Tampere University

JESSE LIETZÉN

Computational Prediction of Impact Sound Insulation of a Timber Floor Based on Simulated Impact Force Excitation of the Standard Tapping Machine

Tampere University Dissertations 977

Tampere University Dissertations 977

JESSE LIETZÉN

Computational Prediction of Impact Sound Insulation of a Timber Floor Based on Simulated Impact Force Excitation of the Standard Tapping Machine

ACADEMIC DISSERTATION
To be presented, with the permission of
the Faculty of Built Environment
of Tampere University,
for public discussion in the auditorium RG202
of the Rakennustalo, Korkeakoulunkatu 5, Tampere,
on 22 March 2024, at 12 o'clock.

ACADEMIC DISSERTATION
Tampere University, Faculty of Built Environment
Finland

Responsible supervisor and Custos	Professor Sami Pajunen Tampere University Finland	
Supervisors	D.Sc. Mikko Kylliäinen Tampere University Finland	D.Sc. Valtteri Hongisto Turku University of Applied Sciences Finland
Pre-examiners	Professor Carl Hopkins University of Liverpool United Kingdom	Ph.D. Catherine Guigou-Carter Scientific and Technical Centre for Buildings CSTB France
Opponent	Professor Edwin Reynders KU Leuven Belgium	

The originality of this thesis has been checked using the Turnitin Originality Check service.

Cover design: Roihu Inc.

ISBN 978-952-03-3340-9 (print)
ISBN 978-952-03-3341-6 (pdf)
ISSN 2489-9860 (print)
ISSN 2490-0028 (pdf)
http://urn.fi/URN:ISBN:978-952-03-3341-6

Carbon dioxide emissions from printing Tampere University dissertations have been compensated.

PunaMusta Oy – Yliopistopaino
Joensuu 2024

PREFACE

My personal interest in acoustics research was awakened probably in 2012 when I had the privilege to take part in a rather vast research project concerning impact sound insulation. During that time, I was supervised by Dr Mikko Kylliäinen, who introduced me to the field of acoustics and has been a source of inspiration to me ever since. Later, my interests in acoustics have been evolving around research and development projects and especially on computational acoustics. However, I also love to operate with building and room acoustics projects, and noise and vibration of different design targets.

My work around the subject of this thesis, on the other hand, started in the beginning of 2017, and during this time I have been working part-time both as a doctoral researcher in Tampere University (former Tampere University of Technology) and as an acoustic consultant at AINS Group (A-Insinöörit). During this period, my responsible supervisor has been Prof. Sami Pajunen. Dr Mikko Kylliäinen has continued to act as my supervisor, and Dr Valtteri Hongisto has been my second supervisor. I am truly grateful for the supervision, support, and all the effort they have given me throughout these years. I would also like to thank all the other co-authors of the publications presented in this thesis: the efforts given by Mr Ville Kovalainen, Dr Juha Miettinen, Mr Juho Sormunen and Mr Saveli Valjakka have been invaluable to me.

From the beginning of 2021, I have been a member of the Doctoral School in Industrial Timber Construction of Tampere University. This community has been of great importance to me and a source of motivation now for three years. I really want to thank Prof. Sami Pajunen for leading the school and all the fellow doctoral researchers in the group: Mika Alanen, Aku Aspila, Juha Franssila, Teemu Hirvilammi, Katja Rodionova, Harri Sivu, Antti Tuure and Ninni Westerholm. All your support, the early-morning and late-night discussions and debates with you have pushed me forward and helped to bring insight into the big picture of construction.

The combination of the two job descriptions has produced an important synergy in my research. I would also like to thank for AINS Group (A-Insinöörit) as an

employer for enabling me to work part-timely during my thesis project. Most of all, I would like to thank all my colleagues who have motivated me to continue with this project. Especially, I would like to thank Mr Ville Kovalainen and Mr Lauri Talus for all the scientifical discussions during the past years.

I would also like to express gratitude to the pre-examiners of this thesis: Prof. Carl Hopkins and Dr Catherine Guigou-Carter. Their efforts in pre-examination and their constructive comments on my work helped me to improve the technical quality of this thesis and encouraged me to carry on.

Of course, this work would not have been possible without the financial support given by different funders. Hence, I would like to thank the funders of the Doctoral School in Industrial Timber Construction of Tampere University, Industrial Research Fund at Tampere University of Technology, and Yrjö ja Senja Koivusen säätiö for their support.

Finally, I am grateful for all the support given by my family during the past seven years. My parents, brothers, and sister: you have always supported me in everything I decided to do, including this work. That cannot be thanked enough. Thank you to my loving wife and children for giving me everyday reasons to think about other than work. Your believe in me has been irreplaceable.

Tampere, 22nd of December 2023

Jesse Lietzén

ABSTRACT

Impact sound insulation (ISI) is one of the principal technical parameters often determining the structural layers of timber intermediate floors. For this reason, in addition to traditional assessment methods such as laboratory and field measurements, researchers have developed several strategies to calculate ISI. The aim of this has been to predict the ISI of timber floors instead of measurements. Recently, there has also been interest among researchers in simulating the ISI of timber floors. The method mainly applied in predictions has been the finite element method (FEM). So far, FEM has been used to evaluate the ISI of full timber floors mainly at low frequencies below 250 Hz, which is why full understanding of the suitability of the method for research or product development purposes of timber floors have not yet been created.

The main purpose of this research was to study the applicability of a FEM simulation procedure for assessing the ISI of a timber floor. Strictly speaking, the investigations of the study were limited to the evaluation of the normalised impact sound pressure level L_n in a computational setup corresponding to the laboratory measurement where the floor is excited by an ISO standard tapping machine (STM). In order to reach this goal, three separate subproblems had to be solved. Related to the first subproblem, the impact force excitation caused by a STM was experimentally investigated with different timber floors. The observations of the study and the obtained measurement results were used to solve the second sub-problem of the study, which concerned a simulation method for determining the impact force excitation. In the third part, the performance of floor coverings with timber floors was investigated experimentally.

Based on the experimental studies, the impact force excitation caused by the STM on timber floors depends on the type of the floor, and naturally the excitation is also affected by the floor covering. The observed differences between magnitude of the amplitude spectra of the impact force were prominent in the entire frequency range studied, but especially at frequencies above 500 Hz. Experimental studies also showed that the performance of floor coverings depends on the type of the bare floor on which the covering is installed. The measured vibration level reductions of the floor coverings differed both between the timber and concrete mock-up slabs.

It was observed that main reason influencing the discrepancies was the different impact force spectra caused by the STM on different floors. Based on the results, the improvement of ISI of floor coverings should be measured with timber floors when they are intended to be used in timber construction projects.

FEM utilising explicit time integration was selected as the simulation tool to determine the impact force excitation of the STM computationally. The simulation results with a cross-laminated timber (CLT) slab showed that the method was able to predict the excitation caused by the apparatus and explain the differences between the results observed in the measurements. The presented post-processing procedure could be used to determine the point force corresponding to the continuous operation of the STM in the time and frequency domains.

The method for determining the impact force excitation was also applied in the simulations of the normalised impact sound pressure level for a full-scale timber floor in its three different construction stages. Based on the results, the simulation procedure enabled predicting the laboratory measurement result of L_n of a full timber floor and the floor without covering with a 0 to 9 dB accuracy in a situation where the exact material properties of the studied timber floors were not known. Single-number-quantities (SNQs) $L_{n,w}$, $L_{n,w} + C_I$, and $L_{n,w} + C_{I,50–2500}$ of the floors were predicted with a 0 to 4 dB accuracy. In case of the bare rib slab, L_n and the SNQs were underestimated by the predictions by 1 to 11 dB, and 4 to 5 dB, respectively. Probable causes for the differences between the simulation and measurement results were uncertain material properties. The applied method can be considered suitable for research and product development use, although the need for further studies and development of the method is obvious.

TIIVISTELMÄ

Askelääneneristävyys on yksi keskeisistä teknisistä ominaisuuksista, joka usein mitoittaa puuvälipohjien rakenteelliset kerrokset. Tästä syystä perinteisten arviointimenetelmien, kuten laboratorio- ja kenttämittausten lisäksi tutkijat ovat kehittäneet useampia strategioita askelääneneristävyyden laskentaan. Tämän tavoitteena on ollut puuvälipohjien askelääneneristävyyden ennustaminen mittausten sijaan. Viime aikoina tutkijoiden keskuudessa on herännyt kiinnostus myös puuvälipohjien askelääneneristävyyden simulointiin. Tähän pääasiallisesti sovellettu menetelmä on ollut elementtimenetelmä (FEM). Toistaiseksi tätä menetelmää on käytetty arvioimaan kokonaisten puuvälipohjien askelääneneristävyyttä lähinnä pienillä, alle 250 Hz taajuuksilla, mistä syystä vielä ei ole syntynyt täyttä käsitystä menetelmän soveltuvuudesta puuvälipohjien tutkimus- tai tuotekehityskäyttöön.

Tämän tutkimuksen päätavoitteena oli tutkia elementtimenetelmään perustuvan simulointiproseduurin soveltuvuutta puuvälipohjan askelääneneristävyyden arviointiin. Tarkkaan ottaen tutkimuksen tarkastelut rajattiin normalisoidun askeläänenpainetason L_n arviointiin laboratoriomittausasetelmaa vastaavassa laskennallisessa tilanteessa, jossa välipohja herätetään askeläänikojeella. Jotta tähän tavoitteeseen päästiin, tuli ratkaista kolme erillistä aliongelmaa. Näistä ensimmäisen yhteydessä tutkittiin kokeellisesti askeläänikojeen aiheuttamaa voimaherätettä erilaisilla puuvälipohjilla. Ensimmäisen tutkimuksen havaintoja ja siinä saatua mittausdataa käytettiin hyväksi tutkimuksen toisen aliongelman ratkaisemiseksi, jossa tarkasteltiin simulointimenetelmää herätteen määrittämiseksi. Kolmannessa osuudessa taas selvitettiin kokeellisesti lattianpäällysteiden suorituskykyä puuvälipohjilla.

Kokeellisten tutkimusten perusteella askeläänikojeen aiheuttama voimaheräte puuvälipohjilla riippuu välipohjan tyypistä ja luonnollisesti herätteeseen vaikuttaa myös lattianpäällyste. Havaitut herätteiden amplitudispektrin magnitudin eroavaisuudet olivat nähtävissä koko tutkitulla taajuusalueella, mutta erityisesti yli 500 Hz taajuuksilla. Kokeelliset tutkimukset osoittivat myös, että lattianpäällysteiden suorituskyky riippuu rakenteesta, jonka päälle päällyste on asennettu. Mitatut värähtelytasoerot erosivat toisistaan sekä puu- että betonilaattojen kesken. Yhtenä näihin eroavaisuuksiin vaikuttavana tekijänä on nimenomaan askeläänikojeen

aiheuttamat erilaiset voimaherätespektrit eri välipohjilla. Tulosten perusteella lattianpäällysteiden askeläänieneristävyyden parannus tulisi mitata puuvälipohjilla, kun niitä on tarkoitus käyttää puurakentamisessa.

Simulointityökaluksi askeläänikojeen voimaherätteen laskennalliseksi määrittämiseksi valikoitui eksplisiittistä aikaintegrointia hyödyntävä elementtimenetelmä. Simulointitulokset ristiinlaminoidulla puulaatalla (CLT) osoittivat, että menetelmä kykeni ennustamaan askeläänikojeen aiheuttaman herätteen ja selittämään mittauksissa havaittuja eroavaisuuksia tulosten välillä. Menetelmän yhteyteen luotua jälkikäsittelyproseduuria voitiin hyödyntää askeläänikojeen jatkuvaa toimintaa vastaavan pistevoiman määrittämiseen aika- ja taajuustasoissa.

Menetelmää askeläänikojeen aiheuttaman voimaherätteen määrittämiseksi sovellettiin myös normalisoidun askeläänenpainetason simuloinneissa kokonaiselle puuvälipohjalle sen kolmessa eri rakennusvaiheessa. Tulosten perusteella simulointiproseduurin avulla kyettiin ennustamaan kokonaisen välipohjan ja lattianpäällysteettömän välipohjan normalisoidun askeläänenpainetason L_n laboratoriomittaustulos 0–9 dB tarkkuudella tilanteessa, jossa tutkittujen puuvälipohjien tarkat materiaaliominaisuudet eivät olleet tiedossa. Askeläänieneristävyyttä kuvaavien yksilukuarvojen $L_{n,w}$, $L_{n,w} + C_I$ ja $L_{n,w} + C_{I,50–2500}$ ennustustarkkuus oli 0–4 dB. Ripalaatan tapauksessa L_n ja yksilukuarvot aliarvioituivat ja ne kyettiin ennustamaan 1–11 dB ja 4–5 dB tarkkuuksilla. Todennäköisenä syynä havaituille simulointi- ja mittaustulosten eroille pidettiin epävarmoja materiaaliominaisuuksia. Käytettyä menetelmää voidaan pitää tutkimus- ja tuotekehityskäyttöön soveltuvana, vaikkakin lisätutkimusten ja menetelmän jatkokehittämisen tarve on ilmeinen.

CONTENTS

ABBREVIATIONS

ΔL	Improvement of impact sound insulation [dB]
ΔL_a	Vibration level reduction [dB]
C_{I}	Spectrum adaptation term [dB]
$C_{\mathrm{I,50\text{-}2500}}$	Spectrum adaptation term for an enlarged frequency range 50–2500 Hz [dB]
CLT	Cross laminated timber
FEM	Finite element method
F_{peak}	Peak value of the impact force pulse [N]
F_{n}	Amplitude spectrum of the force [N]
F_{lf}	Low-frequency magnitude of the amplitude spectrum of the force [N]
I	Mechanical impulse of the force [Ns]
ISI	Impact sound insulation
L_{n}	Normalised impact sound pressure level [dB]
$L_{\mathrm{n,w}}$	Weighted normalised impact sound pressure level [dB]
LVL	Laminated veneer lumber
m	Mass [kg]
m'	Mass per unit area [kg/m^2]
s'	Dynamic stiffness per unit area [MN/m^3]
s_t'	Apparent dynamic stiffness per unit area [MN/m^3]
SNQ	Single-number quantity (such as $L_{\mathrm{n,w}}$, C_{I}, and $C_{\mathrm{I,50\text{-}2500}}$)
STM	ISO standard tapping machine
T_{pulse}	Length of the force pulse [s]
T_{r}	Length of the period between force pulses [s]
v_o	Initial velocity of a hammer of an ISO standard tapping machine before collision to the floor surface [m/s]

ORIGINAL PUBLICATIONS

Publication I Lietzén, J., Miettinen, J., Kylliäinen, M. & Pajunen S. 2021. Impact force excitation generated by an ISO tapping machine on wooden floors. *Applied Acoustics* **175**, article 107821.

Publication II Lietzén, J., Sormunen, J., Pajunen, S. & Kylliäinen, M. 2022. Simulation of impact force generated by an ISO tapping machine on a wooden slab using explicit dynamics analysis. *Engineering Structures* **270**, article 114855.

Publication III Lietzén, J., Kylliäinen, M., Valjakka, S. & Pajunen S. 2022. Vibration level reduction by floor coverings installed on wooden slabs. *Building Acoustics* **29**(2), 221–237.

Publication IV Lietzén, J., Kovalainen, V., Kylliäinen, M. & Pajunen, S. Computational prediction of impact sound insulation of a full-scale timber floor applying a FEM simulation procedure. *Engineering Structures*, submitted 3rd of August 2023, revised 15th of December 2023.

AUTHOR'S CONTRIBUTION

Publication I Lietzén was the corresponding author and responsible for writing the publication. He also conducted the experiments with a help of Miettinen and performed the formal data analysis. Pajunen was responsible of supervising the research activity. The concept and methodology of the research was designed by Lietzén, Kylliäinen and Pajunen. The publication was assessed and edited by Miettinen, Kylliäinen and Pajunen.

Publication II Lietzén was the corresponding author and responsible for writing the publication. Lietzén and Sormunen created the simulation models and computational methodologies. Pajunen was responsible of supervising the research activity. The concept and methodology of the research was designed by all the authors. The publication was assessed and edited by Sormunen, Pajunen and Kylliäinen.

Publication III Lietzén was the corresponding author and responsible for writing the publication. He conducted the experiments on timber floors during the measurement series presented also in Publication I. Valjakka performed the formal data analysis in cooperation with Lietzén. The concept and methodology of the research was designed by Lietzén and Kylliäinen. Pajunen was responsible of supervising the research activity. The publication was assessed and edited by Kylliäinen and Pajunen.

Publication IV Lietzén was the corresponding author and responsible for writing the publication. Lietzén created the simulation models and computational methodologies in cooperation with Kovalainen. Pajunen was responsible of supervising the research activity. Otherwise, the concept and methodology of the research involved all the authors. The publication was assessed and edited by Kovalainen, Kylliäinen and Pajunen.

1 INTRODUCTION

1.1 Motivation to study impact sound insulation of timber floors

Although timber intermediate floors represent classical and practical applications used in the construction industry, they provide perhaps a more topical research subject for acoustical engineers than earlier. Timber floors are subject to various requirements, such as load bearing capacity, deflection, vibration, fire resistance, air tightness, airborne and impact sound insulation. However, in many countries the *impact sound insulation* (ISI) is one of the principal technical parameters dimensioning the structural layers of the timber floors (Rasmussen, 2019). The need to fulfil the ISI requirements has widely led to multi-layered and complex floor structures (Homb *et al.*, 2017, 2016), thus making the timber floors essential building elements also for the competitiveness of timber construction. At the same time, it must be noted that the airborne sound insulation of multi-layered timber floors is generally high and does not usually dimension the floor (Hongisto *et al.*, 2023; Lahtela *et al.*, 2021). These issues make assessing the ISI of the timber floors one of the most important tasks for acoustical engineers working with timber construction.

Designing the ISI of timber floors is still often based on experiences gained in previous projects and from field or laboratory measurements (Balanant *et al.*, 2012; Johansson, 1995; Warnock, 2005; Warnock and Birta, 2000; Zeitler *et al.*, 2010). The application of well-tried structures is often a safe design solution for new buildings but hinders the development of novel structures and introducing state-of-the-art solutions to the building markets. Furthermore, the vast variety of construction materials together with the range of different floor systems makes the development and design work of the timber floors demanding if the acoustical engineers rely only on experience. ISI measurements do not either provide a permanent answer for this challenge since they seldom give reasons for the results but are important for quality control and product approval purposes. Thus, the ability to assess the timber floors by computationally imitating the ISI measurements is a priority. The importance of the matter is emphasised when we consider the necessary changes in the construction methods on a way to a sustainable future.

The combat against climate change is likely to increase timber construction. The global aim (United Nations Framework Convention on Climate Change, 2015) is to reduce the risks and impacts of climate change by holding the global average temperature below 2°C, and preferably below 1.5°C. To meet this aim, greenhouse gas emissions should be mitigated which again challenges the construction markets. One presented mitigation strategy to reduce emissions from building materials involves increasing the share of timber construction by 10% by 2050 (Zhong *et al.*, 2021). However, this strategy together with the other detected mitigation strategies would require doubling the proportional share of emissions of building material sector by 2060 to meet the 1.5°C goal (Zhong *et al.*, 2021). A recent study shows that even more ambitious mitigation strategies, where up to 10%, 50% or 90% of the novel mid-rise buildings would be made using engineered wood during 2020–2100, lead to great emission savings in comparison with the "business as usual" strategy (no timber buildings for new urban citizens) also including land-related emissions (Mishra *et al.*, 2022). Applying the 90% strategy would imply 10% emission savings of the remaining 2°C climate guard rail, and thus can be seen as a viable mitigation option to combat climate change (Mishra *et al.*, 2022). Adopting only a part of this strategy would imply a drastic increase in timber construction markets.

Together with the growth of timber construction, it is essential to develop timber construction to a more resource-efficient and sustainable direction. This requires rethinking the way how we utilize wood in construction (Pramreiter *et al.*, 2023) which probably increases the need to optimize the timber structures (Mayencourt and Mueller, 2020) and is likely to lead to product development of novel solutions for the timber construction markets. This will challenge also the acoustical engineers working with timber buildings within the upcoming decades. Because the timber intermediate floors cause a significant part of embodied carbon emissions in multi-story timber apartment buildings, it is evident that an essential part of the future challenge faced by acoustical engineers is to enable the development of sustainable timber floors fulfilling the requirements for ISI. To reach these goals, this thesis focuses on filling some essential research gaps on a way towards effective tools for research and product development.

1.2 Impact force excitation of timber floors

ISI is measured using standard impact sound sources to achieve a measurable and reproducible *impact force excitation* to the studied floor. Depending on the applied

national legislation or guidelines, the standard impact sound source used in the measurements is either a tapping machine or a rubber ball (ISO 10140-5, 2021; ISO 16283-2, 2015). In special cases, also a modified tapping machine can be used (ISO 10140-5, 2021). The *ISO standard tapping machine* (STM), however, can be considered as the most conventional standard impact sound source because it has been used in measurements since its first standardization in 1938 in Germany (DIN 4110, 1938).

Up to now, the STM is used in the ISI measurements throughout the world (Machimbarrena *et al.*, 2019; Rasmussen, 2019) and is probably the most widely used standard impact sound source. Furthermore, there is some evidence from the psychoacoustic experiments that the alternative impact sound sources do not lead to a better association between the single-numbers quantities (SNQs) rating the impact sound insulation and subjective judgment of the ISI (Gover *et al.*, 2011). The replacement of the STM with a new sound source might not be necessary and the problems associated should be solved by deriving a new rating method based on the tapping machine instead (Zeitler *et al.*, 2013). Such rating method has recently been presented by Kylliäinen *et al.* (2019). These are the main reasons for focusing on the use of STM in the ISI assessments in this thesis.

The STM has five 0.5 kg steel hammers with spherical impact surfaces. Each of the hammers are freely dropped one after another from 40 mm height onto the floor two times per second. Thus, the hammers will impact the floor with an approximate velocity v_0 0.886 m/s at the beginning of the collision. The continuous operation of the apparatus drops the hammers repeatedly resulting in a 2 Hz repetition rate for a single hammer and a 10 Hz rate when all the hammers are accounted for. Full requirements for the STM have been given by the standards ISO 10140-5 (2021) and ISO 16283-2 (2015).

Although the STM excites the floor under study in a reproducible manner, the impact force excitation caused by it is not structure independent. With a focus on the behaviour of the STM on timber floors, an essential feature of the apparatus is that the impact force excitation produced depends on the floor structure. When the hammers hit a stiff and heavy structure with a hard surface, the exerted force pulses are very short but an elastic structure causes the pulses to spread. (Brunskog and Hammer, 2003a; Cremer *et al.*, 2005) Theoretically, the range of low-frequency level difference of the impact force spectrum is 6 dB depending on whether the collision between the hammer and the floor is fully elastic (all the impact energy is preserved in the impact) or fully inelastic (all the impact energy is dissipated in the impact). This range corresponds with the range of the mechanical impulse induced in the collision. Together with the increasing frequency, the theoretical range of level

difference rapidly increases. (Brunskog and Hammer, 2003a) To give an example, the magnitude of the amplitude force spectrum generated by the STM is nearly constant on bare concrete slabs in the frequency range 50–5000 Hz (Gudmundsson, 1984; Rabold *et al.*, 2010), but on timber floors, the spectrum is at its highest in the low frequencies but the values decrease when the frequency increases.

Research literature presents a few measurement results of the impact force generated by the STM. Gudmundsson (1984), Rabold *et al.* (2010), and Olsson and Linderholt (2019) have observed some fundamental differences in the impact force excitation generated by the STM of different floors. Moreover, Jeon *et al.* (2006) have attempted to characterise different impact sound sources, and Amiryarahmadi *et al.* (2016) have compared the measured force spectrum generated by the STM with the spectrum from walking. However, apart from the study by Gudmundsson (1984) who studied mainly concrete structures, measurement results of the impact force excitation have been presented only for few floors (Amiryarahmadi *et al.*, 2016; Jeon *et al.*, 2006; Olsson and Linderholt, 2019; Rabold *et al.*, 2010). Thus, it is not exactly known, how the excitation varies on timber floors, and moreover, how does the floor coverings affect the excitation.

The impact force excitation generated by the STM has been described in the literature with several analytical models. Roughly, these models could be categorised into *simple* and *general models*. The simple models (Cremer *et al.*, 1973; Heckl and Rathe, 1963; Lindblad, 1968; Scholl and Maysenhölder, 1999; Vér, 1971), and the further developed models of Lindblad and Vér presented by Brunskog and Hammer (2003a) and Griffin (2017), respectively, assume a hard slab surface and a large driving-point impedance in comparison with the mass impedance of the hammer. Additionally, the models (Griffin, 2017; Lindblad, 1968; Scholl and Maysenhölder, 1999; Vér, 1971) can take the effect of the resilient floor coverings on the impact force excitation into account. However, these models were mainly developed to describe the excitation of stiff and heavy floor systems, such as concrete floors. According to the author's knowledge, it is not known whether the simple models can reliably be applied for describing the excitation of timber floors.

The general models (Brunskog and Hammer, 2003a; Coguenanff *et al.*, 2015; Rabold *et al.*, 2010) can consider complex features of the floors making them better suitable for describing the impact force excitation generated by the STM on timber floors. The model presented by Rabold *et al.* (2010) even considers the temporally developing process of the relative velocities between the hammer and the slab. Moreover, the model presented by Wittstock (2012) to characterise the interaction between the STM and an infinite reception plate, and the model by Amiryarahmadi

et al. (2011) to model the impact force by applying a Hertzian contact theory, can be regarded as general models although their applicability to model timber floors is slightly limited in this respect. The shortcomings of the models (Brunskog and Hammer, 2003a; Coguenanff *et al.*, 2015; Rabold *et al.*, 2010) lie in their requirements for detailed information from the floor, such as the local and global driving-point mobilities. In case of a general timber floor, determining such input data would require elaborate computational models. Secondly, apart from the model presented by Amiryarahmadi *et al.* (2011), the general models do not take into account the geometric non-linearity caused by the spherical surfaces of the hammers. An appealing alternative for these general models would be to solve the impact force excitation straight with the numerical simulation models. One possibility for this is to apply techniques from *computational impact mechanics* when both the geometric non-linearity and complex features of the floors can be simultaneously considered without the need for determination of input data with computational models.

1.3 Prediction of impact sound insulation of timber floors

Instead of the measurements, an interesting and efficient approach would be to assess the ISI of the floors computationally. Since the standardised methods for calculating the ISI (EN ISO 12354-2, 2017) are not applicable to timber floors, various strategies for the calculation have been shown in the research (Brunskog and Hammer, 2000; Forssén *et al.*, 2008). The strategies can roughly be divided into experimental, analytical and numerical models (Atalla and Sgard, 2015).

Several parametric measurements have been carried out in attempts to interpret the effects of different structural parts on the ISI of the timber floors (Balanant *et al.*, 2012; Chung *et al.*, 2006; Johansson, 1995; Warnock, 2005; Warnock and Birta, 2000; Zeitler *et al.*, 2010, 2008). The variated structural parts in these measurements have been, e.g., the surface structures, beams of the rib slab floor, ceilings and the rate of absorption material in the airspace of the floor (Latvanne, 2015). One simple experimental prediction model, partly based on the parametric measurements, has been presented by Latvanne *et al.* (2018). The aim of the model is to allow a fast evaluation of ISI by combining the available measurement results. To predict the ISI of different timber floors properly the model requires a substantial number of measurement data. The shortcoming of the parametric models usually lies in the lack of input data.

Since measuring every possible parameter in detail is not possible in practice, artificial neural networks have recently been applied to predict the ISI of timber floors with products not measured (Bader Eddin *et al.*, 2022). This method also requires a great amount of measurement data. However, the approach is problematic for the product developers because the artificial neural network method is unable to explain the reasons for the ISI results. Another way to cover the deficiencies of the experimental models and simultaneously bring insights into the causes of the results is to combine the measurement results with the results of analytical models. Analytical models in general are highly effective when they can be applied in sound insulation prediction tools. The shortcoming of the models is, however, that analytical solutions can be found only for relatively simple applications (Atalla and Sgard, 2015). To give an example: two models predicting the ISI of timber rib slabs have been presented in the literature (Brunskog and Hammer, 2003b; Mosharrof *et al.*, 2011), but their applicability is limited for this specific purpose. While novel and sophisticated analytical models can be further developed, the problem lies in their limitations to answer general questions about the development of timber floors.

Recently, the application of numerical simulation methods (later briefly called *simulations*) in the prediction of ISI of timber floors has raised interests. In addition to the complexity of the timber floors, one particular reason for this is the acknowledged importance to consider the low-frequency behaviour of the timber floors (Ljunggren *et al.*, 2017, 2014; Ljunggren and Simmons, 2022; Öqvist *et al.*, 2018). The principal numerical method used in the prediction has been the *finite element method* (FEM). The deterministic nature of FEM, however, means that the quality of the input data is of great importance for the prediction accuracy. This can be seen as a shortcoming of the method when it is used to analyse the behaviour of structures with uncertain and highly variable material properties. Nevertheless, in case of timber slabs and floors, FEM has previously been successfully applied to assess the low-frequency vibration, sound radiation and impact sound insulation of the structures below 500 Hz, but usually below 250 Hz.

FEM has been applied to simulate issues affecting the low-frequency ISI of timber floors and slabs. For example, the low-frequency vibration of timber slabs and floors – related to the acoustical performance of the structures – has been studied with FEM by several researchers. The simulations have included investigations on the vibrational performance of timber rib slabs (sole load-bearing structure) and rib slab floors (load-bearing structure together with other structural layers) (Bard *et al.*, 2017, 2008; Negreira *et al.*, 2016; Negreira and Bard, 2016; Persson and Flodén, 2019; Shen and Hopkins, 2022, 2020, 2019), mass timber slabs

(Filippoupolitis *et al.*, 2017, 2014; Qian *et al.*, 2019a, 2019b), and full-scale timber mock-ups (Bolmsvik *et al.*, 2014; Bolmsvik and Brandt, 2013; Flodén *et al.*, 2015). Moreover, simulations have been carried out to solve the sound radiation of different point-excited structures by using FEM in the low frequencies. These studies have involved simulations on mass timber slabs (Buchschmid *et al.*, 2015; Hopkins *et al.*, 2016; Kohrmann *et al.*, 2013), a timber rib slab floor (Olsson and Linderholt, 2021) and hybrid timber slabs (Linderholt and Olsson, 2017; Olsson and Linderholt, 2021). Overall, FEM has proven to be a versatile tool offering several possibilities to solve vibrational behaviour and sound radiation of timber structures.

In addition, FEM has been used to simulate the ISI of timber floors excited with the STM. Rabold (2010), Rabold *et al.* (2009, 2008, 2007), Kohrmann (2017), Kohrmann *et al.* (2016), and Coguenanff (2016) simulated the low-frequency ISI of different timber floors below 200 or 250 Hz applying FEM. To consider the impact force excitation generated by the STM, Rabold *et al.* applied a general impact force model (Rabold *et al.*, 2010), Kohrmann *et al.* used a simple impact force model (Cremer *et al.*, 2005) and Coguenanff used a probabilistic model (Coguenanff, 2016; Coguenanff *et al.*, 2015) in their simulations. FEM has recently also been applied for ISI computations of a timber slab in a broad frequency range. Previously, this has successfully been carried out for concrete slabs (Jean *et al.*, 2006; Vastiau *et al.*, 2022), but Wang *et al.* (2020) have presented a FEM model simulating the radiating impact sound pressure level of a timber rib slab. Wang *et al.* applied a general impact force model (Brunskog and Hammer, 2003a) to characterise the excitation generated by the STM.

Apart from the study by Wang *et al.* (2020) on a timber slab, FEM has previously been applied to predict the ISI of timber floors only in the low-frequency range. The agreement between the simulation and measurement results presented by Wang *et al.* was good in a broad frequency range despite some evident discrepancies between the simulated and measured mid-frequency results. These were explained, e.g., with the applied impact force excitation in the simulations. (Wang *et al.*, 2020) According to the author's knowledge, validated FEM models predicting the ISI of *full timber floors* in a broader frequency range have not been published so far. The term *full floor*, in this respect, means that the floor under investigation has all the structural and acoustical layers (a floor covering, a load-bearing timber slab, a structural surface layer to add mass of the slab, a suspended ceiling, and absorptive material in the air cavity), and that the dimensions of the floor also correspond to the dimensions of a room in an apartment building.

1.4 Floor coverings on timber floors

Floor coverings, such as cushion vinyls, wall-to-wall carpets, and multilayer parquets or laminates on their underlayments, constitute an important and effective way to affect the ISI of floors. By reducing the impact force excitation to the bare intermediate floor, the floor coverings improve the ISI of the whole structure. This relative *improvement of impact sound insulation* (ΔL) caused by the floor covering is a function of frequency and it is usually determined in a laboratory by following standardised measurement procedures (ISO 10140-1, 2016; ISO 10140-3, 2021; ISO 10140-5, 2021). The procedures involve measuring the impact sound pressure levels radiated by the floor with and without the floor covering using the STM as the impact sound source. Optionally, the ΔL of a light floor covering can be measured with a small concrete mock-up slab according to the standard ISO 16251-1 (2014) by deriving the ΔL from the measured vibrational acceleration of the slab.

In addition to the concrete slab, the performance of the floor coverings can be measured according to the standard ISO 10140-5 (2021) on three different lightweight reference floors and on a timber mock-up floor. However, currently there exist no standardised method for timber floors corresponding to the one presented by the standard ISO 16251-1 (2014). Despite the possibilities to perform ISI measurements of floor coverings on the lightweight reference floors, construction industry has made measurements of floor coverings mainly on concrete slabs. Thus, an important question is whether these measurement results for ΔL can be applied in the ISI assessment of timber floors. And more specifically, how does the type of the subfloor affect the ΔL.

According to the research literature, there is little evidence that ΔL depends on the type of the slab although this has previously been identified as a problem (Hopkins, 2007; ISO 10140-5, 2021; Kartous and Jonasson, 2001; Zeitler *et al.*, 2009). For example, several studies show that resilient floor coverings have different abilities to reduce impact sound on concrete and timber slabs (Alonso *et al.*, 2019; Nowotny and Nurzyński, 2020; Pereira *et al.*, 2016; Schmitz, 2000; Scholl and Maysenhölder, 1999; Warnock, 2000). This performance difference has also been noted by Guigou-Carter *et al.* (2009) who studied prediction of the ΔL of two floating floor coverings on concrete and lightweight floors. However, there has been a lack of a systematic study where results of different floor coverings on concrete and timber slabs have been compared. In the product development of timber slabs but also in the design tasks it is preferable that measured values for ΔL of different floor

coverings are available. To avoid tedious simulation setups, ΔL values should correspond with the performance of the covering on the slab under consideration.

1.5 Objectives

The principal objective of this thesis was to study the applicability of a FEM simulation procedure to predict the ISI of full timber floors. Specifically, the study was limited to the evaluation of the normalised impact sound pressure level L_n in a computational setup corresponding to laboratory measurements where the floors are excited by a STM. The aim behind this objective is to enable the development of accurate simulation tools for acoustical research and product development purposes but eventually also for design tasks concerning the ISI of timber floors. As discussed in Section 1.1, it is likely that needs for such tools are increasing. Due to the research gaps mentioned above, the objective was supported with simulations and experimental research. The aim of the experimental parts of the research was to create a more profound insight to the addressed problems concerning the impact force excitation generated by the STM and the performance of floor coverings on timber floors, and to produce validation data for the simulations.

To serve these objectives, the study presented in this thesis was divided into four sub-problems (see also Section 2.1):

- Measurements of the impact force excitation generated by the STM on different timber floors with and without floor coverings,
- Simulations of the impact force excitation generated by the STM on a timber slab,
- Measurements of the performance of floor coverings on different timber slabs and on a concrete slab,
- ISI simulations to study the applicability of a simulation procedure to predict ISI of full timber floors.

2 MATERIALS AND METHODS

2.1 Structure of the research

The sub-problems formulated in Section 1.5 were studied in four publications I–IV as follows:

- **Publication I** describes the experimental results for impact force excitation generated by the STM at five source positions on ten different timber slabs with and without floor coverings. Additionally, the publication describes the applied method to instrument the STM for impact force measurement purposes.
- **Publication II** describes a validated simulation procedure for the determination of the impact force excitation generated by the STM. The applied techniques, e.g., allow considering the geometric non-linearity of the contact between the hammers and the slab, as well as post-processing the simulation results for ISI simulation purposes. The publication also presents the results of the model validation together with the sensitivity analysis.
- **Publication III** presents the experimental results for the vibration level reduction by floor coverings installed on eight timber slabs and a concrete mock-up slab. In addition to the bare load-bearing timber slabs, the publication studies the effect of adding mass of the timber slabs by conventional structural means on the performance of the floor coverings.
- **Publication IV** studies the applicability of the applied FEM simulation procedure to predict the normalised impact sound pressure levels L_n of a full-scale timber floor in three construction stages. The publication describes the results from the simulations performed in two different manners and compares the results with the laboratory measurement results.

The following sections of this thesis report an overview of the entire study comprised by the publications. More detailed descriptions of the individual studies can be found from the original publications I–IV together with comprehensive descriptions of background, materials and methods, as well as results.

2.2 Experiments on timber floors

2.2.1 Impact force and vibration experiments

The experiments were carried out on 24 timber floor mock-ups (**Figure 1**). The sizes of the floors were 2.4 m x 2.7 m with a span of 2.7 m. The two studied load-bearing slabs comprised a 100 mm thick cross laminated timber (CLT) slab (floors F1–F5) and a prefabricated rib slab (floors F6–F10). The slabs were installed between vibration isolated steel structures located on the floor of the construction laboratory. The CLT slab was a 3-layered construction with lamellas of thicknesses 30, 40 and 30 mm. Individual structural timber boards of the slab were laminated to each other only from their broader sides. Therefore, slight gaps between the narrow sides of the boards were present. The rib slab was constructed from 25 mm thick laminated veneer lumber (LVL) panel deck and 45 mm x 260 mm LVL beams (c/c 578–600 mm). The LVL panel was both screwed and glued to the LVL beams. In few experiments, 15.5 mm thick plasterboards were attached to the surface of the load-bearing slabs to increase the mass of the floor. The boards were glued and screwed to each other and screwed to the timber slabs.

The surface structures of the floors included two floor coverings and a floating floor (see **Figure 1**). The multilayer parquet (floor covering C1) was a 14 mm thick maple parquet (mass per unit area m' = 7.73 kg/m^2) equipped with tongue-and-groove joints. In all the measurements, the parquet was installed in identical order on the soft 3 mm thick underlayment (m' = 0.15 kg/m^2, dynamic stiffness per unit area s' = 65.1 MN/m^3). The cushion vinyl (floor covering C2) was a soft 3 mm thick product especially used in apartment houses (m' = 0.15 kg/m^2, s' = 2282 MN/m^3). The vinyl was glued to the substructure under and around each source position. The floating floor was constructed from a 30 mm thick mineral wool layer (apparent dynamic stiffness per unit area s'_t = 12.8 MN/m^3, s' = 16.4 MN/m^3) and two 15 mm thick plasterboard layers (m' = 15.4 kg/m^2) glued and screwed to each other according to instructions provided by the manufacturer.

The measurements were carried out at five STM positions S1–S5 per structure. During the measurements, both the impact force generated by the centre hammer of the STM at different source positions and the vibrational acceleration of the floors at measurement positions M1–M6 were recorded (**Figure 2**). The positions were at least at half a meter apart from the edges of the structure (cf. requirements in ISO 16283-2 (2015)). The frequency range of interest in the force measurements was 16–

3600 Hz, since the low frequency behaviour often determines the subjective rating of the timber floor structures (Ljunggren *et al.*, 2017, 2014). The vibration of the floors was studied in the frequency range 50–5000 Hz.

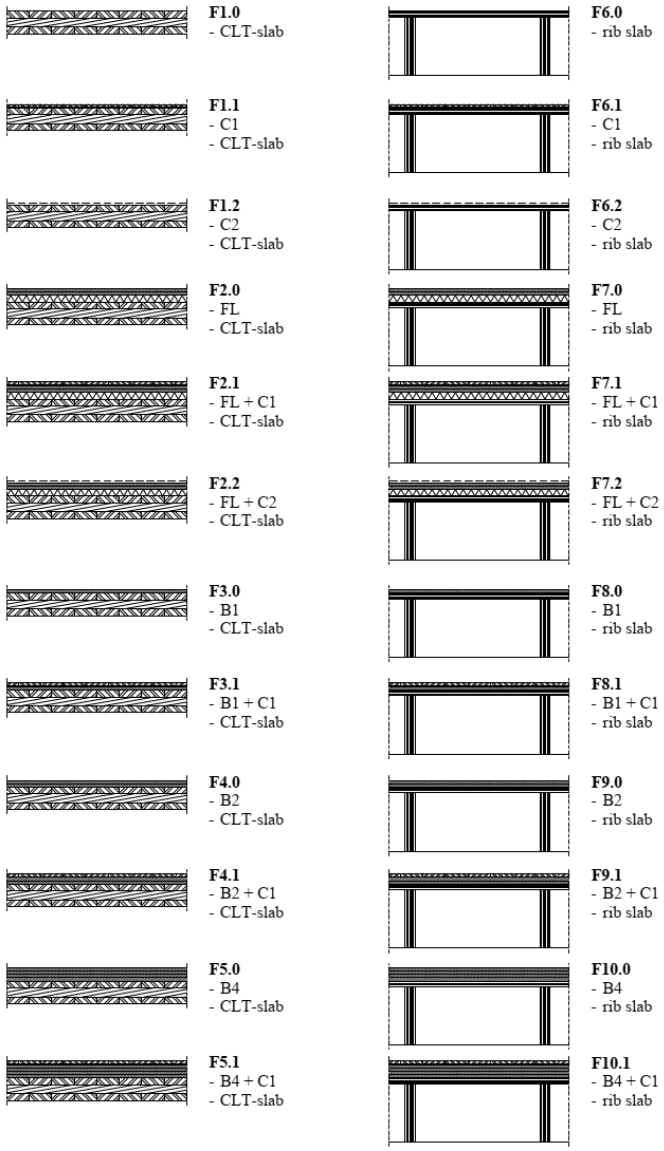

Figure 1. Experimentally studied floors F1–F10. The numbers after the points indicate the surface structures: (0) no floor covering, (1) floor covering C1, and (2) floor covering C2. FL denotes the floating floor, and B indicates the additional plasterboards on the slab, where the following number denotes the number of board layers (B1, B2, B4).

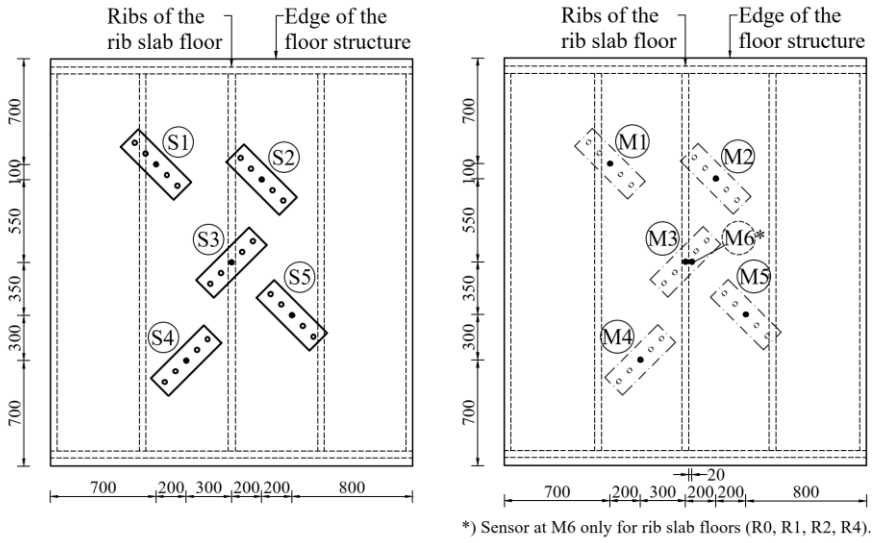

Figure 2. Source positions (left) and measurement positions (right) of the floors F1–F10. The presented dimensions (in millimetres) illustrate the area of the rib slab, spacing of the ribs, and the location of the centre hammer of the STM in different positions.

Impact force excitation generated by the STM was measured *using an instrumented ISO standard tapping machine*. The centre hammer of the STM was modified and equipped with both force and acceleration sensors (**Figure 3**). The force sensor, covered with a custom-built impact cap, was calibrated at the factory prior to the measurements and placed at the bottom of the hammer to measure the impact force input into the floor. The acceleration sensor was placed at the top of the hammer to get further information on the motion of the hammer. The modifications of the hammer were performed such that the hammer fulfilled the standard requirements for the STM (ISO 10140-5, 2010; ISO 16283-2, 2015) together with the attached sensors and additional parts.

The impact force was directly measured from the hammer during the operation of the apparatus. This was performed also to investigate the variation of the impact force pulses. All measurements were recorded in the time domain, and therefore the time histories of the impact force were received. The length of each measurement was approximately 30 s, the sampling frequency was 12800 Hz, and the length of the period T_r between the pulses was 0.5 s. In the **Publication I**, the post-processed measurement signals during the contact of the hammer and the floor were shown. However, as noted later in the **Publication II,** the effect of the mass of the impact cap should be considered in the derivation of the forces driving the floors. This effect can be accounted for multiplying the time and frequency domain results with

a correction factor (see **Publication II**). This has been performed in the results shown in this thesis.

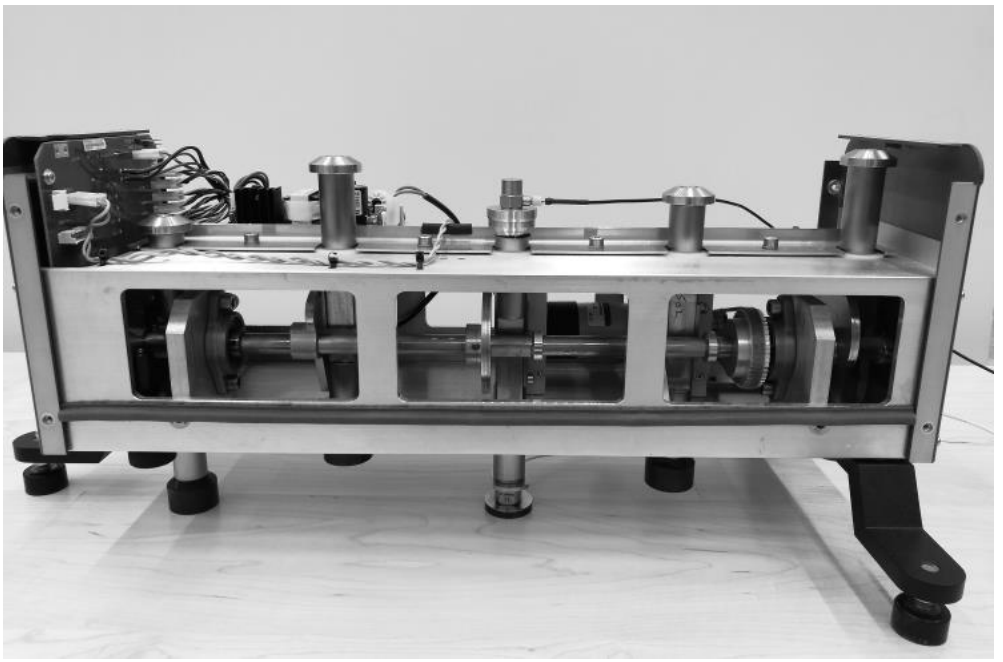

Figure 3. Instrumented ISO standard tapping machine (STM). The centre hammer was modified and equipped with a force sensor covered with a custom-built impact cap (at the bottom of the hammer), and with an acceleration sensor (at the top of the hammer).

To determine the performance of the floor coverings on the timber slabs, *vibration level reductions* (ΔL_a) were derived from the vibratory acceleration levels of the floors (see **Publication III**). The ΔL_a of the floor coverings were determined for the multilayer parquet with the underlayment (C1), and the cushion vinyl (C2) on the timber slabs F1, F3, F4, F5, F6, F8, F9, F10 by adopting the measurement methods from Sommerfeld (2009) presented in the standard ISO 16251-1 (2014). In cases where the performance of the covering C1 was measured on the timber slabs with plasterboard surfaces, measurements with the covering were performed first. However, in the derivation of the results on the timber floors the vibratory acceleration levels directly below the source position were neglected. The tests were repeated for the same floor coverings on a concrete mock-up slab in accordance with the standard ISO 16251-1 (2014). The aim of this was to find out how the results differ on timber and concrete slabs, and the reasons for the possible discrepancies. These latter tests were performed by Acoustics Laboratory of Turku

University of Applied Sciences. The results for the ΔL_a were calculated from the measured vibratory acceleration levels both on the timber and the concrete mock-up slabs in a similar manner according to ISO 16251-1 (2014).

2.2.2 Impact sound insulation measurements

To enable the validation of the simulations of impact sound insulation described in Section 2.3, ISI measurements were conducted for full-scale timber floors. The structure under study was a full timber floor with a rib slab as its load-bearing structure (F11). Additionally, the floor F11 consisted of a floor covering, plasterboards attached onto the slab, a suspended plasterboard ceiling, and a glass wool installed between the ribs. The floor was studied in three construction stages: F11 (the full floor), F12 (the floor without floor covering), and F13 (the bare rib slab) (**Figure 4**). The length of the floor was 3870 mm, and the width 3020 mm.

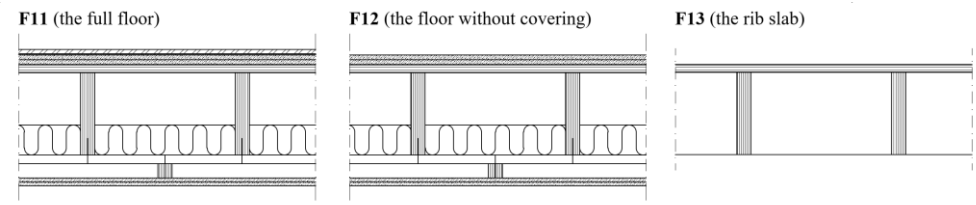

Figure 4. Floor structure F11 and its construction stages F12 and F13. The layers of the floor F11 from top to bottom were: a multilayer parquet (thickness h = 14 mm) on an underlayment (h = 3 mm), two plasterboard layers (h = 15.5 mm), rib slab with a LVL deck (h = 27 mm) and LVL beams (h = 260 mm, width b = 45 mm, c/c = 490 mm), a glass wool layer (h = 95 mm) between the ribs, boards from LVL deck (h = 27 mm, b = 100 mm, c/c = 550 mm) screwed below the ribs, LVL battens from LVL beams (h = 45 mm, b = 45 mm, c/c = 490 mm) screwed to the overhead boards between the ribs, and two plasterboard layers (h = 12.5 mm).

The rib slab was constructed from a 27 mm thick LVL panel deck and 45 x 260 mm LVL beams (c/c 490 mm). The panel was both screwed and glued to the beams. Two plasterboard layers of thickness 15.5 mm were screwed and glued on the top of the LVL panel deck and to each other. The boards had carton liners with an approximate thickness 0.5 mm on both sides of the boards. The ceiling included two plasterboard layers of thickness 12.5 mm suspended from the rib slab with LVL battens. These plasterboards were installed with screws. The overhead boards of the LVL battens were of the same material than used for the LVL panel deck of the rib slab. The lower battens were sawn from similar LVL beams than used in the rib slab.

To absorb the air cavity within the structure, a 95 mm layer of glass wool was installed between the ribs. The floor covering installed onto the floor F11 was a 14 mm thick multilayer oak parquet installed on a 3 mm thick, soft underlayment.

ISI of the floors F11, F12, and F13 was measured in accordance with the standard ISO 10140-3 (2021) by Eurofins Expert Services Oy in an accredited building acoustics laboratory. The experiments were performed to achieve the *normalised impact sound pressure level* L_n in the 1/3-octave bands 50 to 5000 Hz. STM was applied as an impact sound source in the experiments at source positions S1–S5 as depicted in **Figure 5**. Additionally, the reverberation time of the receiving room was measured.

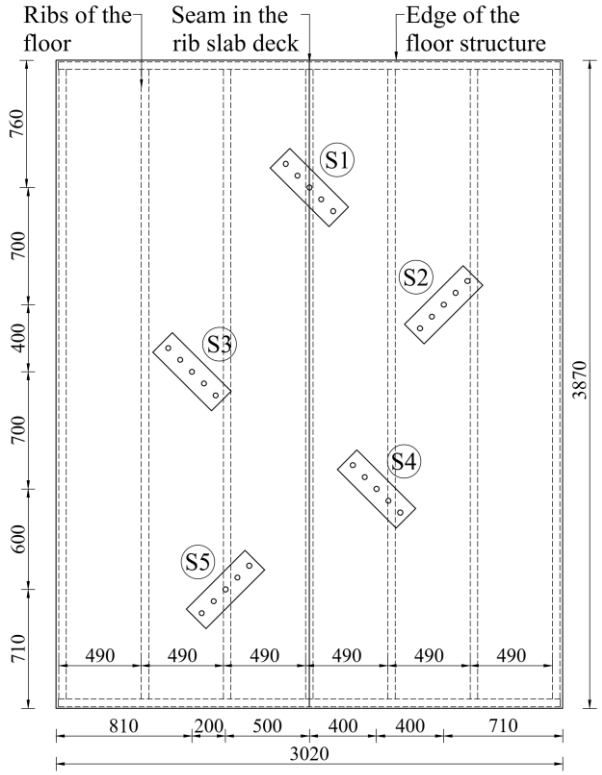

Figure 5. Source positions S1–S5 of the floors F11–F13. The presented dimensions (in millimetres) illustrate the area of the rib slab, spacing of the ribs, and the location of the centre hammer of the STM in different positions.

The floors were supported to the laboratory opening at their short ends by 12.5 mm thick elastomer strips installed between the rib slab and the supporting steel

frame of the opening (**Figure 6**, detail 1). Otherwise, the floors were kept mechanically unattached to the supporting frame apart from the sealing compounds and linen wool installed between the floors and the frame (**Figure 6**, detail 2). Due to the supporting structures of the laboratory opening, the suspended plasterboard ceiling had an area of 2.83 m x 3.68 m.

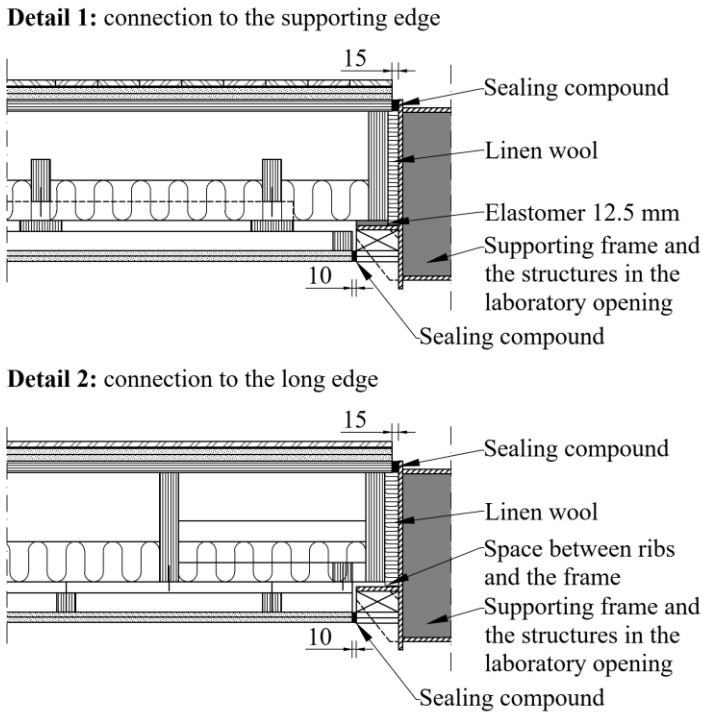

Figure 6. Details describing the floor supports. Dimensions have been presented in millimetres.

2.3 Simulations

The simulations presented in this thesis focused on three significant stages in predicting the ISI of timber floors. **Figure 7** illustrates the applied FEM simulation procedure enveloping these stages in a frequency domain analysis. The aim of the procedure is to be applicable to research and product development of timber floors, in addition to research purposes. In the first stage, the impact force excitation generated by the STM is determined via simulations. To study this issue on timber floors, **Publication II** presented a validated procedure to predict the excitation

applying the techniques used in the field of *computational impact mechanics* (see Section 2.3.1). As a validation data, results from the experiments (Section 2.2.1) were applied. The second stage focuses on the determination of the impact sound radiation from the floor driven by the previously derived impact force excitation. **Publication IV** studied applicability of *a FEM simulation procedure* to predict the normalised impact sound pressure level L_n of timber floors (see Section 2.3.2). As a validation, the results of the simulations were compared with the results of the ISI measurements (Section 2.2.2).

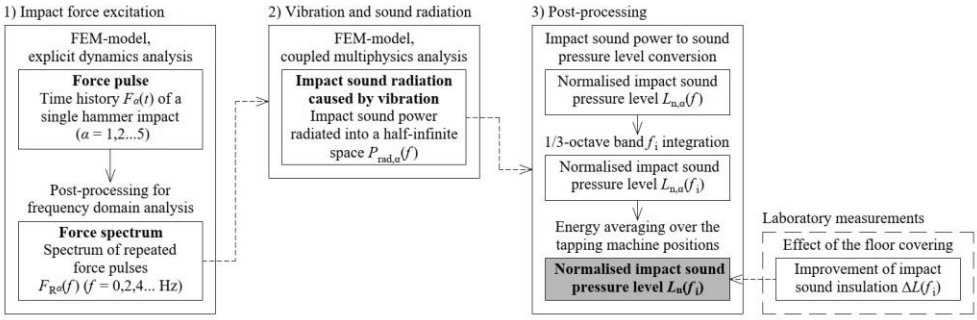

Figure 7. FEM procedure applied to determine the normalised impact sound pressure level L_n of the timber floors excited by the STM.

2.3.1 Simulations on impact force excitation of a timber slab

Impact force simulations were performed to digitally imitate the impact force experiments on the CLT slab (floor F1.0) (see **Figure 1**) at different source positions (see **Figure 2**). The simulation procedure involved determination of the impact force pulse generated by a hammer of STM and a post-processing method (**Figure 8**). The procedure aimed to define the point forces driving the CLT slab both in time and frequency domains. These again can be utilised in ISI prediction models. The impact force pulse was computed applying explicit time integration and FEM (briefly *explicit dynamics analysis*) since it enables describing the non-linear behaviour of the impact between the hammer and the floor (Rao *et al.*, 2017; Wu and Gu, 2012). One of the main features of the explicit dynamics analysis is that the system consists of lumped elements, which are calculated separately due to the diagonal mass matrix (Wu, 2006). This increases cost-efficiency of explicit dynamics analysis in the problem. The post-processing can be performed both for time and frequency domain

simulations to describe the continuous operation of the STM on the floor under study (see **Publication II**).

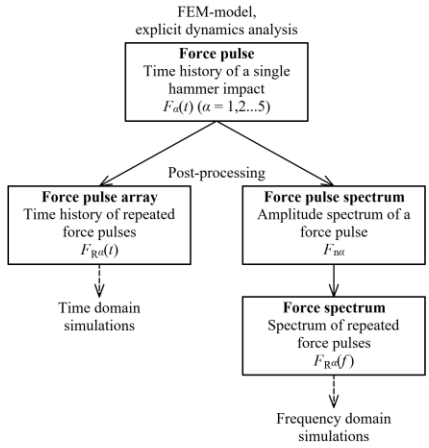

Figure 8. FEM procedure applied to determine the point force generated by the STM.

The explicit dynamics analyses were performed using a FEM program Ansys LS-DYNA (version: smp s R10.1.0 Revision: 123264). The simulations were used to describe the collision between the hammer and the slab. The contacts of the interacting bodies were modelled by using a penalty method (*LS-DYNA Theory Manual (r:8571)*, 2017). Both the static and the dynamic frictional coefficients between the contacting bodies were initially set to a value 0.5. The effect of the friction to the impact force was further studied in the sensitivity analysis.

The model of the STM hammer represented a simplification of the instrumented hammer used in the experiments (see Section 2.2.1). The impacting head of the hammer was modelled to closely represent the real hammer head in the measurements, but the body with the sensors and additional parts of the hammer was considered as a simplified cylinder. The height of the cylinder was adjusted so that the total masses of the modelled and experimental hammers were equal. The hammer was treated as an ideal impact source in the simulations and thus, all the possible imperfections of the STM (ISO 10140-5, 2021; Wittstock, 2012), such as the acceptable variations in the shape of the hammer head, repetition time of impacts or in initial velocity at impact, were neglected.

The material of the hammer was described as linear isotropic elastic (EN 1993-1-1, 2005; EN 1993-1-4, 2006) and the timber of the CLT slab was spruce mainly in the strength class C24 (EN 338, 2016; ETA-14/0349, 2014) (see **Publication II**). The boards of the CLT slab were described as a linear orthotropic elastic material

whose three principal axes were longitudinal (L), radial (R), and tangential (T) axes in cartesian coordinate system with respect to the fibre direction and annual rings of the timber (Forest Products Laboratory, 2010). It was assumed that glue layers between the structural timber layers were very thin, and the glue perfectly connects the layers. Thus, the layers were meshed together in the same part. To account for the gaps between the boards of the CLT, the outer lamellae of the slab were modelled as individual structural timber boards. In this configuration, no contacts were defined between the narrow sides of the lamellae.

Figure 9 shows the computational mesh and the geometry of the model near the impact area. In the initial state of the simulations, the tip of the hammer head was in contact with the slab in a single point and the hammer was just dropped to the slab.

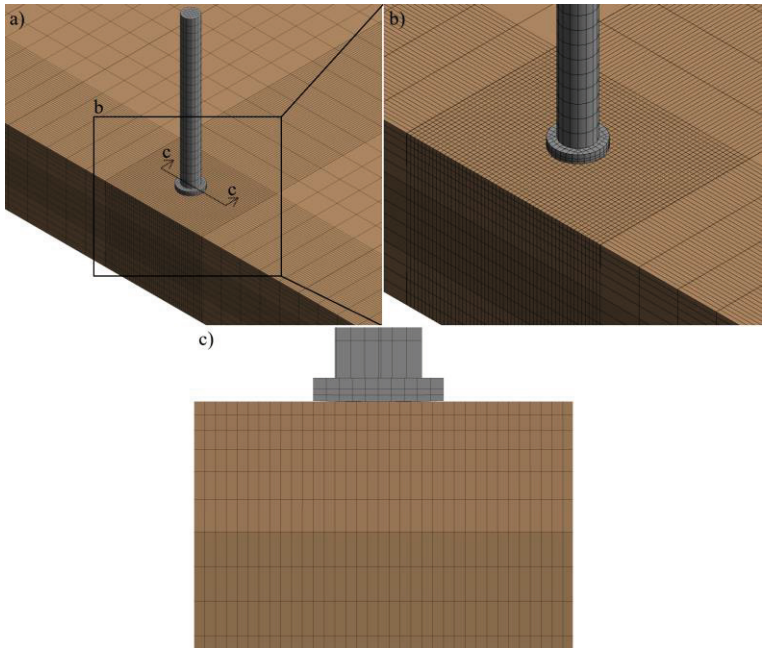

Figure 9. Computational mesh of the hammer and the CLT slab: a) hammer and impact area, b) magnification of a), c) cross section of impact area. The elements on the left side of the a) and b) have been hidden to present the mesh in the sectional direction.

In addition to the model validation, a sensitivity analysis was performed. In the analysis, different parameters such as the size, configuration, and material parameters of the CLT slab and the friction coefficients between the impacting bodies were varied. The analysis aimed to investigate how to model a CLT slab in sufficient detail and which parameters are most important to the results.

2.3.2 Simulations on impact sound insulation of timber floors

In the last part of the thesis, simulations were performed to digitally imitate the laboratory measurements of the normalised impact sound pressure levels L_n of the timber floors F11, F12, and F13 (see **Figure 4**). The simulations were conducted in the frequency range 50–1000 Hz following the procedure presented in **Figure 7**. Thus, in addition to the low-frequency range, the computations were carried out in an important frequency range often dimensioning the SNQs of timber apartment floors (Latvanne, 2015). In case of the full floor F11, the floor covering was taken into consideration at the post-processing stage.

The first stage of the simulations involved determination of the impact force excitation generated by the STM. Instead of using the impact force models presented in the research literature (Amiryarahmadi *et al.*, 2011; Brunskog and Hammer, 2003a; Coguenanff *et al.*, 2015; Rabold *et al.*, 2010; Wittstock, 2012), the force pulses generated by each of the STM hammer were simulated applying the procedures and the same tools as presented in **Publication II** (Section 2.3.1). The impact force pulses were converted into frequency domain to present continuous operation of the STM. As a result, complex 2 Hz line spectra presenting the five individual point forces driving the floor were derived for each studied source position S1–S5 (see **Figure 5**). To validate the computational model predicting the impact force excitation, the results were compared with the measurement results presented in **Publication I** for the floors F6.0 and F9.0 due to their close resemblance with the floors F13 and F12, respectively.

At the second stage, FEM simulations were performed to compute the impact sound radiation of the floors excited by the predetermined point. The computations were performed in frequency domain as a linear system to provide accurate results with less computational effort than with time domain simulations (Negreira and Bard, 2016). The simulations were performed as a fully coupled harmonic multiphysics analysis by using a program COMSOL Multiphysics 6.1 with a 2 Hz frequency spacing corresponding to the previously determined complex excitation line spectra. The radiated sound power of the floor was solved directly with the FEM model by applying an acoustical half-infinite receiving fluid domain below the floor. The fully absorptive boundary conditions were set to the faces of the domain excluding the radiating plane by applying perfectly matched layers (PML) (COMSOL, 2022). This approach slightly differs from the methods shown previously in the research literature (Hopkins *et al.*, 2016; Linderholt and Olsson, 2017; Olsson and Linderholt, 2021).

At the post-processing stage, the radiated sound power was converted to present the normalised impact sound pressure level L_n in an ideal receiving room. The narrow-band results were converted to present the L_n in a diffuse sound field, and the results were integrated to present the 1/3-octave band results. The last part involved energy averaging over the STM positions. In case of the floor F11, the ΔL of the floor covering on the ISI was derived from the laboratory measurements and added to the simulation result.

To describe the behaviour of the materials in the floors F11–F13, mainly data provided by the product manufacturers was applied in the simulations (see **Publication IV**). Since every property was not given by the manufacturers, the input data was supplemented with information based on the values reported in the research literature (Cremer *et al.*, 2005; Hopkins, 2007; Niskanen *et al.*, 2011). This included the frequency-independent loss factors applied to describe damping in structural materials. The LVL products as well as the carton layer of the floor plasterboards was modelled as linear orthotropic elastic materials. However, the information from the carton layers was applied only at the first stage when determining the impact force excitation generated by the STM on the floor F12. Other structural materials were considered as linear isotropic elastic, and the mineral wool was taken into account with an equivalent fluid model (Allard and Champoux, 1992; COMSOL, 2022). **Figure 10** illustrates the geometry of the models the floors F12 and F13 together with their computational meshes at 1000 Hz.

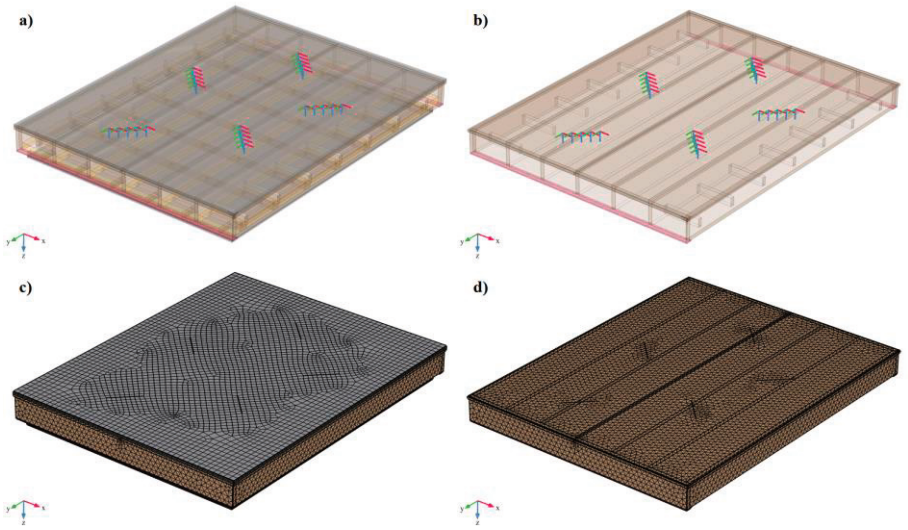

Figure 10. Geometry and mesh (at 1000 Hz) of the FEM models for the floors F12 (a, c) and F13 (b, d). The airspaces and PMLs have been hidden to emphasise the features of the floors.

The models of the floors F12 and F13 were constructed two different ways (see **Publication IV**). The first models were created to represent *ideal* boundary conditions and constraints. This approach is comparable to a task where idealisation is needed since the exact conditions of the structures are not known. Secondly, the models were modified to represent the *in-situ* boundary conditions and constraints of the laboratory experiments. This way the effect of boundary conditions and smaller details on the results could be analysed.

3 RESULTS

3.1 Impact force excitation generated by the STM on the timber floors

3.1.1 Experimental results

An example of the measurement results for the impact force is illustrated in **Figure 11** in case of the CLT slab (floor F1.0). The figure presents the time history of the force driving the floor for the whole measurement period, the individual force pulses caused by the hammer, and the magnitudes of the amplitude spectra F_n for the individual force periods. The five columns of the figure represent results for each source position S1–S5. The number of full impacts ranged from 60 to 61 during the measurement period of different floors. The variation of the impacts on different source positions can be seen both from the time histories and from the impact force spectra. However, the variation was best evident in the individual force pulses, where the shape of the pulses was prominent, but the spectra indicated the variation of the excitation as well. For a detailed description of the results, see **Publication I**.

Figure 12 presents the arithmetic averages of all the magnitudes of the amplitude spectra F_n of the individual force periods for all the floors at the source position S1. The low-frequency variation of the results can be seen from the magnified results. For example, the results show how different floor coverings affect the impact force spectra: they seemed to lower the force input into the floors but especially in mid- and high frequencies but their effect on the force was prominent also in the low-frequency range. Moreover, it was evident that the excitation spectrum was not constant over the bare timber floors.

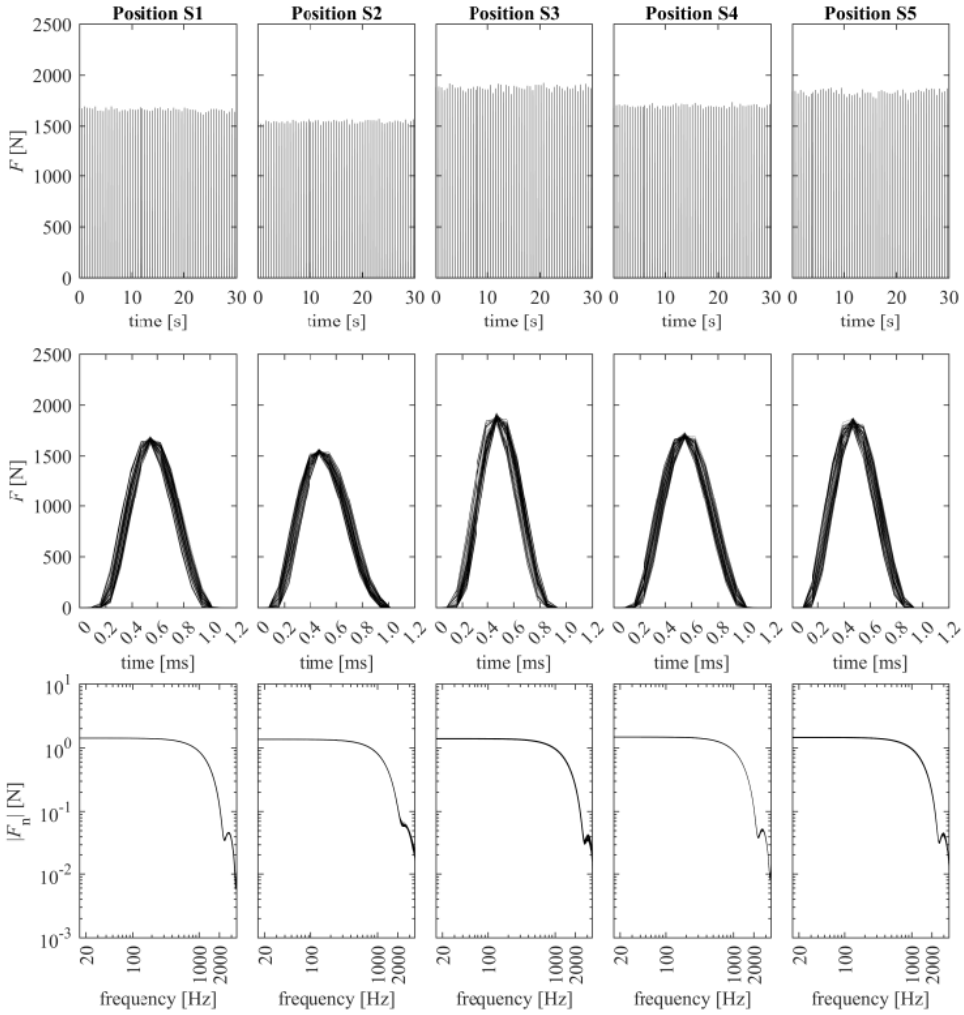

Figure 11. Measurement results of the floor F1.0. Results at the source positions S1–S5 have been depicted in three rows from top to bottom: the time histories of the force driving the floor, the individual force pulses, and the magnitudes of the amplitude spectra F_n of the force.

Figure 13 shows the average impulses I for all the floors at the source positions S1–S5. The scale of the figure was set to represent the extreme boundaries corresponding to the theoretical limits for ideal inelastic and ideal elastic impulses (Brunskog and Hammer, 2003a). The geometrical mean value of the impulse ($\sqrt{2}mv_0 \approx 0.626$ Ns) has been illustrated in the figure with dotted line. The figure shows that the measured impulses depended on the floor structure and the results ranged from nearly inelastic to well over geometrical mean value. Additionally, spatial variation can be seen from the figure.

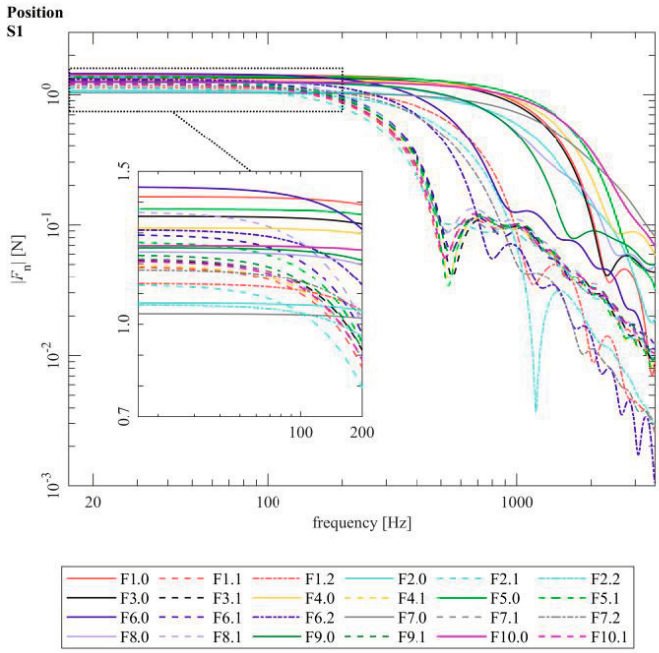

Figure 12. Averages of the magnitudes of the two-sided amplitude spectra F_n of the force at the source position S1. The solid lines illustrate the result on a floor without any floor covering, the dashed and dash-dotted lines present the results when the floor covering was the C1, and the C2, respectively.

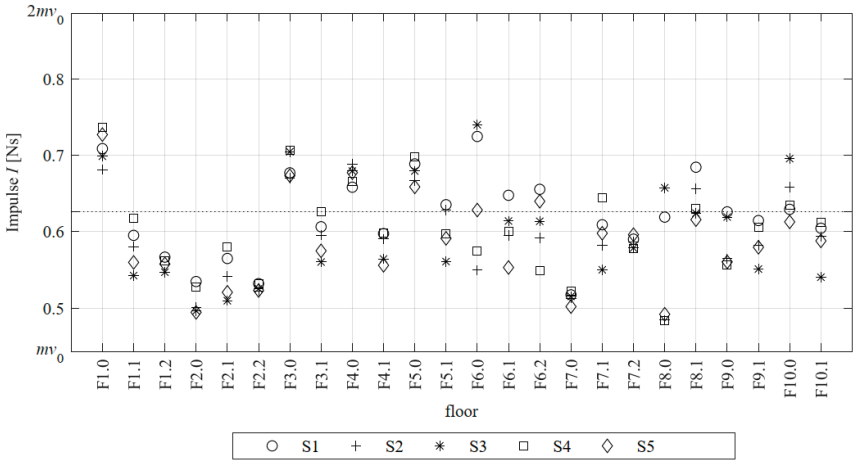

Figure 13. Average impulses I at the positions S1–S5. The extreme boundaries represent the theoretical limits for I from 0.443 Ns (mv_0) to 0.886 Ns ($2mv_0$) corresponding to the ideal inelastic and elastic collisions, respectively. The geometrical mean value of the impulse 0.626 Ns ($\sqrt{2}mv_0$) has been shown with the dotted line.

3.1.2 Simulation results

Figure 14 depicts the comparison of the simulated and measured force pulses on the CLT slab (floor F1.0) in time and frequency domains. The figure shows the measured and the simulated contact force pulses and magnitudes of their amplitude spectra at the source positions S1–S5. Note that the measured force pulses were centred according to the peak values of the simulation results. Hence the nonzero values before $t = 0$ ms. The peak value of the force pulse F_{peak}, the low-frequency force F_{lf}, the mechanical impulse I, and the length of the pulse T_{pulse} have been presented in **Table 1** for the measured and simulated force pulses.

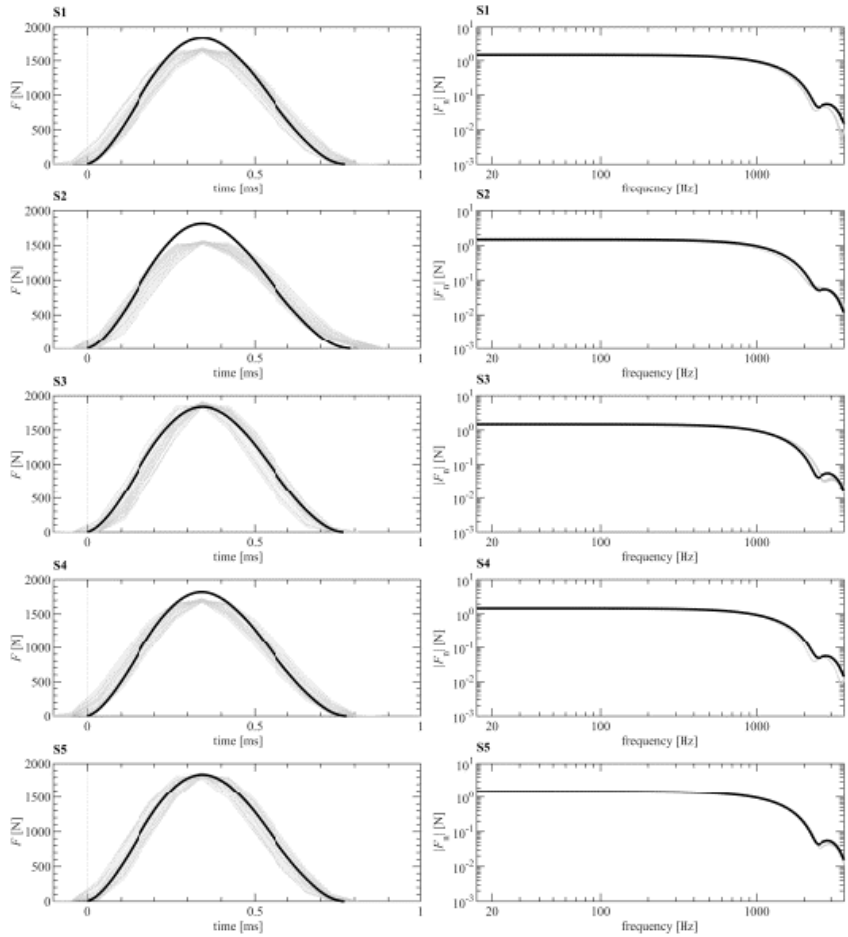

Figure 14. Simulated force pulses $F(t)$ and magnitudes for their two-sided amplitude spectra F_n at the source positions S1–S5 (black lines) and the corresponding measurement results from the experiments (thin grey lines). Note the overlapping of the results.

Table 1. Scalar values determined based on the measured and simulated force pulses. Measured values represent the average results of all the measured pulses.

Source position	Measured (M)/ Simulated (S)	F_{peak} [N]	F_{lf} [N]	I [Ns]	T_{pulse} [ms]
S1	M	1662.5	1.42	0.71	0.99
	S	1833.4	1.48	0.74	0.77
S2	M	1546.3	1.36	0.68	1.02
	S	1813.3	1.47	0.74	0.79
S3	M	1878.5	1.40	0.70	0.91
	S	1839.3	1.48	0.74	0.77
S4	M	1699.4	1.47	0.74	1.01
	S	1822.2	1.48	0.74	0.78
S5	M	1832.8	1.45	0.73	0.94
	S	1838.2	1.48	0.74	0.77

Figure 14 and **Table 1** indicated reasonable equivalency of the measurement and simulation results. Because of this, the simulation model was regarded valid. However, it is noticeable that the computational model led to minor spatial variation in comparison with the measurement results. The simulation seemed to closely predict the measured peak value of the force F_{peak} at the source positions S3, and S5. Additionally, the low-frequency force F_{lf}, and the mechanical impulse I of the simulation results were near equivalent with the measurement result at the source position S4. Minor discrepancies between the measurement and simulation results at the source positions S1, and S2 were prominent. The simulations produced results near the measured maximum both in time and frequency domains. As can be seen, there was little spatial variation in the simulation results whereas the measured results varied greater (see **Table 1**).

To illustrate the effect of the local properties to the impact force pulse, **Figure 15** presents the deformation process of the CLT slab under the hammer during the impact at the source positions S1, S2, and S3. The positions lied locally in different locations. The results show that the maximum deformation occurred straight under the tip of the hammer head when the impact force pulse was near its peak value (see **Figure 14**). Furthermore, only a minor part of the slab was deformed during the impact, which suggests that for a short impact the global behaviour of the slab is not of importance from the point of view of the single impact force pulse. Additionally,

the non-linear interaction between the hammer and the slab can be seen from **Figure 15** since the contact surface between the hammer and the slab is a function of time.

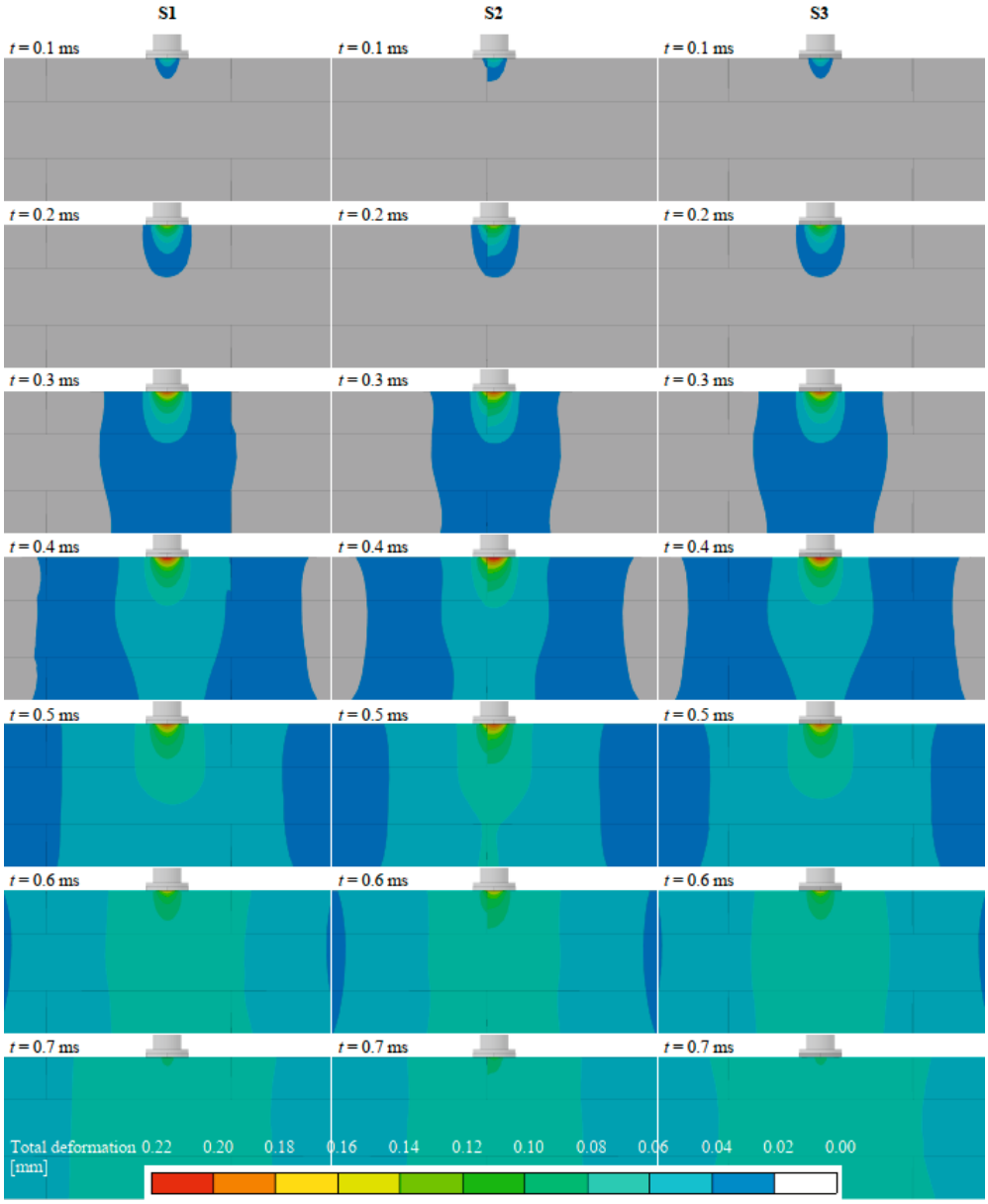

Figure 15. Total elastic deformation process of the floor F1.0 during the collision of the hammer and the floor at the source positions S1, S2, and S3.

A sensitivity analysis was performed to further study the effect of the local and global properties to the impact force and to find out reasons causing the differences between the measurement results at different source positions. According to the analysis, it was evident that the global properties of the slab did not affect the simulation results of a single impact force pulse (see **Publication II**). For example, ignoring the gaps between the CLT boards and decreasing the size of the slab did not significantly decrease the accuracy of the simulations. Additionally, the model was found to be insensitive to the contact friction (see **Publication II**). Because of these issues, the sensitivity analysis was continued with a slab having size 1000 mm x 1000 mm and the friction coefficient was kept the same as in the validated model.

Because of the abovementioned observations, the effect of local properties on the results was studied with three additional analyses (**Figure 16**). First, the local effects in the sectional direction of the CLT slab were studied (**Figure 16a**) by varying the strength class of the centre lamella of the slab from C24 to C16 and C30 while keeping the outer lamellae as C24, as well as by introducing an imaginary material X10 with tenfold elastic and shear moduli to different slab layers. Secondly, the effect of the material properties on the impact force was studied by varying all the material parameters a single value at a time (**Figure 16b**). An exception of this were the Poisson's ratios which were varied simultaneously. The range of the varied material parameters corresponded to the change in the strength class from C16 to C30. Third, since the CLT slab in the measurements was mainly made from heartwood, the effect of heartwood and sapwood (**Figure 16c**) on the impact force was studied (**Figure 16d**). This was conducted by solving the impact force presenting the material of the upmost lamella in different locally rotated cartesian coordinate systems A–D.

According to the results of the analysis, the strength class of the centre lamella had a minor effect on the impact force, but drastic changes in the stiffness properties can affect the force majorly especially if the properties of the upper lamellae change (c.f. tree knots) (see **Figure 16a**). Based on the analysis, the modulus of elasticity E_R, the shear modulus G_{LR}, and the density were the most important material properties for the impact force (see **Figure 16b**). Furthermore, the results indicate that the spatial differences in the measurement results can be explained with the presence of heartwood in the CLT slab (see **Figure 16d**). Hence, if the annual rings of wood are evident and the specimen is well known, the use of rotated cartesian or cylindrical coordinate system is justified for improving the computational accuracy. Modelling timber boards as continuous layers, however, produced results on the safe side, thus offering an engineering approach for design stage analyses.

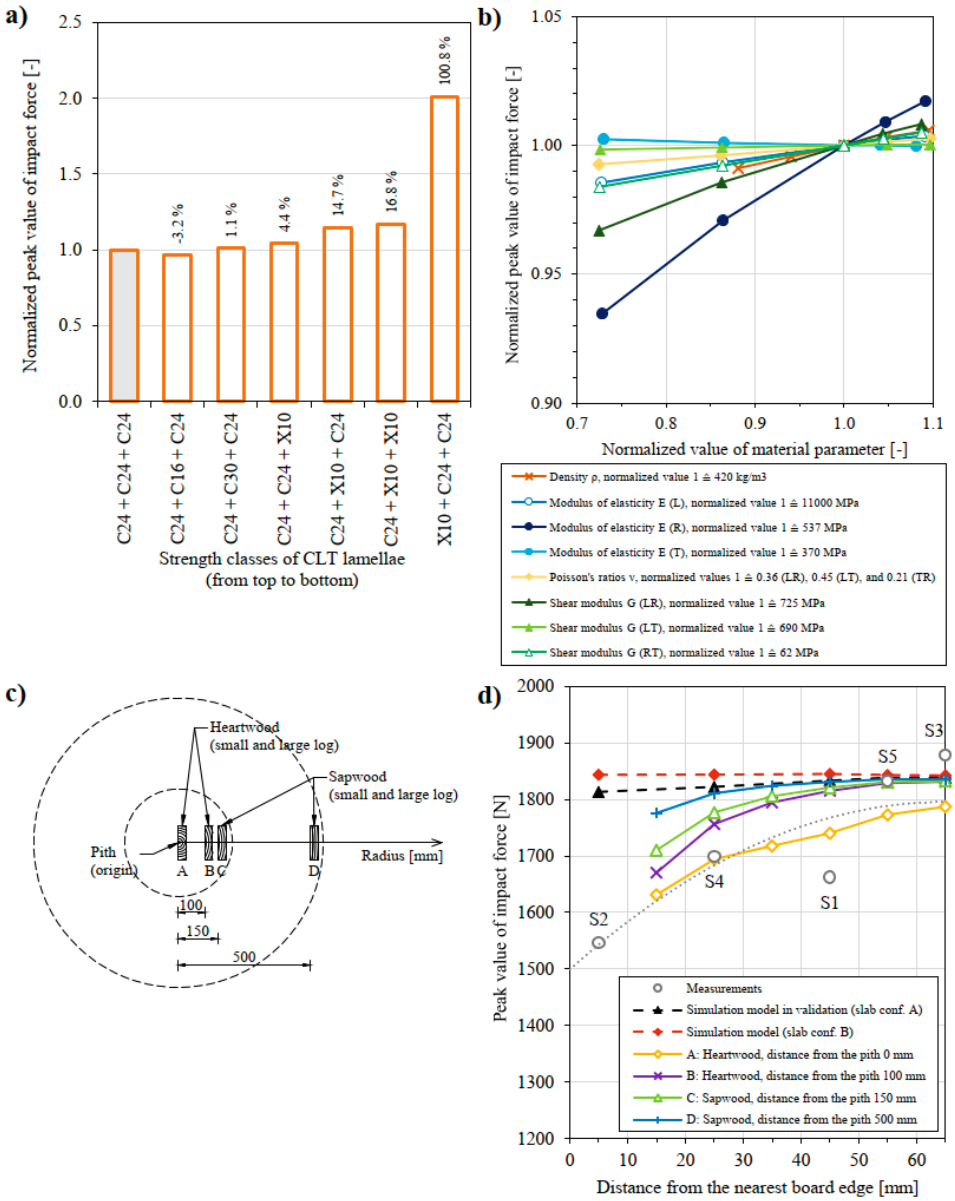

Figure 16. Sensitivity of the simulated (peak) impact force to the local properties of the CLT slab. a) sensitivity of the lamellae's strength class on the force (normalised to the result in grey colour), b) sensitivity of material parameters of the CLT slab on the force, c) locally rotated coordinate systems to study the effect of the heart wood and sapwood on the force, d) effect of the heartwood and sapwood on the force: comparison of the measurement and simulation results. Average measurement results at different source positions have been indicated with labels S1–S5 and with a polynomial trend line of order two (dotted (:) grey line).

To use the simulated force pulses as inputs for point forces in time or frequency domain ISI simulations, the results must be post-processed to describe the continuous operation of the STM (see **Publication II**). To demonstrate this procedure (see **Figure 8**), the validated model was applied to compute the force pulse for each of the five hammers of the STM on the floor F1.0 at the source position S3. The post-processed force results have been depicted in **Figure 17** both in time and frequency domains. The figure shows the force pulse arrays for the two first pulses in time domain, and the single-sided force spectrum for individual hammers at the source position. The time shift of the force pulses causes phase shift to the force spectra which can be seen as fluctuation of real and imaginary parts of the force spectra.

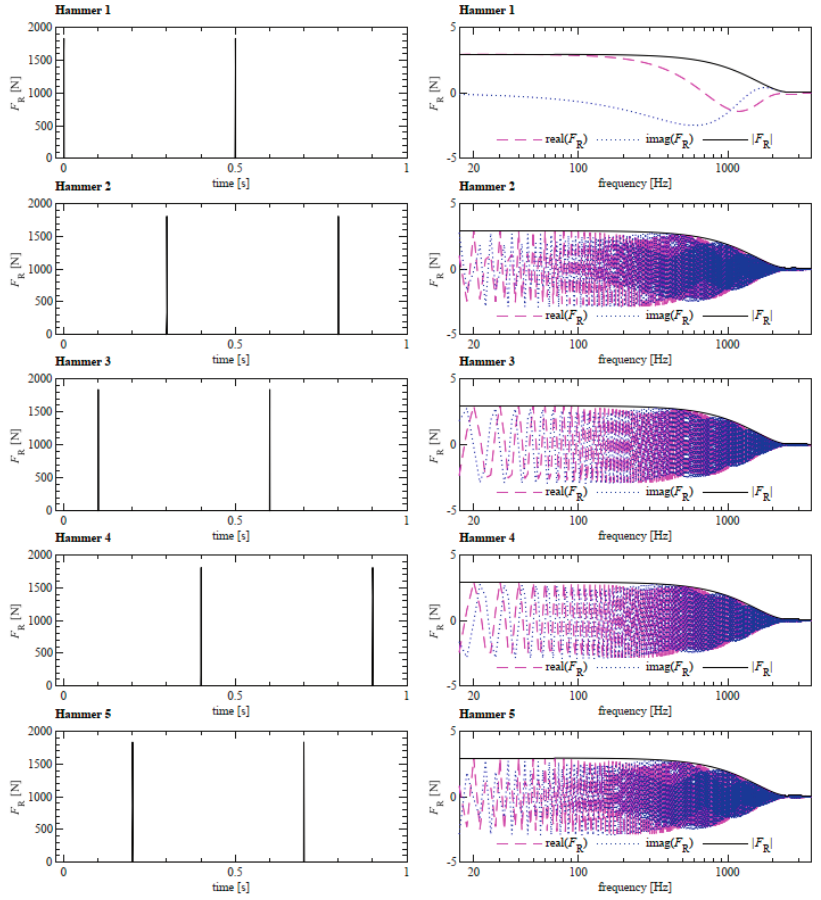

Figure 17. Post-processed impact force for time and frequency domain simulations: the magnitude (solid black line), real part (dashed (--) magenta line), and imaginary part (dotted (:) blue line) of the single-sided force spectra.

3.2 Vibration level reduction of the floor coverings

The average measurement results for the vibration level reduction ΔL_a by the floor coverings C1 and C2 on the studied timber slabs have been illustrated in **Figure 18** for the CLT and rib slabs. The vibration level reductions were derived from the acceleration levels of the timber floors with and without the floor coverings. Thus, the first two characters denoted in the figure legend indicate the bare timber slab where the comparison has been made. For example, the curve F1.1 illustrates the ΔL_a for the floor covering C1 (the multilayer parquet on the soft underlayment) on the bare CLT slab (floor F1.0).

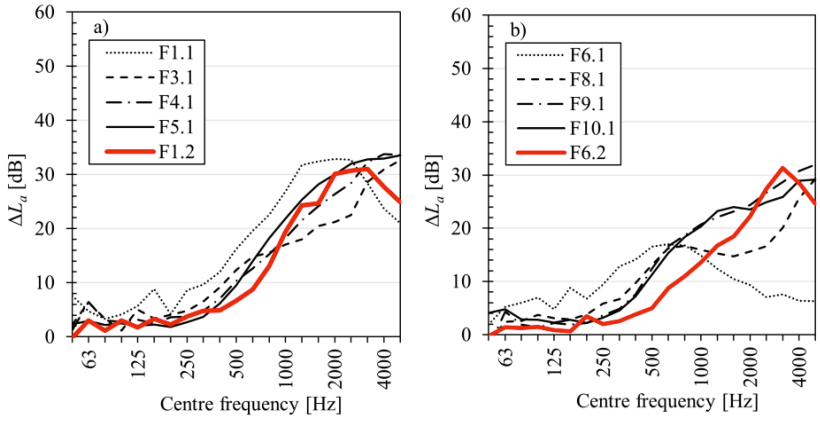

Figure 18. Measurement results of ΔL_a on a) CLT slabs, and on b) rib slabs.

The results presented by **Figure 18** show that the ΔL_a was positive almost in the entire frequency range for both floor coverings when their performance was measured on the timber slabs. In the low-frequency range up to 250 Hz band, the values were rather constant apart from some individual peaks. The values of ΔL_a in this range varied between 1 and 9 dB. In the mid-frequency range above the 250 Hz band, the ΔL_a began to increase until at higher frequencies the values decreased or at least remained at a constant level compared to the latter.

The measured ΔL_a levels of the floor coverings depended on the type of the timber slabs (see **Figure 18**). The results for the floor covering C1 showed high dependency between the ΔL_a and the bare timber slab. For the floor covering C2, the differences of the ΔL_a results F1.2 and F6.2 were minor but prominent in the frequency range between 800–2500 Hz. It can also be noted that the ΔL_a levels for the floor coverings C1 and C2 were different when measured on the same timber slab. When comparing the results F1.1 to F1.2 and F6.1 to F6.2, it can be seen that

the floor covering C1 produced larger ΔL_a levels than C2 in the low- and mid-frequency ranges. Adding the plasterboards to the load-bearing slabs gradually evened out the differences between the floors on the same load-bearing timber slab. Furthermore, the additional mass reduced the ΔL_a in low- and mid-frequencies and increased it at high frequencies.

The ΔL_a results for the concrete mock-up slab are shown in **Figure 19** for both the floor coverings. The differences between ΔL_a on the concrete mock-up slab and on the timber slabs, i.e. $\Delta L_{a,conc} - \Delta L_{a,wood}$, have been illustrated by **Figure 20**.

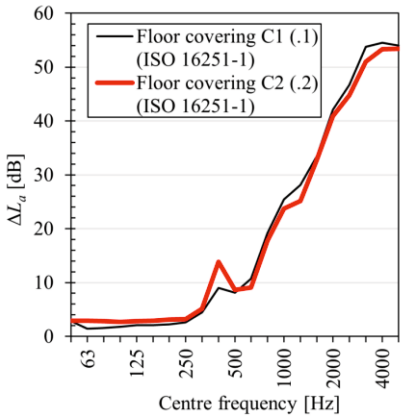

Figure 19. Measurement results of ΔL_a of the floor coverings C1 and C2 on the concrete mock-up slab.

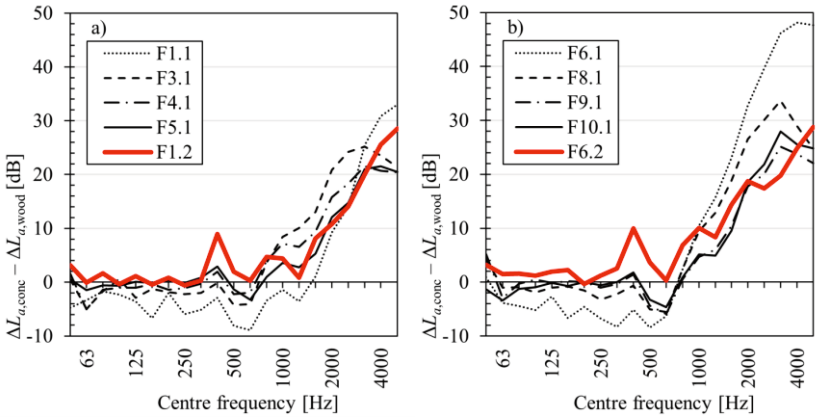

Figure 20. The difference between the measurement results on the concrete mock-up ($\Delta L_{a,conc}$) and timber slabs ($\Delta L_{a,wood}$). The figure a) compares the results on the concrete mock-up and the CLT slabs and b) compares the results on the concrete mock-up and the rib slabs.

The ΔL_a results for the two floor coverings on the concrete mock-up slab seemed to be close to each other (see **Figure 19**), which was not the case for the timber slabs (see **Figure 18**). In the mid-frequencies, resonance frequencies were evident for both floor coverings probably due to the interaction between the hammers and the soft cushion vinyl, and due to the floating floor constituted by the multilayer parquet and the soft underlayment. At the higher frequencies, the values increased until the highest studied frequency bands.

The differences between the measurement results of ΔL_a on the concrete mock-up slabs and the timber slabs were major especially in the high frequencies (see **Figure 20**). A significant characteristic of the differences was that in the low-frequency range, the differences were rather constant and in the mid-frequencies a turning point was prominent after which the differences began to increase. In the low frequencies, the ΔL_a on timber slabs was larger than on the concrete mock-up for the floor covering C1, especially in case of the lightest floors. The turning point frequency seemed to vary slightly depending on the floor covering and on the timber slab. Moreover, differences between the measurement results of ΔL_a on the concrete mock-up slabs and the timber slabs for the floor covering C1 diminished when the plasterboards were added to the timber floors.

3.3 Simulation results for impact sound insulation of the timber floors

Figure 21 illustrates the comparison of the simulated and measured impact force pulses in time and frequency domains. According to these validation results, the applied procedure closely predicted the measured impact force pulse on the floor F6.0 at the source position S3, but at S4 (see **Publication I**) the simulation underestimated the T_{pulse} and I and overestimated the F_{peak}. These issues were also seen from the frequency domain results where the simulated and measured force spectra were nearly equivalent in the low frequencies, but prominent discrepancies occurred around mid-frequencies. In case of the floor F9.0, similarity of the results was rather good although the simulations slightly overestimated the F_{peak} and I. This again can be seen as a resemblance of the results in the frequency domain.

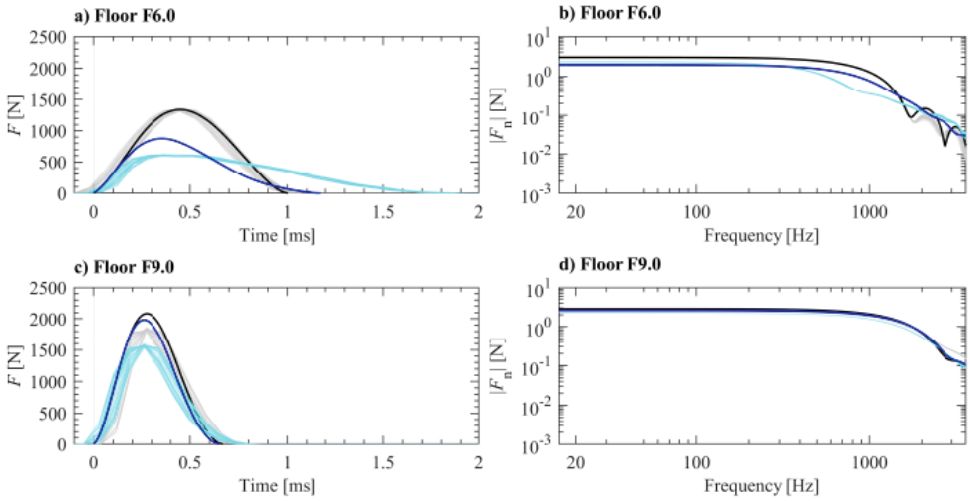

Figure 21. Simulated impact force pulses $F(t)$ and magnitudes of their single-sided amplitude spectra F_n (black (S3) and blue (S4) lines) and the corresponding measurement results from the experiments (thin grey (S3) and light blue (S4) lines).

Even though some discrepancies between simulation and measurement results were observed, the impact force simulation model was regarded as valid to be applied in predicting the impact force excitations of the floors F12 and F13. Probable causes for the deviation between the simulation and measurement results of the impact force are the local inhomogeneities in the measured rib slab and differences between the real and simulated material properties. However, the best available information from the floors led to acceptable equivalency between the impact force results. The validation models were modified to correspond with the timber slabs of the floors F12 and F13 and applied to compute their impact force excitations in frequency domain following the post-processing procedure (see **Figure 8**). In the ISI simulations, the magnitude and phase spectra of the repeated force pulses were applied to excite the floors in the frequency domain analyses (see **Publication IV**).

Simulation results for the normalised impact sound pressure level L_n have been presented for the floors F12 and F13 in **Figure 22**. The figure presents the spatially averaged narrow-band results (2 Hz frequency resolution) in a frequency range covering the 1/3-octave bands from 50 to 1000 Hz, and the effect of the source positions on the L_n as a range of results. It is evident that the excitation generated by the STM induces large peaks to L_n on multiples of 10 Hz. This occurs due to the excitation model applied to describe the continuous operation of the apparatus but the behaviour also corresponds with the findings presented in the literature for real STMs (Wittstock, 2012).

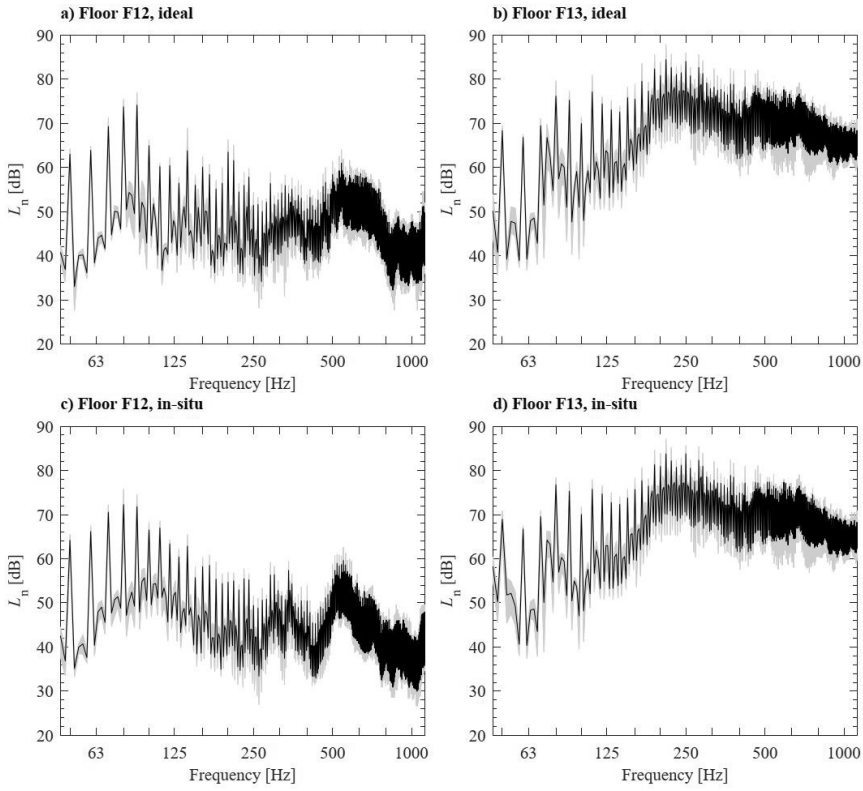

Figure 22. Simulated narrow-band L_n levels for the floors F12 (a, c) and F13 (b, d). The black lines show the spatially averaged results, and the grey areas depict the range of results caused by different source positions.

Laboratory measurement results for the L_n have been illustrated in **Figure 23** for the floors F11–F13 and for the ΔL of the floor covering. The results represent the energy averaged levels based on all the source positions in the frequency range 50–5000 Hz. Additionally, the figure presents the results as SNQs $L_{n,w}$, C_I, and $C_{I,50\text{-}2500}$ calculated according to the standard ISO 717-2 (2020). $L_{n,w}$, $L_{n,w} + C_I$, and $L_{n,w} + C_{I,50–2500}$ for the floor F1 were fully determined based on the results below 200 Hz. In case of the floor F2, the SNQs $L_{n,w} + C_I$, and $L_{n,w} + C_{I,50–2500}$ were determined by the results below 1000 Hz. Thus, the chosen frequency range covering the 1/3-octave bands 50–1000 Hz can be regarded justified for the L_n simulations.

1/3-octave band integrated measurement and simulation results for the floor construction stages F11–F13 were compared in **Figure 24** in the frequency range 50–1000 Hz. The similar correspondence with the simulation and measurement results of the floors F11 and F12 occurred due to the inclusion of the floor covering from the measurement results (see **Figure 23**).

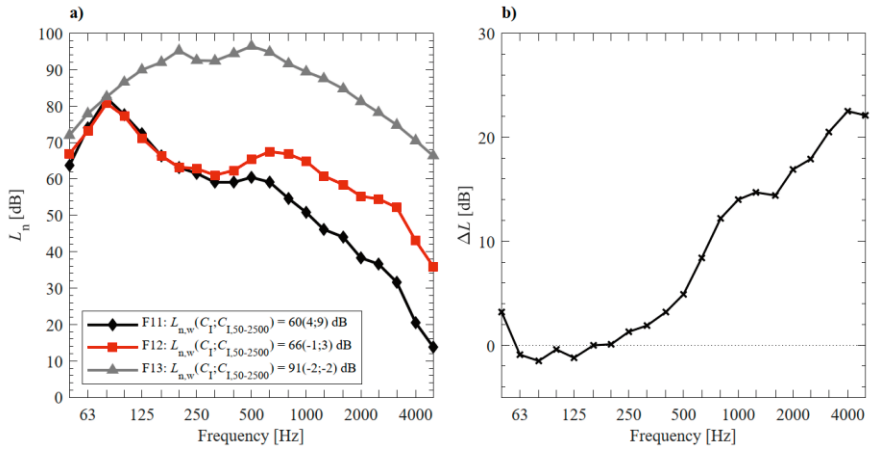

Figure 23. Measurement results for the L_n and the SNQs for the studied floors F11–F13 (a) and the ΔL of the floor covering (b).

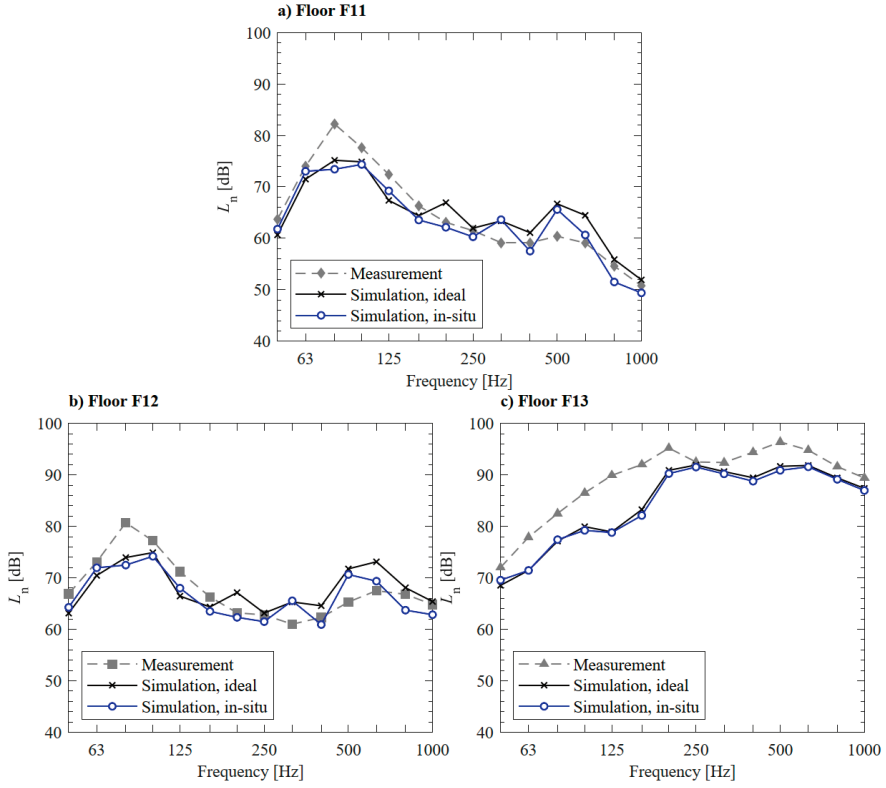

Figure 24. Simulated and measured 1/3-octave band integrated normalised impact sound pressure levels L_n for the floors F11–F13.

4 DISCUSSION

4.1 Impact force excitation of timber floors

Results from the impact force experiments indicated that the impact force excitation generated by the STM depends strongly on the type of the timber floor (see **Figure 12**). When comparing the results for the force spectra with the spectra measured on concrete and steel structures (Gudmundsson, 1984; Jeon *et al.*, 2006; Rabold *et al.*, 2010), it is obvious that excitation caused by the apparatus is different on the timber floors. The variation of the results for the force spectra on different timber floors was evident in the whole frequency range of interest, but the differences were major above 500 Hz. In this frequency range, also the effect of the floor coverings was prominent. At frequencies below 100 Hz, the values of the magnitude of the force spectra stayed rather constant and the differences between the floors were minor in comparison with the high-frequency range results. However, the variation corresponded to the level difference of over 3 dB of the force input in the low-frequency range. The variation of the results in the low-frequency range was evident from the determined impulses I (see **Figure 13**). On the basis of these results, the geometrical mean value of the impulse does not represent the actual value of the impulse on timber floors in general.

Based on the experimental results, two important practical implications could be drawn. First, according to the results the model describing the impact force excitation generated by the STM should include the ability to predict the value of the impulse on timber floors. This means that the model should account for the energy dissipation depending on the floor. Secondly, it was observed that the process of excitation with the STM was not transient for the structures studied (see, e.g., **Figure 11**, and **Publication I**). Thus, minor time dependency of the impact force was detected after the operation of the STM was started, and the vibration of the measured timber floors did not seem to influence the excitation force. This again suggests that modelling a single impact would be sufficient in describing the full excitation generated by the STM.

Considering the abovementioned conclusions, a simulation procedure was proposed to model the impact force excitation using explicit dynamics analysis (see

Publication II). The model validation showed that the procedure is applicable in predicting the impact force generated by the STM on a timber slab (see **Figure 14**, and **Table 1**) when the calculation mesh is appropriate, and the material parameters represent the behaviour of the slab. These are especially important issues for the analysis due to the deterministic nature of the applied prediction method. Comparison of the simulation and experimental results for the CLT slab indicated that in time domain, the measured force pulses varied more than the simulated ones with respect to the source position. However, the finite element model seemed to closely predict the maximum force pulse regardless. Discrepancies between the measurement results of different source positions were partly explained with the different distances from the closest board edges. The differences between the simulated and measured values were, however, minor in the low-frequency range.

Reasons explaining the differences between the measurement and simulation results, and the minor spatial variation of the simulation results were found in the sensitivity analysis (see **Figure 16**). The findings of the sensitivity analysis indicated that the local properties of the CLT slab close to the impacted area are important to the impact force. In addition, it was found that the impact force was insensitive to the global properties of the slab. These findings support modelling only a part of the slab around the impact area to still compute the impact force pulse accurately. This occurs because the stress waves caused by the impact to the slab cannot reach the impact area from the boundaries during the time of contact (see **Figure 15**).

4.2 Floor coverings on timber floors

Possible reasons for the discrepancies between the ΔL_a results on different slabs were found from the behaviour of the slabs and floor coverings (see **Publication III**). The main reason for the different results for the studied floor coverings on different slabs was the different impact force levels generated by the STM on the bare slabs (see **Figure 12**, and **Publication I**). Secondly, the behaviour of the ΔL_a of the parquet on the underlayment was explained by the floating structure composed by the floor covering. In the low-frequency range, the relative increase of mass brought by the parquet to the slab increased the ΔL_a levels on timber slabs in comparison with the concrete mock-up slab. In high frequencies it was noted that it is possible that the parquet acts resonantly, thus reducing its ability to improve ISI. Adding plasterboards to the floors seemed to diminish the discrepancies. Third, in

case of the cushion vinyl, it is possible that the results were affected by the damping effects of the floor covering.

According to the results in **Figures 18–20** and to the literature (Alonso *et al.*, 2019; Nowotny and Nurzyński, 2020; Pereira *et al.*, 2016; Schmitz, 2000; Scholl and Maysenhölder, 1999; Warnock, 2000), it is obvious that the ΔL measured on concrete slabs do not fully correspond to the ΔL gained on timber slabs in the whole frequency range of interest. Using the ΔL measured on concrete slabs instead of the ΔL measured on timber slabs could lead to mispredictions when designing the ISI of timber floors. This should raise an interest to measure the floor covering products also on the timber slabs. In any case, this would increase the applicability of the products for use in the timber construction. However, the results also illustrate that there are differences between timber slabs. Thus, it is important to measure the floor covering products on similar types of slabs where the products are expected to be used.

4.3 Impact sound insulation simulations of timber floors

The correspondence between the simulation and measurement results for the normalised impact sound pressure levels L_n was the best with the floors F11 and F12 (see **Figure 24**). In case of these floors, the low-frequency simulation results were lower than the measurement results. The most prominent differences between the simulation and measurement results, where the simulation results deviated from the measurement results around 5 to 9 dB, occurred around 80 Hz and 500 Hz bands. In case of the floor F3, the simulation results were considerably lower than the measured ones in the entire frequency range 50–1000 Hz. The simulations underestimated the measured L_n by 1 to 11 dB.

Although the simulated frequency range 50–1000 Hz did not cover all the frequencies needed in the standardised SNQ rating, the differences between the measurement and simulation results for the floors F11 and F12 correspond to 0–2 dB differences in $L_{n,w}$ and $L_{n,w} + C_I$, and 0–4 dB differences in $L_{n,w} + C_{I,50-2500}$ if values beyond the studied frequency range are omitted. The larger scale for the latter is caused by the differences seen in the 80 Hz frequency band for the floors F11 and F12. In case of the floor F13, the corresponding differences were 4–5 dB for all the abovementioned SNQs. For the sake of comparison, the standard deviation of the differences between single and mean SNQs simulated with Monte Carlo method on concrete floors has been found to be between 0.1–0.6 dB and 0.1–0.8 dB for the

SNQs $L'_{n,w}$ and $L'_{n,w} + C_I$, respectively (Kylliäinen, 2014), and the standard ISO 12999-1 (2020) reports the uncertainty of the respective SNQs as 1.5 dB.

The differences between the simulation and measurement results indicated for probable reasons for the discrepancies. The two evident peaks in the mid-frequency simulation results for the floor F13 appeared to be shifted to adjacent frequency bands in comparison with the measurement (see **Figure 24c**). This implies that the orthotropic properties of the floor in the simulations do not fully correspond to those of the measured floor. Moreover, since the L_n levels were underestimated by the simulations, it is possible that the mass or the damping of the floor were overestimated in the models. The differences were also probably affected by underestimated impact force spectra predicted for the STM positions between the beams (see **Figure 21**). Additionally, it must be noted that the applied simulation procedure does not take into account the mode coupling between the floor and the receiving room, which could have improved the correspondence between measurement and simulation results (Wang et al., 2020). These are probable causes leading to differences between the prediction and measurement results of the floors F11 and F12, as well.

The abovementioned issues highlight the common problem with all the deterministic models, including FEM, when the material properties are highly variable. The computations were performed by using information from the materials presenting the best available data at the design stage of a building. However, it is likely that the differences between simulation and measurement results were caused by uncertain material properties, although modelling inaccuracies can also occur.

Since the ideal and in-situ conditions resulted in rather similar L_n levels for the floor F13, it seems that the result for the rib slab was quite insensitive for small changes in boundary conditions. Interestingly, however, including the in-situ boundary conditions to the simulation model improved the similarity of the simulation and measurement results for the floors F11 and F12 (see Fig. **Figure 24a-b**). This suggests that it is preferred to model the floors in detail to reach better equivalency between the simulation and measurement results. It was also evident that the simulation results of the floors F11 and F12 were sensitive to the contact between the supporting structures of the ceiling and that the accuracy of the simulation depended on the source position (see **Publication IV**).

5 CONCLUSIONS

5.1 Computational prediction of impact sound insulation of timber floors

The applied FEM simulation procedure to predict the normalised impact sound pressure level L_n involved a three-stage process (see **Figure 7**). First, it is evident that information from the impact force excitation is required for the ISI simulations. Since the experimental study indicated that excitation force depends strongly on the type of the timber floor, the excitation must be computationally determined for each studied case. At this stage, the explicit dynamics analysis proved to be an accurate tool serving the assessment purposes. This tool was chosen due to the practical implications drawn from the impact force experiments: the model should be able to predict a single impact force pulse and account for the energy dissipation in the collision. The model predicted the peak value of the maximum impact force pulses on the CLT slab (floor F1.0) with a 40 N and the mechanical impulse with a 0.04 Ns accuracy. The FEM models created were able to explain the effect of complex features on the excitation generated by the STM. Based on the sensitivity analysis performed for the CLT slab (see **Figure 16**), the local properties of the slab were important to the impact force, but the simulated impact force pulses were insensitive to the global features, such as the size of the slab. These new findings from the analysis are significant since they offer possibilities to further develop tools predicting the excitation force for both engineering and research purposes.

The second stage involved the actual sound radiation simulations requiring most of the computational efforts in the simulations. According to the simulation results, the applied FEM simulation procedure was able to predict the normalised impact sound pressure levels L_n of the studied full timber floor and the floor without the covering with a reasonable equivalency between the simulation and measurement results in a broad frequency range (see **Figure 24a–b**). The difference between the 1/3-octave simulation and measurement results varied between 0 and 9 dB, and for the SNQs between 0 and 4 dB. In case of the bare rib slab, the simulation underestimated the L_n by 1 to 11 dB, and the SNQs by 4 to 5 dB. It must be emphasised that this was achieved although the exact properties of the used materials

were not known. This indicates that the simulation procedure can be applied for research and product development purposes of timber floors. However, it is obvious that further research is needed to improve both the accuracy and efficiency of the applied procedures. The differences between the simulation and measurement results indicated for probable reasons for the discrepancies. This suggests that it is preferred to model the floors in detail to reach better equivalency between the simulation and measurement results. Hopefully this also encourages the product manufacturers to provide their material data precisely and even on a larger scale.

The last part involved post-processing where the effect of the floor coverings and other additional structures can be introduced to the simulations. To maintain accuracy also at this stage, the ΔL of the floor covering products should be measured also on timber slabs. This would give information on the suitability of the products for use in the timber construction and would enable the development of new floor coverings to the timber construction markets. As discovered, the ISI performance of the floor coverings C1 and C2 depended on the type of the bare slab they were installed on. Possible reasons for this were found from the behaviour of the slabs and floor coverings. The different impact force levels generated by the STM on the bare slabs was considered as one of the main reasons for the differing results on different slabs.

5.2 Limitations and further research

Instead of actual material properties, the ISI simulations were based on data provided by the product manufacturers of the floors representing the best available data. However, because of the chosen approach, it is unclear whether the actual material properties would improve the equivalence between the simulation and measurement results for the ISI. Thus, it is recommended to repeat this study with known material properties including information from the elastic and damping properties of the materials. This would also bring insight into the possible modelling inaccuracies. Furthermore, it is not known how sensitive the analysis is for changes in the floors including variations in materials, dimensions, and joints. Because of this, it is recommended to perform a sensitivity analysis for the simulations. Modal analyses would also give information from the behaviour of the structures.

The applied simulation procedure was computationally rather expensive. Thus, it is obvious that further studies are required to improve the efficiency of the simulations. This could be done by applying less expensive element types into the

models instead of full solid elements, and possibly by a coarser frequency resolution outside the low-frequency range, to give examples.

The computational model simulating the impact force excitation generated by the STM was used under a few assumptions. The main assumption considered the initial states of the colliding bodies: the studied floor was initially at rest in the simulations. This initial state was based on the findings from the experimental study (see **Publication I**). For this reason, the analysis was performed to compute the force pulse generated by a single hammer drop. Hence, studying the effect of the vibration of the slab on the impact force in further research would be interesting. Furthermore, the post-processing procedure converting the impact force pulses to present continuous operation of the STM leads to an excitation spectrum with a 2 Hz frequency resolution. This occurs due to the assumption of ideal behaviour of a STM. If the repetition time between the force pulses deviates largely from the ideal, this would influence the resolution and magnitude of the impact force spectrum. Again, this would have an effect on the predicted ISI of the studied floors.

The vibration level reduction ΔL_a by the floor coverings has not been confirmed to correspond with the improvement of impact sound insulation ΔL on timber slabs. Thus, increasing the measurement positions below the timber slabs would have improved the accuracy of the analysis. Therefore, the results of the study for the performance of the floor coverings on the timber floors should not be considered absolute, but the conclusions should be confirmed by further research conducted in a full-scale building acoustics laboratory.

REFERENCES

Allard, J.-F., Champoux, Y., 1992. New empirical equations for sound propagation in rigid frame fibrous materials. Journal of the Acoustical Society of America 91, 3346–3353.

Alonso, A., Patricio, J., Suárez, R., 2019. On the efficiency of impact sound insulation systems on prefabricated lightweight floor and on standard homogeneous base-floor. Engineering Structures 191, 649–657.

Amiryarahmadi, N., Kropp, W., Bard, D., Larsson, K., 2011. Time-domain model of a tapping machine. In: Proceedings of Forum Acusticum 2011. Aalborg, Denmark, pp. 1713–1718.

Amiryarahmadi, N., Kropp, W., Larsson, K., 2016. Identification of low-frequency forces induced by footsteps on lightweight floors. Acta Acustica united with Acustica 102, 45–57.

Atalla, N., Sgard, F., 2015. Finite Element and Boundary Methods in Structural Acoustics and Vibration. CRC Press.

Bader Eddin, M., Ménard, S., Bard Hagberg, D., Kouyoumji, J.-L., Vardaxis, N.-G., 2022. Prediction of Sound Insulation Using Artificial Neural Networks—Part I: Lightweight Wooden Floor Structures. Acoustics 4, 203–226.

Balanant, N., Guigou, C., Villenave, M., 2012. Acoubois, Respect des exigences acoustiques dans les bâtiments à ossature bois, à vocation logements, Etape 2, Rapport final. Qualitel, FCBA, CSTB, France.

Bard, D., Negreira, J., Guigou Carter, C., Borello, G., Kouyoumji, J., Speranza, A., Coguenanff, C., Hagberg, K., 2017. Modelling prerequisites – FEM/SEA Impact and Airborne Sound. Silent Timber Build, report no STB01 WG1. RISE Research Institutes of Sweden AB.

Bard, D., Sonnerup, J., Sandberg, G., 2008. A Finite Element Solution of Structure-Borne Sound Attenuation for a Lightweight Timber Floor. Building Acoustics 15, 137–152.

Bolmsvik, Å., Brandt, A., 2013. Damping assessment of light wooden assembly with and without damping material. Engineering Structures 49, 434–447.

Bolmsvik, Å., Linderholt, A., Brandt, A., Ekevid, T., 2014. FE modelling of light weight wooden assemblies - Parameter study and comparison between analyses and experiments. Engineering Structures 73, 125–142.

Brunskog, J., Hammer, P., 2000. Prediction Models of Impact Sound Insulation on Timber Floor Structures; A Literature Survey. Building Acoustics 7, 89–112.

Brunskog, J., Hammer, P., 2003a. The interaction between the ISO tapping machine and lightweight floors. Acta Acustica united with Acustica 89, 296–308.

Brunskog, J., Hammer, P., 2003b. Prediction model for the impact sound level of lightweight floors. Acta Acustica united with Acustica 89, 309–322.

Buchschmid, M., Kohrmann, M., Müller, G., Schanda, U., 2015. Vibroacoustic Investigation of Light-Weight Ceilings - Modeling aspects and Design Guidelines. In: Proceedings of EuroNoise 2015. Maastricht, Netherlands, pp. 2497–2502.

Chung, H., Dodd, G., Schmid, G., Emms, G., McGunnigle, K., 2006. Maximising impact sound resistance of timber framed floor/ ceiling systems, Volumes 1–3 (No. Project number: Pn04.2005). Forest and Wood Products Research and Development Corporation, Australia.

Coguenanff, C., 2016. Robust design of lightweight wood-based systems in linear vibroacoustics (Dissertation). Universite Paris-Est.

Coguenanff, C., Guigou-Carter, C., Jean, P., Desceliers, C., 2015. Probabilistic model of the impact force spectrum for the standard ISO tapping machine. In: Proceedings of the 22nd International Congress on Sound and Vibration ICSV 2015. Florence, Italy, pp. 5551–5558.

COMSOL, 2022. Acoustics Module User's Guide.

Cremer, L., Heckl, M., Petersson, B.A.T., 2005. Structure-Borne Sound. Springer-Verlag, Berlin Heidelberg.

Cremer, L., Heckl, M., Ungar, E.E., 1973. Structure-Borne Sound. Springer-Verlag, Berlin Heidelberg.

DIN 4110, 1938. Technische Bestimmungen für Zulassung neuer Bauweisen. Deutcher Normenausschuß, Berlin.

EN 338, 2016. Structural timber – Strength classes. Brussels.

EN 1993-1-1, 2005. Eurocode 3: Design of steel structures - Part 1-1: General rules and rules for buildings. European Committee for Standardization, Brussels.

EN 1993-1-4, 2006. Eurocode 3: Design of steel structures - Part 1-4: General rules - Supplementary rules for stainless steels. European Committee for Standardization, Brussels.

EN ISO 12354-2, 2017. Building acoustics – Estimation of acoustic performance of buildings from the performance of elements – Part 2: Impact sound insulation between rooms. European Committee for Standardization, Brussels.

ETA-14/0349, 2014. European Technical Assessment. Austrian Institute of Construction Engineering.

Filippoupolitis, M., Hopkins, C., Völtl, R., Schanda, U., Mahn, J., Krajci, L., 2014. Experimentally validated finite element models for the modal response of a solid timber floor formed from dowel–connected joists. In: Proceedings of Forum Acusticum 2014. Krakow, Poland.

Filippoupolitis, M., Hopkins, C., Völtl, R., Schanda, U., Mahn, J., Krajči, L., 2017. Structural dynamics of a dowelled-joist timber floor in the low-frequency range modelled using finite element simulation. Engineering Structures 148, 602–620.

Flodén, O., Negreira, J., Persson, K., Sandberg, G., 2015. The effect of modelling acoustic media in cavities of lightweight buildings on the transmission of structural vibrations. Engineering Structures 83, 7–16.

Forest Products Laboratory, 2010. Wood Handbook – Wood as an Engineering Material, General Technical Report FPL-GTR-190. U.S. Department of Agriculture, Forest Service, Forest Products Laboratory, Madison, Wisconsin.

Forssén, J., Kropp, W., Brunskog, J., Ljunggren, S., Bard, D., Sandberg, G., Ljunggren Fredrik, Ågren, A., Hallström, O., Dybro, H., Larsson, K., Tillberg, K., Järnero, K., Sjökvist, L.-G., Östman, B., Hagberg, K., Bolmsvik, Å., Olsson, A., Ekstrand, C.-G., Johansson, M., 2008. Acoustics in wooden buildings – State of the art 2008. Vinnova project 2007-01653. SP Rapport 2008:16. SP Technial Research Institute of Sweden, Stockholm, Sweden.

Gover, B.N., Bradley, J., Schoenwald, S., Zeitler, B., 2011. Subjective ranking of footstep and low-frequency impact sounds on lightweight wood-framed floor assemblies. In: Proceedings of Forum Acusticum 2011. Aalborg, Denmark, pp. 1755–1760.

Griffin, D., 2017. Accuracy of prediction methods for the improvement of impact sound pressure levels using floor coverings. In: Proceedings of Internoise 2017. Hong Kong, China, pp. 3805–3813.

Gudmundsson, S., 1984. Sound insulation improvement of floating floors. A study of parameters. Lund Institute of Technology, Department of Building Acoustics, Report TVBA-3017, Lund, Sweden.

Guigou-Carter, C., Foret, R., Chéné, J.B., Villot, M., 2009. Prediction of the acoustic performance of floor coverings on lightweight floors. In: Proceedings of Internoise 2009.

Heckl, M., Rathe, E.J., 1963. Relationship between the transmission loss and the impact-noise isolation of floor structures. Journal of the Acoustical Society of America 35, 1825–1830.

Homb, A., Guigou-Carter, C., Hagberg, K., Schmid, H., 2016. Impact sound insulation of wooden joist constructions: Collection of laboratory measurements and trend analysis. Building Acoustics 23, 73–91.

Homb, A., Guigou-Carter, C., Rabold, A., 2017. Impact sound insulation of cross-laminated timber/massive wood floor constructions: Collection of laboratory measurements and result evaluation. Building Acoustics 24, 35–52.

Hongisto, V., Alakoivu, R., Virtanen, J., Hakala, J., Saarinen, P., Laukka, J., Linderholt, A., Olsson, J., Jarnerö, K., Keränen, J., 2023. Sound insulation dataset of 30 wooden and 8 concrete floors tested in laboratory conditions. Data in Brief 49, 109393.

Hopkins, C., 2007. Sound Insulation. Elsevier Ltd, Oxford, United Kingdom.

Hopkins, C., Filippoupolitis, M., Ferreira, N., Völtl, R., Schanda, U., Mahn, J., Krajči, L., 2016. Vibroacoustic finite element modelling of the low-frequency performance of a solid timber floor formed from dowel-connected joists. In: Proceedings of Inter-Noise 2016. Hamburg, Germany, pp. 1115–1122.

ISO 717-2, 2020. Acoustics – Rating of sound insulation in buildings and of building elements – Part 2: Impact sound insulation. International Organization for Standardization, Geneva.

ISO 10140-1, 2016. Acoustics – Laboratory measurement of sound insulation of building elements – Part 1: Application rules for specific products. International Organization for Standardization, Geneva.

ISO 10140-3, 2021. Acoustics – Laboratory measurement of sound insulation of building elements – Part 3: Measurement of impact sound insulation. International Organization for Standardization, Geneva.

ISO 10140-5, 2010. Acoustics – Laboratory measurement of sound insulation of building elements – Part 5: Requirements for test facilities and equipment. International Organization for Standardization, Geneva.

ISO 10140-5, 2021. Acoustics – Laboratory measurement of sound insulation of building elements – Part 5: Requirements for test facilities and equipment. International Organization for Standardization, Geneva.

ISO 12999-1, 2020. Acoustics – Determination and application of measurement uncertainties in buildings acoustics – Part 1: Sound insulation. International Organization for Standardization, Geneva.

ISO 16251-1, 2014. Acoustics – Laboratory measurement of the reduction of transmitted impact noise by floor coverings on a small floor mock-up – Part 1: Heavyweight compact floor. International Organization for Standardization, Geneva.

ISO 16283-2, 2015. Acoustics – Field measurement of sound insulation in buildings and of building elements – Part 2: Impact sound insulation. International Organization for Standardization, Geneve.

Jean, P., Siwiak, H., Joubert, G., 2006. A decoupled vibro-acoustic development of FEM: Application to laboratory modelling. Building Acoustics 13, 83–98.

Jeon, J.Y., Ryu, J.K., Jeong, H., Tachibana, H., 2006. Review of the impact ball in evaluating floor impact sound. Acta Acustica united with Acustica 92, 777–786.

Johansson, C., 1995. Low-frequency impact sound insulation of a light weight wooden joist floor. Applied Acoustics 44, 133–147.

Kartous, M., Jonasson, H.G., 2001. A Simplified Method to Determine Impact Sound Improvement on Light-Weight Floors. Nordtest Project 1544-01.

Kohrmann, M., 2017. Numerical Methods for the Vibro-Acoustic Assessment of Timber Floor Constructions (Dissertation). Technische Universität München.

Kohrmann, M., Buchschmid, M., Müller, G., Völtl, R., Schanda, U., 2013. Numerical models for the prediction of vibro-acoustical characteristics of light-weighted ceilings. In: Proceedings of Inter-Noise 2013. Innsbruck, Austria.

Kohrmann, M., Buchschmid, M., Schanda, U., Müller, G., 2016. A FEM-based planning tool for the vibro-acoustic design of wooden floors at low frequencies. In: Proceedings of the INTER-NOISE 2016 - 45th International Congress and Exposition on Noise

Control Engineering: Towards a Quieter Future. Hamburg, Germany, pp. 3743–3751.

Kylliäinen, M., 2014. The Measurement Uncertainty of Single-Number Quantities for Rating the Impact Sound Insulation of Concrete Floors. Acta Acustica united with Acustica 100, 640–648.

Kylliäinen, M., Virjonen, P., Hongisto, V., 2019. Optimized reference spectrum for rating the impact sound insulation of concrete floors. The Journal of the Acoustical Society of America 145, 407–416.

Lahtela, T., Kylliäinen, M., Lietzén, J., Kovalainen, V., Talus, L., 2021. Ääneneristys puutalossa. Puuinfo Oy, Helsinki, Finland.

Latvanne, P., 2015. The acoustical properties and the calculation models of the wooden intermediate floor constructions (in Finnish) (Master of Science Thesis). Tampere University of Technology.

Latvanne, P., Kylliäinen, M., Kovalainen, V., Lietzén, J., 2018. An engineering method for the calculation of impact sound insulation of wooden floor constructions. In: Proceedings of Baltic-Nordic Acoustics Meeting BNAM 2018. Reykjavík, Iceland.

Lindblad, S., 1968. Impact sound characteristics of resilient floor coverings. Lund Institute of Technology, Division of Building Technology, Bulletin 2, Lund, Sweden.

Linderholt, A., Olsson, J., 2017. A simulation based study of low frequency transient sound radiation from floors - A concrete vs. a hybrid floor. In: Proceedings of International Congress on Sound and Vibration ICSV 24. London, United Kingdom, pp. 23–27.

Ljunggren, F., Simmons, C., 2022. Correlation between sound insulation and occupants' perception – Proposal of alternative single number rating of impact sound, Part III. Applied Acoustics 197, 108955.

Ljunggren, F., Simmons, C., Hagberg, K., 2014. Correlation between sound insulation and occupants' perception - Proposal of alternative single number rating of impact sound. Applied Acoustics 85, 57–68.

Ljunggren, F., Simmons, C., Öqvist, R., 2017. Correlation between sound insulation and occupants' perception – Proposal of alternative single number rating of impact sound, part II. Applied Acoustics 123, 143–151.

LS-DYNA Theory Manual (r:8571), 2017. . Livermore Software Technology Corporation (LSTC), Livermore, California.

Machimbarrena, M., Rasmussen, B., Alves Monteiro, C., 2019. Regulatory sound insulation requirements in South America – Status for housing, schools, hospitals and office buildings. In: Proceedings of the Inter-Noise 2019. Madrid, Spain.

Mayencourt, P., Mueller, C., 2020. Hybrid analytical and computational optimization methodology for structural shaping: Material-efficient mass timber beams. Engineering Structures 215, 110532.

Mishra, A., Humpenöder, F., Churkina, G., Reyer, C.P.O., Beier, F., Bodirsky, B.L., Schellnhuber, H.J., Lotze-Campen, H., Popp, A., 2022. Land use change and carbon emissions of a transformation to timber cities. Nat Commun 13, 4889.

Mosharrof, M.S., Brunskog, J., Ljunggren, F., Ågren, A., 2011. An improved prediction model for the impact sound level of lightweight floors: Introducing decoupled floor-ceiling and beam-plate moment. Acta Acustica united with Acustica 97, 254–265.

Negreira, J., Bard, D., 2016. Modelling of the tapping machine for finite element prediction tools -Preliminary parametric studies. In: Proceedings of International Congress on Acoustics. Buenos Aires, Argentina, p. 132.

Negreira, J., Sjöström, A., Bard, D., 2016. Low frequency vibroacoustic investigation of wooden T-junctions. Applied Acoustics 105, 1–12.

Niskanen, K., Gustafsson, P.-J., Berglund, L., Kulachenko, A., Nygards, M., Hägglund, R., Uesaka, T., Mäkelä, P., Östlund, S., 2011. Mechanics of Paper Products, 1st ed, De Gruyter Textbook Ser. De Gruyter, Inc.

Nowotny, Ł., Nurzyński, J., 2020. Proposal of an Assessment Method of the Impact Sound Insulation of Lightweight Floors. Buildings 10, 13.

Olsson, J., Linderholt, A., 2019. Force to sound pressure frequency response measurements using a modified tapping machine on timber floor structures. Engineering Structures 196, 109343.

Olsson, J., Linderholt, A., 2021. Low-frequency impact sound of timber floors: A finite element–based study of conceptual designs. Building Acoustics 28, 17–34.

Öqvist, R., Ljunggren, F., Johnsson, R., 2018. Walking sound annoyance vs. impact sound insulation from 20 Hz. Applied Acoustics 135, 1–7.

Pereira, A., Mateus, D., Godinho, L., Monteiro, S., Dias, A., 2016. Evaluation of impact sound reduction of floor coverings on timber and timber-concrete floors using vibration measurements. In: Proceedings of EuroRegio2016. Porto, Portugal.

Persson, P., Flodén, O., 2019. Effect of material parameter variability on vibroacoustic response in wood floors. Applied Acoustics 146, 38–49.

Pramreiter, M., Nenning, T., Malzl, L., Konnerth, J., 2023. A plea for the efficient use of wood in construction. Nat Rev Mater.

Qian, C., Ménard, S., Bard, D., Negreira, J., 2019a. Development of a vibroacoustic stochastic finite element prediction tool for a CLT floor. Applied Sciences 9, 1–25.

Qian, C., Ménard, S., Bard-Hagberg, D., Kouyoumji, J.L., Negreira, J., 2019b. Calibration of the ISO tapping machine for finite-element prediction tool on a wooden-base floor. Building Acoustics 26, 157–167.

Rabold, A., 2010. Anwendung der Finite Element Methode auf die Trittschallberechnung (Dissertation). Technische Universität München.

Rabold, A., Buchschmid, M., Düster, A., Müller, G., Rank, E., 2010. Modelling the excitation force of a standard tapping machine on lightweight floor structures. Building Acoustics 17, 175–197.

Rabold, A., Düster, A., Hessinger, J., Rank, E., 2009. Optimization of lightweight floors in the low frequency range with a FEM based prediction model. In: Proceedings of NAG/DAGA 2009. Rotterdam, Netherlands, pp. 1514–1517.

Rabold, A., Düster, A., Rank, E., 2007. Anwendung der Finiten Elemente Methode auf die Trittschallberechnung von Holzdecken. In: Proceedings of DAGA 2007. Stuttgart, Germany, pp. 261–262.

Rabold, A., Düster, A., Rank, E., 2008. FEM based prediction model for the impact sound level of floors. In: Proceedings of the Meetings in Acoustics. Paris, France, pp. 2993–2998.

Rao, C.L., Narayanamurthy, V., Simha, K.R.Y., 2017. Applied Impact Mechanics. John Wiley & Sons Inc.

Rasmussen, B., 2019. Sound insulation between dwellings - Comparison of national requirements in Europe and interaction with acoustic classification schemes. In: Proceedings of the International Congress on Acoustics. Aachen, Germany, pp. 5102–5109.

Schmitz, A., 2000. Comparison of impact sound insulation measurements of floor coverings using different floor types and excitation sources. In: Proceedings of Inter-Noise 2000. Nice, France, pp. 1–9.

Scholl, W., Maysenhölder, W., 1999. Impact sound insulation of timber floors: interaction between source, floor coverings and load bearing floor. Building Acoustics 6, 43–61.

Shen, X., Hopkins, C., 2019. Experimental validation of a finite element model for a heavy impact from the standard rubber ball on a timber floor. In: Proceedings of International Congress on Acoustics ICA 2019. Aachen, Germany, pp. 1271–1277.

Shen, X., Hopkins, C., 2020. Prediction of maximum fast time-weighted velocity levels from a rubber ball impact on a timber floor. In: Proceedings of Forum Acusticum 2020. Lyon, France, pp. 1651–1655.

Shen, X., Hopkins, C., 2022. Low-frequency vibration of a timber joist floor section connected by metal screws: experimental validation of FEM model. In: Proceedings of Inter-Noise 2022. Glasgow, Scotland.

Sommerfeld, M., 2009. A simplified measurement method for the determination of impact sound reduction. In: Proceedings of DAGA. Rotterdam, Netherlands.

United Nations Framework Convention on Climate Change, 2015. Paris Agreement. United Nations, Paris Climate Change Conference.

Vastiau, J., Van hoorickx, C., Reynders, E., 2022. Numerical and experimental investigation of the narrow-band impact sound insulation of layered floors. In: Proceedings of Inter-Noise 2022. Glasgow, Scotland.

Vér, I.L., 1971. Impact noise isolation of composite floors. The Journal of the Acoustical Society of America 50, 1043–1050.

Wang, P., Van hoorickx, C., Lombaert, G., Reynders, E., 2020. Numerical prediction and experimental validation of impact sound radiation by timber joist floors. Applied Acoustics 162, 107182.

Warnock, A.C.C., 2000. Impact Sound Measurements on Floors Covered with Small Patches of Resilient Materials or Floating Assemblies. National Research Council Canada.

Warnock, A.C.C., 2005. Summary Report for Consortium on Fire Resistance and Sound Insulation of Floors: Sound Transmission and Impact Insulation Data. National Research Council Canada.

Warnock, A.C.C., Birta, J.A., 2000. Detailed Report for Consortium on Fire Resistance and Sound Insulation of Floors: Sound Transmission and Impact Insulation Data in 1/3 Octave Bands. National Research Council Canada.

Wittstock, V., 2012. On the spectral shape of the sound generated by standard tapping machines. Acta Acustica united with Acustica 98, 301–308.

Wu, S.R., 2006. Lumped mass matrix in explicit finite element method for transient dynamics of elasticity. Computer Methods in Applied Mechanics and Engineering 195, 5983–5994.

Wu, S.R., Gu, L., 2012. Introduction to the explicit finite element method for nonlinear transient dynamics. John Wiley & Sons Inc., Hoboken, New Jersey.

Zeitler, B., Nightingale, T.R.T., King, F., 2008. Methods to control low frequency impact noise in wood-frame construction. In: Proceedings of Acoustics '08. Paris, France, pp. 5589–5594.

Zeitler, B., Nightingale, T.R.T., Schoenwald, S., 2009. Effect of floor treatments on direct impact sound pressure level. In: Proceedings of Euronoise 2009. Edinburgh, Scotland, pp. 1–9.

Zeitler, B., Schoenwald, S., Gover, B., 2013. On the relevance of impact source impedance at low frequencies. In: Proceedings of Meetings in Acoustics 19. Montreal, Canada, p. 015125.

Zeitler, B., Schoenwald, S., Nightingale, T.R.T., 2010. Parametric study of sound transmission through lightweight floors. In: Proceedings of 39th International Congress on Noise Control Engineering Internoise 2010. Lisbon, Portugal, pp. 1–10.

Zhong, X., Hu, M., Deetman, S., Steubing, B., Lin, H.X., Hernandez, G.A., Harpprecht, C., Zhang, C., Tukker, A., Behrens, P., 2021. Global greenhouse gas emissions from residential and commercial building materials and mitigation strategies to 2060. Nat Commun 12, 6126.

PUBLICATION I

Impact force excitation generated by an ISO tapping machine on wooden floors

Jesse Lietzén, Juha Miettinen, Mikko Kylliäinen, Sami Pajunen

Applied Acoustics 175, article 107821
https://doi.org/10.1016/j.apacoust.2020.107821

Applied Acoustics 175 (2021) 107821

Contents lists available at ScienceDirect

Applied Acoustics

journal homepage: www.elsevier.com/locate/apacoust

Impact force excitation generated by an ISO tapping machine on wooden floors

Jesse Lietzén [a,*], Juha Miettinen [b], Mikko Kylliäinen [a], Sami Pajunen [a]

[a] Tampere University, Faculty of Built Environment, Civil Engineering, Hervanta Campus, P.O. Box 600, 33014 Tampere University, Tampere, Finland
[b] Tampere University, Faculty of Engineering and Natural Sciences, Material Sciences and Environmental Engineering, Hervanta Campus, P.O. Box 589, 33014 Tampere University, Tampere, Finland

ARTICLE INFO

Article history:
Received 24 June 2020
Received in revised form 8 October 2020
Accepted 25 November 2020
Available online 16 December 2020

Keywords:
Impact sound insulation
Impact force
Tapping machine
Wooden floor

ABSTRACT

Prediction of the impact sound insulation of wooden floors requires information of the excitation forces driving the structure. According to earlier research, it is evident, that the impact force generated by the ISO tapping machine on the wooden floors is different than on bare concrete floors. However, only a few measurement results of the force have been shown in the literature. The purpose of our study was to experimentally determine the impact force excitation with an instrumented ISO tapping machine on a large range of wooden floors. One of the hammers of the tapping machine was equipped with both force and acceleration sensors. The hammer itself was modified to fulfil the requirements for the tapping machine presented in the standards ISO 10140-5 and ISO 16283-2. Based on the measured force signals, force spectra and impulses exerted by the instrumented hammer were determined. According to the results, differences between the force spectra on the wooden floors were prominent in the frequencies above 500 Hz. In the low-frequency range, the variation of the driving force corresponded to a level difference of more than 3 dB. In addition, the results showed that the process of excitation was not transient for the structures studied. Thus, the vibration of the measured wooden floors did not seem to influence the impact force. The findings of this paper are of very high importance for those developing mathematical calculation tools to predict the impact sound insulation of wooden floors.

1. Introduction

The conventional and the most used standard impact sound source is the ISO standard tapping machine (presented in the standards ISO 10140-5 [1] and ISO 16283-2 [2]). The apparatus consists of five steel hammers, which are repeatedly dropped one at the time on the floor two times per second, thus resulting in a total repetition rate of 10 Hz. Hence, the tapping machine generates a quasi-stationary impact force excitation to the surface of the floor. The use of alternative sound sources has not become a common practice at least in Europe and the ISO tapping machine will most probably remain as the primary impact sound source [3]. Therefore, only the impact force excitation generated by the ISO tapping machine is studied in this paper.

Interaction between the tapping machine and the floor structure, i.e. the manner how the hammers hit the floor, depends on the type of the floor [4]. Since the tapping machine repeatedly drops its five hammers freely on to the surface of the floor, the force and the sound power input into the floor depends on the behaviour of the structure under the hammers. The peak impact force the apparatus produces is at its highest when the hammers hit a rigid and heavy structure, whereas it can be significantly lower when the structure under the hammers is elastic or when the surface structure of the floor is resilient, cf. [4]. These issues have also an effect on the length of the force pulses as well as on the spectrum of the impact force [4,5]. Due to these effects, it is obvious that the impact force excitation of lightweight structures differs from the force on a bare concrete structure.

Several models describing the impact force excitation of the floors generated by the ISO tapping machine have been presented in the literature [4,6–14]. A comparison between some of the models can be found for example in ref. [11]. Despite the models, only a few measurement results of the force have been shown in the literature. The studies conducted by Gudmundsson [15], Rabold et al. [11] and Olsson and Linderholt [16] distinguished some fundamental differences of the impact force generated by the ISO tapping machine on different floors. Furthermore, Jeon et al. [17] attempted to characterise the force input of different impact sources, and Amiryarahmadi et al. [18] compared the measured force spectrum

* Corresponding author.
E-mail address: jesse.lietzen@tuni.fi (J. Lietzén).

https://doi.org/10.1016/j.apacoust.2020.107821
0003-682X/

generated by the tapping machine with the force spectrum caused by walking.

Apart from the study of Gudmundsson [15], measurement results of the impact force on different floor structures caused by ISO tapping machine have been presented only for a few floor structures. One reason for this is probably the tedious measurement setups. Secondly, the amplitude spectrum of the impact force generated by a single hammer blow of the hammer of the ISO tapping machine on bare concrete structures can often be considered rather constant [11,15]. Thus, there has probably been a minor need for investigating the impact force in the countries having buildings made mainly out of concrete. However, the force spectrum depends on the type of the floor as discussed above. Hence, more information of the impact force is required in order to understand better the behaviour of the tapping machine on lightweight structures. This is of particular importance for the acoustical engineers developing mathematical calculation tools applicable for the evaluation of the impact sound insulation of the wooden floors. One possibility to measure the impact force is to modify the hammers of the tapping machine.

In this study, the impact force excitation was measured with an instrumented tapping machine. The objective of the research was to study experimentally the spectrum and the impulse of the impact force excitation generated by the ISO tapping on wooden floors. The study included measurements for a large range of wooden floors with conventional floor coverings. Moreover, the aim was to study how the impact force was affected by the source position, the surface structures and the load-bearing structures. Additionally, the time dependency of the impact force excitation was discussed, referring to the requirements for the generation of sound field presented in the standards [1,2].

2. Methods

2.1. Excitation generated by the hammers of the ISO tapping machine

The drop height of the hammers of the ISO tapping machine is 40 mm and the mass of each hammer is 500 g. The full requirements for the ISO tapping machine are presented in the standards [1,2] which state, e.g. that the velocity of a hammer at impact v_0 shall be 0.886 m/s ± 0.022 m/s. This arises from the maximum permitted deviation of the mass of each hammer (12 g). Nevertheless, the impact force excitation cannot be generalized for all floor systems.

The formulation of the impact force excitation generated by the ISO tapping machine can be found from several sources in literature (see e.g. [4,5,8,11,12]). Here the formulation follows the presentation given by Brunskog and Hammer [4,19], where a two-sided representation of the spectrum of the force was used. The model considers a single hammer, but the excitation generated by every hammer could be formulated from this following the work of Wittstock [12].

The excitation force generated by the ISO tapping machine can be regarded as an infinite time series of separate force pulses $F(t)$ [4]. The length of the period T_r between the pulses for a single hammer is 0.5 s and the repetition rate $f_r = 1/T_r = 2$ Hz. Thus, the time history of the force pulse array $F_R(t)$ is a periodic signal and it can be represented by a two-sided complex Fourier series [4]

$$F_R(t) = \sum_{n=-\infty}^{\infty} F(t - nT_r) = \sum_{n=-\infty}^{\infty} F_n e^{i2\pi nt/T_r}, \quad (1)$$

where $i = \sqrt{-1}$ represents the imaginary unit and F_n is the amplitude of the discrete frequency components as follows

$$F_n = \frac{1}{T_r}\int_0^{T_r} F(t) e^{-\frac{i2\pi nt}{T_r}} dt. \quad (2)$$

The Fourier spectrum of the time history of the force is a tonal spectrum [4]

$$F_R(f) = \sum_{n=-\infty}^{\infty} F_n \delta(f - nf_r), \quad (3)$$

where δ denotes the Dirac delta function. The expression implicates that the single hammer of the tapping machine generates a spectrum with harmonics with a 2 Hz frequency step [12].

In case of a real tapping machine, some variation between the individual force pulses may be expected. If only a single force pulse $F(t)$ of the hammer is being considered, the amplitude spectrum is

$$F_n = \int_0^{T_r} F(t) e^{-i2\pi nt} dt. \quad (4)$$

The mechanical impulse I exerted by a hammer in the impact can be determined by integrating the time history $F(t)$ of a force pulse [4,5]

$$I = \int_0^{T_r} F(t) dt. \quad (5)$$

According to [4,5], the value of the impulse I ranges from mv_0 to $2mv_0$ depending on whether the impact is ideal inelastic or ideal elastic. The geometric mean value of the impulse I is $\sqrt{2}mv_0$. Further on, the low-frequency force F_{lf} can be determined dividing the impulse with the period between the pulses T_r

$$F_{lf} = \frac{I}{T_r}. \quad (6)$$

The low-frequency force F_{lf} (or the impulse I divided with the force period T_r) is equivalent with the low-frequency values of the magnitude of the amplitude spectrum $|F_n|$. Theoretically, the range of variation of the level of the F_{lf} is 6 dB [4]. This corresponds the maximum possible change in the momentum exerted by the apparatus.

The force level in [dB] can be calculated, e.g. in 1/3-octave-band frequencies, as follows

$$L_{force} = 20\log\left(\frac{F_{rms}}{F_{ref}}\right), \quad (7)$$

where F_{rms} denotes the root-mean-square force for each frequency band, and F_{ref} is the reference force.

When comparing the excitation of different floors in the frequency domain, the magnitude of the amplitude spectrum $|F_n|$ of the single force pulses (later also briefly called *the force spectrum*) is of particular interest. Additionally, the differences in the excitation force can be seen from the force level results. Moreover, the impulse I (or the low-frequency force F_{lf}) exerted by an impact represents the interaction between the hammer and the floor.

2.2. Procedure of the experiments

Impact force excitation was studied using an instrumented ISO tapping machine. The centre hammer of the machine (Norsonic Nor277) was modified and equipped with both force and acceleration sensors (see Fig. 1). The force sensor (Kistler type 9712B5000), covered with a custom-built impact cap, was placed at the bottom of the hammer in order to measure the impact force input into the floor. The acceleration sensor (Kistler type 8202A10) was placed at the top of the hammer to get further information on the motion of the hammer.

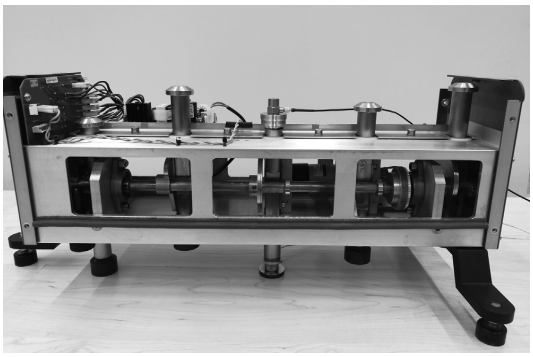

Fig. 1. The instrumented ISO tapping machine. The centre hammer was modified and equipped with force and acceleration sensors.

The hammer itself was modified to fulfil the requirements for the tapping machine presented in the standards [1,2] together with the attached sensors and additional parts. Thus, e.g. the diameter of the custom-built impact cap was 30 mm and the curvature of the impact surface of the cap was 500 mm. Additionally, the mass of the instrumented hammer was set to 503 g and the falling height of the hammer was kept at 40 mm. The permitted range of the mass of the hammer is 488–512 g [1,2], so the hammer fulfilled this requirement. The unmodified original hammer of the tapping machine weighted 502 g. Fig. 2 depicts the original hammer and the instrumented hammer used in the measurements. The sensors

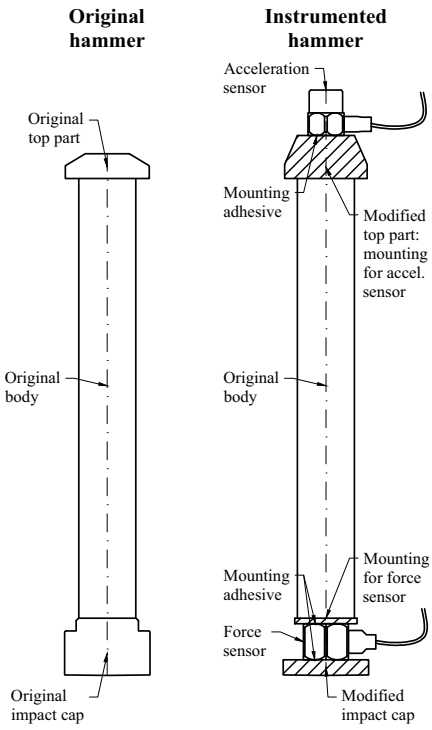

Fig. 2. The original and the instrumented hammer of the ISO tapping machine.

were mounted to the body of the hammer with studs. Moreover, adhesive was used in the mounting between the sensors and the body.

The impact force was directly measured from the hammer during the normal operation of the apparatus. This way the variation of the impact force pulses could be investigated. In the research [15], Gudmundsson noticed that the motion of the other hammers disturbed the signal when the force measurements were carried out using an acceleration sensor. Because of this, all the measurement results presented in this paper were derived from the signal of the force sensor in order to neglect the contribution of the other hammers to the impact force under study. It was assumed that the hammer behaved in these measurements as a rigid body. Therefore, the actual driving force would be the counterforce of the measurement signal during the contact of the hammer and the floor.

At the beginning of each measurement, the hammers of the tapping machine were at rest in arbitrary positions. The measurement started when the instrumented hammer first hit the surface of the floor. All measurements were performed in the time-domain, and therefore the time history of the impact force was recorded. The length of each measurement was approximately 30 s and the sampling frequency was 12800 Hz. During the experiments, the measurement cables were fastened with tape to the body of the tapping machine, in order to not interfere with the acceleration and force measurements.

2.3. Floor structures and source positions

The experiments were carried out on 24 wooden floors (see Fig. 3). The sizes of the floors were 2.4 m $\times$ 2.7 m with a span of 2.7 m. Two bearing floor structures were studied: a 100 mm thick cross-laminated-timber (CLT) slab (floors F1–F5) and a prefabricated rib slab (floors F6–F10). The CLT-slab was 3-layered with lamellas of thicknesses 30, 40, and 30 mm. The rib slab was constructed from 25 mm thick LVL panel deck and 45 mm $\times$ 260 mm LVL beams (c/c 578–600 mm). The LVL panel was both screwed and glued to the beams of the rib slab. For more information of the load bearing floors, see the Appendix 1 presented in the supplemental material. In few experiments, additional plasterboards were attached to the surface of the bearing structures in order to increase the mass of the floor. The plasterboards were glued and screwed to each other.

The surface structures of the floors included a multilayer parquet on an underlayment, a cushion vinyl, and a floating floor. The dynamic stiffness per unit area s' and the apparent dynamic stiffness per unit area s_t' [20] of the resilient products were measured. The multilayer parquet used in the measurements was a 14 mm thick maple parquet equipped with tongue-and-groove joints. In all the measurements, the parquet was installed in identical order on the soft 3 mm thick underlayment. The cushion vinyl was a soft 3 mm thick product especially used in apartment houses. The vinyl was glued to the substructure under and around each source position. The floating floor was constructed from a 30 mm thick mineral wool layer and two plasterboard layers glued and screwed to each other according to manufacturer's instructions. Since the floating floor was constructed from individual plasterboard sheets, there were small gaps between adjacent boards. One gap between the lower layer of the plasterboards lied in the centre of the span.

The load bearing structures were installed between vibration isolated massive steel structures placed on the floor of the construction laboratory. The structures were fixed from their both ends to the load supports with screw connections (see supplemental material, Appendix 2). The natural frequency of the vibration isolation was set under 10 Hz in order to attenuate possible vibrations from the surroundings. The frequency range of interest was

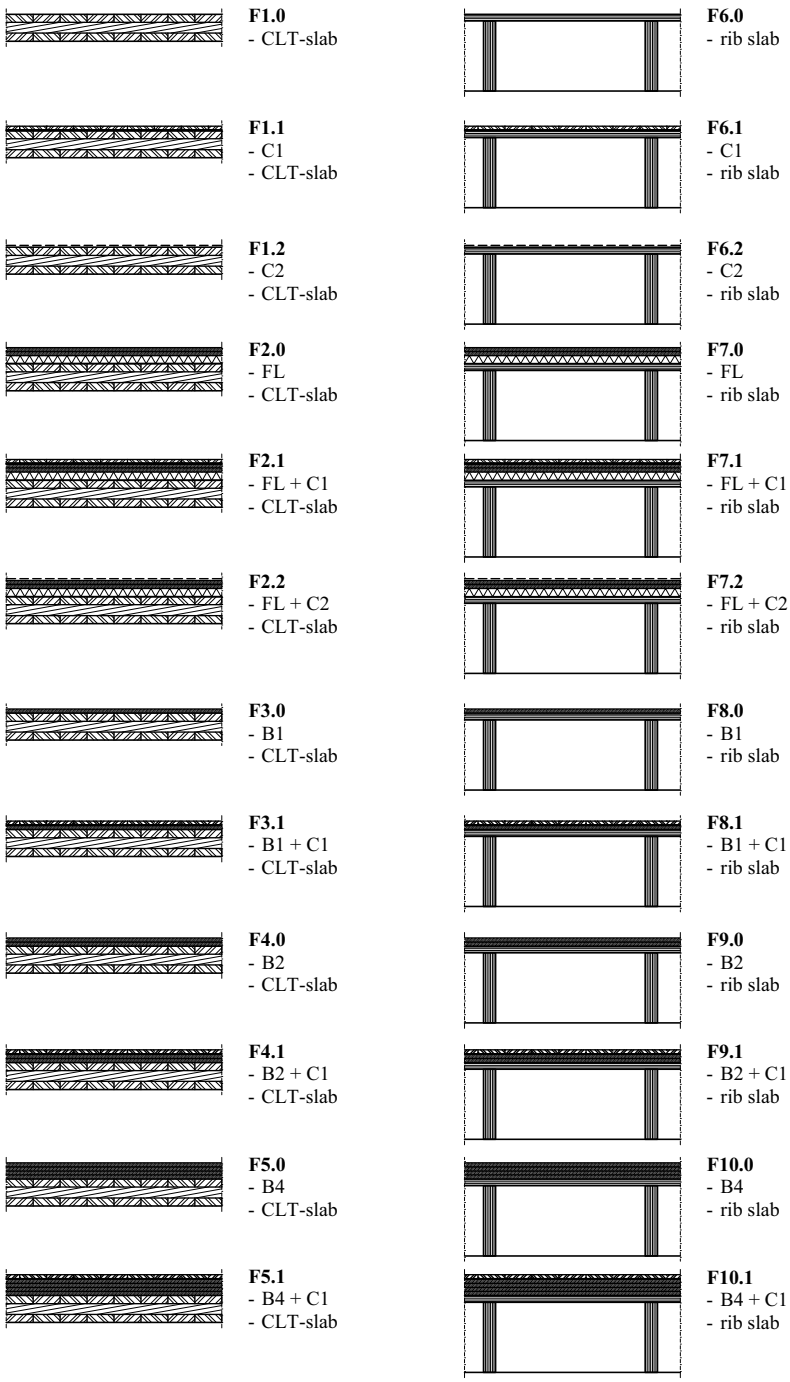

Fig. 3. Floor structures F1–F10. The number after the point indicates the type of the floor covering on the floor as follows: (0) no floor covering; (1) C1, the multilayer parquet (thickness h = 14 mm) on an underlayment (h = 3 mm, s' = 65,1 MN/m^3); and (2) C2, the cushion vinyl (h = 3 mm, s' = 2282 MN/m^3). The other abbreviations are: FL, a floating floor with two plasterboards (h = 15 mm, mass per unit area m' = 15.4 kg/m^2) on a mineral wool layer (h = 30 mm, s'_t = 12,8 MN/m^3, s' = 16,4 MN/m^3); and B, additional plasterboards ((h = 15 mm, m' = 15.4 kg/m^2) on the bearing structure, where the number following B denotes the number of the plasterboards layers (B1, B2, B4).

16–3600 Hz, since the low frequency behaviour often determines the subjective rating of the wooden floor structures, cf. [21,22].

The measurements were performed at five source positions S1–S5 per structure. Fig. 4 shows the source positions and the orientation of the ISO tapping machine at the positions. The positions were at least at a range of 0.5 m from the edges of the structure (cf. requirements in ISO 16283-2 [2]). The position S3 was located at the centre of the structures. All the positions were kept the same for all studied floor structures.

2.4. Post-processing of the measurement results

Fig. 5**a** shows an example of the entire measured time history of the force. As the impact force generated by the ISO tapping machine was measured with the sensor attached to the hammer, a slight additional force occurred between the impacts upon the floor (see Fig. 5**b**). This was due to the acceleration of the instrumented hammer and due to the impacts generated by the hammers not involved in the measurement. However, the counterforce of the force being measured drives the floor only when the hammer and the surface of the floor are in contact. Thus, in order to get information from the actual driving force of the floors, all the impact force pulses were sought, and the force was set to zero between the impacts.

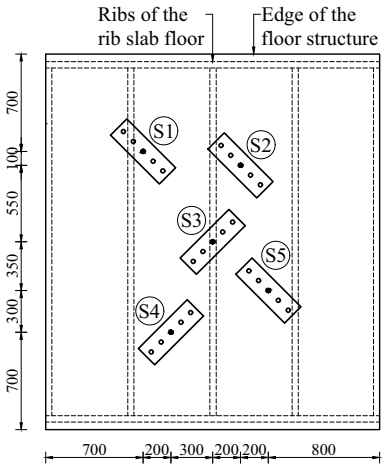

Fig. 4. Source positions S1–S5 on the floor structure. The rectangular boxes illustrate the orientation of the ISO tapping machine on the source positions and the black circles show the location of the instrumented hammer used in the measurements. Dimensions in the figure are presented in millimetres.

Since the position of the hammer in the beginning of each measurement was arbitrary, not resulting in a full initial impact, the first impact was omitted from the time history of the force. In addition, the time history from the beginning of the last impact to the end of the measurement was deleted, because of the lack of information of the beginning of the next impact after the measurement (the time between the impacts was not exactly 0.5 s, which can also be seen from Fig. 5**b**).

The spectrum of the driving force was determined from the time history of the force processed in accordance with the method described above. The amplitude spectrum F_n of the driving force was determined for every force pulse according to Eq. (4). The calculations were carried out with the FFT algorithm implemented in MATLAB®. In order to compare different force pulses in the frequency domain, the length of the period between the pulses T_r was set to 500 ms. The amount of the samples in a single force period was 6400, thus resulting in frequency spacing of the spectrum of 2 Hz.

Additionally, the time history of the force was filtered using 1/3-octave-band filters in the frequency range from 20 to 3150 Hz. The root-mean-square force F_{rms} was calculated for each frequency band and the force level L_{force} was determined by using Eq. (7).

In order to determine the effect of the floor on the momentum exerted by the hammer, the mechanical impulse I was determined according to Eq. (5) for every force pulse. The calculations of the integral were performed via the trapezoidal method implemented in MATLAB®. Hence, the results for I represent the approximate values of the impulse.

The calculations were done for every floor under study and for every source position S1–S5. Note that the values of the calculated force spectra were low compared to the measured peak values of the impact force pulses in time domain. This occurred, since between the short impacts upon the floor, the force driving the floor was zero, and the calculation of the force spectra was carried

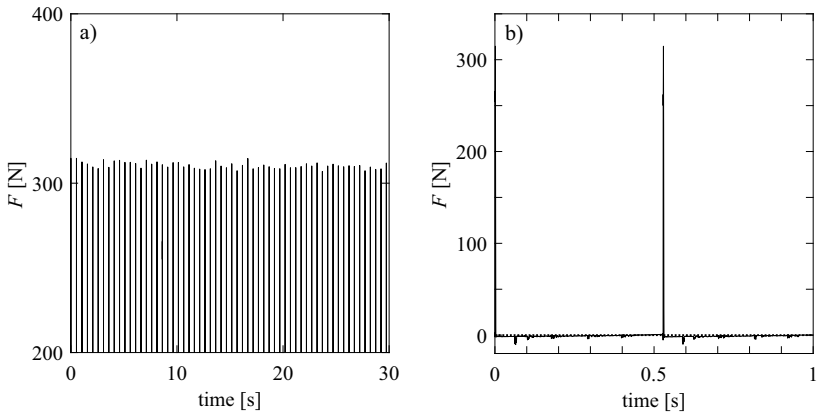

Fig. 5. Time history of the force (floor F1.1, source position S1): a) an example of the entire time history; b) an example of the additional force occurring between the first two impacts of the instrumented hammer (the black solid line depicts the measurement result and the dotted line the force level of zero Newtons).

out also for these moments (see Eq. (4)). If the results were compared with the one-sided formulation of the Fourier series, the values of the magnitude of the amplitude spectra and the impulses should be multiplied with the factor of 2.

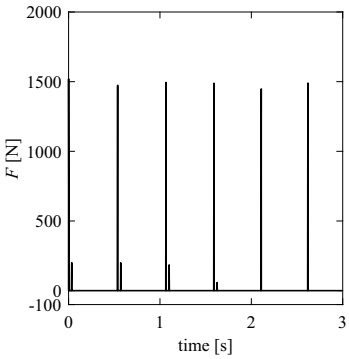

Fig. 6. The secondary impacts of the hammer during the force measurement (floor F7.0, source position S5). The second impacts occurred 34 ms after each of the first four impacts on this floor. These first impacts were omitted from the calculation of the results. No secondary impacts occurred on the other floors under study.

2.5. The secondary impacts of the hammer

In theory, it is possible that the hammer of the ISO tapping machine would rebound and hit the floor at least a second time. These secondary impacts could occur when the first impact is nearly inelastic and almost all the energy is dissipated in the collision. The standards ISO 10140-5 and ISO 16283-2 have set a requirement that the time between the impact and the lift of the hammer should be less than 80 ms [1,2]. This sets the possible time window for the secondary impacts. Wittstock showed a measurement result in [12] where the hammer of the mechanical tapping machine began to fall again after the actual impact and before its lift. His experiments were performed on a small reception plate made of artificial stone. However, in this occasion the hammer did not hit the plate a second time.

In this study, it was also investigated whether the measurement results included secondary impacts. This was carried out by comparing the modified force signal (see Section 2.4) with the original force signal between the actual impacts. According to the results, second impacts occurred approximately 34 ms after the first four full impacts on the floor F7.0 at the source position S5 (see Fig. 6). These first impacts were omitted from the calculations and no spectra for these impacts were determined. This was the only occasion where the second impacts were prominent and no

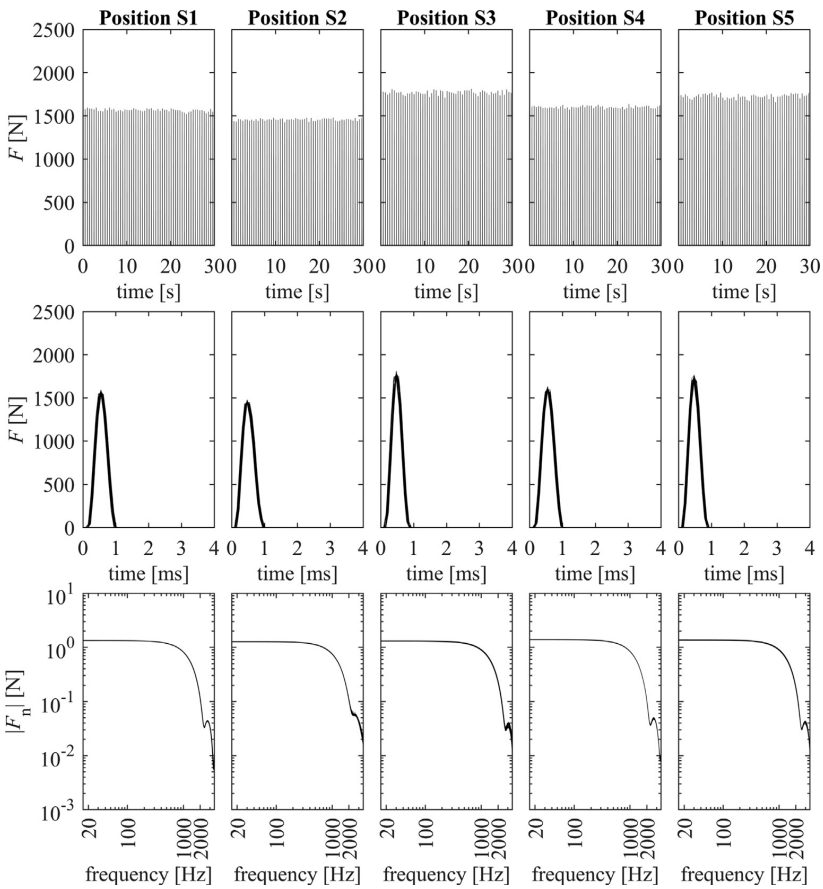

Fig. 7. An example of the measurement results (floor F1.0). Results for source positions S1–S5 are shown in three rows. The top row shows the time history of the force driving the floor, the individual force pulses are presented in the middle row and the bottom row depicts the magnitude of the amplitude spectra $|F_n|$.

secondary impacts occurred on the other floors under study. Hence, it is justified to carry out the calculation of the force spectrum on basis of the post-processing method described in the previous Section 2.4.

3. Results

3.1. The impact force in time and frequency domains

All the measurement results of the impact force have been shown in the Appendix 3 of the supplemental material. An example of the presentation of the results is illustrated in Fig. 7. The results in the appendix were arranged on three rows as follows: the top row shows the time history of the force driving the floor for the whole measurement period, the second row presents the individual force pulses in time domain, and the magnitudes of the amplitude spectra $|F_n|$ of the single force periods is depicted on the bottom row. The five columns of the figure represent results for each source position S1–S5. The individual force pulses were centred based on their peak values in order to make them better comparable. In a few cases, the pulse had two local maxima, when the pulses were primarily centred based on the first one. The amount of impacts ranged from 60 to 61 during the measurements (without the first and the last impact).

In Fig. 7 the variation of the impacts on different source positions can be seen both from the time histories and from the spectra of the forces. However, since the measured values were discrete, the variation of the excitation force was best evident in the individual force pulses, where the shape of the pulses was prominent. The results for the spectra of the force presented for a single source position form a set of curves, for the calculations were carried out for every individual force period. Thus, these results also indicate the variation of the excitation in the frequency domain.

The force spectra presented in the results were derived by assuming that the hammer would behave as a rigid body. However, if the joints between the parts of the instrumented hammer and the force sensor would behave elastically, this would affect the behaviour of the hammer. Hence, it should be noted that in some cases and in the whole frequency range presented, the spectra may not correspond to the impacting force correctly.

The dependence of the force pulses in the time domain on the floor and source position can also be seen from Table 1, where the peak values of the individual force pulses and their durations have been listed. The durations of the pulses represent the length

Table 1
The average peak values and the average durations of the individual force pulses.

Floor		Pos. S1	Pos. S2	Pos. S3	Pos. S4	Pos. S5
F1.0	Peak value [N]	1566.6	1457.1	1770.2	1601.4	1727.2
	Duration [ms]	0.99	1.02	0.91	1.01	0.94
F1.1	Peak value [N]	310.5	345.1	421.1	439.9	397.4
	Duration [ms]	3.02	2.44	2.41	2.20	2.38
F1.2	Peak value [N]	624.0	647.1	661.9	627.8	623.4
	Duration [ms]	2.10	2.15	2.00	2.16	2.24
F2.0	Peak value [N]	1149.8	1523.0	1008.5	1474.7	1564.0
	Duration [ms]	1.08	0.94	1.26	0.94	0.95
F2.1	Peak value [N]	287.4	338.2	410.8	445.5	400.2
	Duration [ms]	3.26	2.56	2.44	2.10	2.35
F2.2	Peak value [N]	540.2	556.6	547.5	580.6	559.8
	Duration [ms]	2.43	2.36	2.45	2.32	2.45
F3.0	Peak value [N]	1471.2	1831.4	1918.8	1764.3	1712.5
	Duration [ms]	0.98	0.82	0.85	0.87	0.88
F3.1	Peak value [N]	341.5	359.4	419.8	462.1	412.5
	Duration [ms]	2.83	2.46	2.36	2.15	2.33
F4.0	Peak value [N]	1604.3	1967.3	1792.3	1704.1	1524.1
	Duration [ms]	0.87	0.81	0.86	0.85	0.95
F4.1	Peak value [N]	324.0	351.5	422.5	420.9	407.2
	Duration [ms]	2.92	2.50	2.33	2.28	2.37
F5.0	Peak value [N]	1885.9	1820.5	2150.6	2178.3	1693.1
	Duration [ms]	0.83	0.86	0.77	0.78	0.88
F5.1	Peak value [N]	345.3	374.3	423.8	417.2	423.8
	Duration [ms]	2.90	2.49	2.36	2.26	2.30
F6.0	Peak value [N]	673.1	613.0	1252.0	575.1	577.9
	Duration [ms]	1.91	1.82	1.24	2.10	2.49
F6.1	Peak value [N]	358.9	412.7	440.9	508.9	420.6
	Duration [ms]	2.83	2.58	2.35	1.94	2.68
F6.2	Peak value [N]	502.6	458.0	567.2	444.3	425.7
	Duration [ms]	2.35	3.02	2.19	2.42	3.21
F7.0	Peak value [N]	1502.7	1470.7	1127.2	1566.4	1501.0
	Duration [ms]	0.89	1.04	1.07	0.90	0.92
F7.1	Peak value [N]	321.7	366.0	407.0	481.2	435.8
	Duration [ms]	3.04	2.59	2.52	2.14	2.24
F7.2	Peak value [N]	544.7	539.3	523.4	529.6	546.9
	Duration [ms]	3.02	2.70	2.74	2.90	2.58
F8.0	Peak value [N]	1124.4	1255.7	1435.5	1192.0	1170.3
	Duration [ms]	1.20	1.13	0.96	1.14	1.13
F8.1	Peak value [N]	361.1	396.4	470.5	477.4	436.8
	Duration [ms]	2.96	2.56	2.48	2.14	2.59
F9.0	Peak value [N]	992.0	1917.5	1728.8	1476.0	1833.9
	Duration [ms]	1.20	0.79	0.85	0.93	0.81
F9.1	Peak value [N]	336.8	352.9	425.3	469.8	388.2
	Duration [ms]	2.90	2.51	2.46	2.05	2.36
F10.0	Peak value [N]	1820.2	2045.7	1180.0	1387.6	1358.2
	Duration [ms]	0.84	0.80	1.15	1.02	1.01
F10.1	Peak value [N]	316.2	362.6	419.7	455.9	393.1
	Duration [ms]	2.96	2.39	2.47	2.13	2.33

of the pulse from the beginning to the end of it. The values presented in the table correspond to the averaged results for the respective floor and source position.

3.2. The average impact force in the frequency domain

Fig. 8 shows the average of all the magnitudes of the amplitude spectra $|F_n|$ of the individual force periods for each floor in the frequency range 16 to 3600 Hz. The figure illustrates the results for the source position S1. The spectra depicted in the figure represent the arithmetic averages of the spectra of all the individual force periods of the respective floor. The figure includes a small window for magnified results in the low frequencies from 16 to 200 Hz, where the variation of the results in this frequency range can be seen.

Fig. 9 shows the force levels L_{force} in 1/3-octave-bands from 20 to 3150 Hz for each floor structure. The results are arithmetic averages over all the source positions S1–S5. In the Fig. 10, the standard deviations of these levels over the source positions are shown. Thus, the figure depicts the effect of the source position on the force measured on each floor.

In the Figs. 8–10, the results for the floors without any floor covering (floor types Fx.0) are presented with solid lines, the dashed lines show the results for the floors with the multilayer parquet on the underlayment (floor types Fx.1), and the results for the floors with the cushion vinyl as the floor covering (floor types Fx.2) are depicted with dash-dotted lines.

3.3. The mechanical impulses generated by the ISO tapping machine

Table 2 shows the average impulses I and their standard deviations calculated for all the floors at the source positions S1–S5. Additionally, the average values are depicted in Fig. 11, where the scale is set such that the extreme boundaries represent the theoretical limits for the ideal inelastic and ideal elastic impulse discussed in the Section 2.1. The geometrical mean value of the impulse ($\sqrt{2}mv_0 \approx 0.626$ Ns) is illustrated in Fig. 11 with dotted line. If the low-frequency force F_{lf} were determined on the basis of the impulses (see Eq. (6)), they would correspond the low-frequency values of the magnitude spectra presented in Fig. 8.

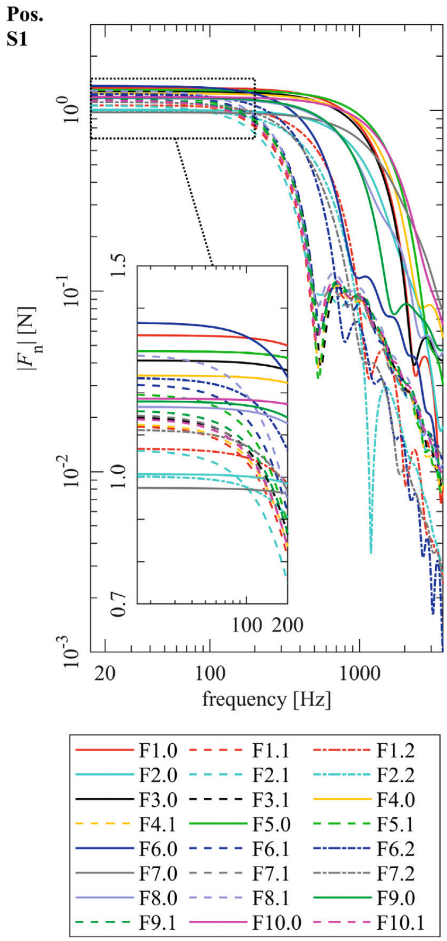

Fig. 8. The average of the magnitudes of the amplitude spectra $|F_n|$ of the force on all the floors at the source position S1. The solid lines depict the result on a floor without any floor covering, the dashed lines present the result when the floor covering was the multilayer parquet on the underlayment, and the dash-dotted lines illustrate the results on the cushion vinyl.

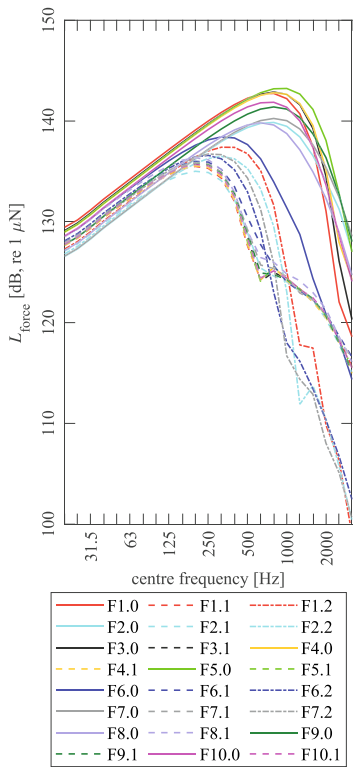

Fig. 9. The average force level L_{force} over all the source positions S1–S5 in 1/3-octave-bands on all the floors. The solid lines depict the result on a floor without any floor covering, the dashed lines present the result when the floor covering was the multilayer parquet on the underlayment, and the dash-dotted lines illustrate the results on the cushion vinyl.

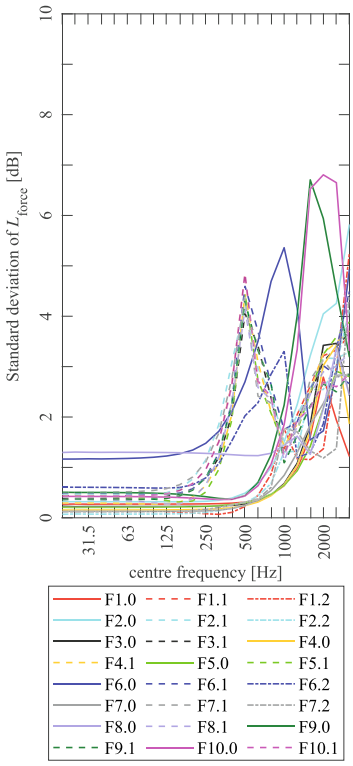

Fig. 10. The standard deviation of the force level L_{force} over the source positions S1–S5 in 1/3-octave-bands on all the floors. The solid lines depict the result on a floor without any floor covering, the dashed lines present the result when the floor covering was the multilayer parquet on the underlayment, and the dash-dotted lines illustrate the results on the cushion vinyl.

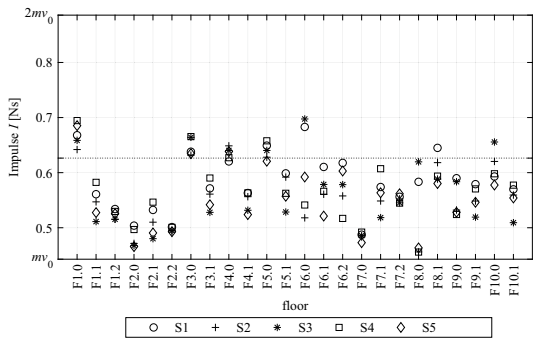

Fig. 11. The average impulses I on different floors at the positions S1–S5. The extreme boundaries represent the theoretical limits for the impulse from 0.443 Ns (mv_0) to 0.886 Ns ($2mv_0$) which correspond to the ideal inelastic and ideal elastic collisions, respectively. The theoretical geometrical mean value of the impulse 0.626 Ns ($\sqrt{2}mv_0$) is illustrated with the dotted line.

4. Discussion

4.1. The impact force excitation on different wooden floors

The results for the peak values of the force pulses caused by the tapping machine and their durations (Table 1), and for the force spectra (Fig. 8), as well as for the force level spectra (Fig. 9), indicate that the excitation driving the wooden floors depends strongly on the type of the structure. The finding is of very high practical importance. Such a wide experimental evidence has not been published previously in this field. When comparing the results for the force spectra with the spectra measured on concrete and steel structures in [11,15,17], it is obvious that the impact force excitation generated by the ISO tapping machine is different on the wooden floors. The variation of the results for the force spectra on different wooden floors is evident in the whole frequency range of interest, but the differences are major above 500 Hz. At frequen-

Table 2
The average values and the standard deviations of the impulses I in [Ns] determined from all the individual force pulses. The standard deviations are presented in brackets. The average values (AVG) and standard deviations (STDEV) of the results are shown for each floor (on the right part of the table).

Floor	Pos. S1	Pos. S2	Pos. S3	Pos. S4	Pos. S5	AVG	STDEV
F1.0	0.67 (0.0031)	0.64 (0.0031)	0.66 (0.0050)	0.69 (0.0037)	0.69 (0.0051)	0.67	0.0192
F1.1	0.56 (0.0033)	0.55 (0.0028)	0.51 (0.0030)	0.58 (0.0031)	0.53 (0.0032)	0.55	0.0251
F1.2	0.53 (0.0021)	0.52 (0.0017)	0.52 (0.0021)	0.53 (0.0026)	0.53 (0.0026)	0.52	0.0079
F2.0	0.50 (0.0019)	0.47 (0.0020)	0.47 (0.0017)	0.50 (0.0024)	0.47 (0.0013)	0.48	0.0161
F2.1	0.53 (0.0028)	0.51 (0.0021)	0.48 (0.0019)	0.55 (0.0034)	0.49 (0.0018)	0.51	0.0250
F2.2	0.50 (0.0013)	0.49 (0.0018)	0.49 (0.0018)	0.50 (0.0018)	0.49 (0.0013)	0.50	0.0041
F3.0	0.64 (0.0030)	0.63 (0.0031)	0.66 (0.0036)	0.67 (0.0037)	0.63 (0.0028)	0.65	0.0152
F3.1	0.57 (0.0036)	0.56 (0.0021)	0.53 (0.0024)	0.59 (0.0032)	0.54 (0.0029)	0.56	0.0221
F4.0	0.62 (0.0024)	0.65 (0.0034)	0.64 (0.0038)	0.63 (0.0024)	0.64 (0.0023)	0.63	0.0104
F4.1	0.56 (0.0050)	0.56 (0.0023)	0.53 (0.0025)	0.56 (0.0028)	0.52 (0.0023)	0.55	0.0169
F5.0	0.65 (0.0026)	0.63 (0.0036)	0.64 (0.0039)	0.66 (0.0033)	0.62 (0.0031)	0.64	0.0139
F5.1	0.60 (0.0044)	0.59 (0.0033)	0.53 (0.0034)	0.56 (0.0029)	0.56 (0.0031)	0.57	0.0256
F6.0	0.68 (0.0058)	0.52 (0.0063)	0.70 (0.0056)	0.54 (0.0052)	0.59 (0.0062)	0.61	0.0730
F6.1	0.61 (0.0078)	0.56 (0.0053)	0.58 (0.0056)	0.57 (0.0037)	0.52 (0.0048)	0.57	0.0295
F6.2	0.62 (0.0040)	0.56 (0.0051)	0.58 (0.0024)	0.52 (0.0048)	0.60 (0.0053)	0.57	0.0358
F7.0	0.49 (0.0013)	0.48 (0.0014)	0.49 (0.0013)	0.49 (0.0014)	0.47 (0.0015)	0.48	0.0065
F7.1	0.57 (0.0094)	0.55 (0.0073)	0.52 (0.0058)	0.61 (0.0059)	0.56 (0.0071)	0.56	0.0301
F7.2	0.56 (0.0019)	0.55 (0.0031)	0.55 (0.0031)	0.54 (0.0029)	0.56 (0.0020)	0.55	0.0070
F8.0	0.58 (0.0023)	0.46 (0.0021)	0.62 (0.0021)	0.46 (0.0016)	0.46 (0.0023)	0.52	0.0712
F8.1	0.65 (0.0077)	0.62 (0.0035)	0.59 (0.0042)	0.59 (0.0061)	0.58 (0.0054)	0.61	0.0243
F9.0	0.59 (0.0023)	0.53 (0.0026)	0.58 (0.0025)	0.52 (0.0021)	0.53 (0.0023)	0.55	0.0291
F9.1	0.58 (0.0022)	0.55 (0.0018)	0.52 (0.0018)	0.57 (0.0024)	0.55 (0.0022)	0.55	0.0211
F10.0	0.59 (0.0035)	0.62 (0.0024)	0.66 (0.0028)	0.60 (0.0019)	0.58 (0.0022)	0.61	0.0273
F10.1	0.57 (0.0020)	0.56 (0.0035)	0.51 (0.0018)	0.58 (0.0017)	0.55 (0.0017)	0.55	0.0239

cies below 100 Hz, the values of the force spectra stay rather constant and the differences between the floors were minor in comparison with the high-frequency range results. However, the value of the magnitude force spectra ranged from 0.9 to 1.4 N. This variation corresponds to the level difference of over 3 dB of the force input in the low-frequency range (see Fig. 9).

The variation of the results in the low-frequency range can also be seen from the impulses I shown in Table 2 and Fig. 11, as discussed in Section 2.1. On the basis of these results, the geometrical mean value of the impulse does not represent the actual value of the impulse on wooden floors in general. The results imply that the model describing the impact force excitation generated by the ISO tapping machine on wooden floors should include the ability to predict the value of the impulse. This is especially important when developing mathematical calculation tools predicting the impact sound insulation of wooden floors in the low-frequency range.

In case of the CLT-floors (F1.0, F3.0, F4.0 and F5.0), the impulses and the force spectra had on average the greatest values of all the results. The shapes of the force spectra on different CLT-floors were rather uniform and they began to decrease around 500 Hz, while the first local minima occurred at over 2000 Hz. On the bare CLT-floor (F1.0), the force was between 1.28 and 1.39 N in the low-frequency range. The respective values ranged from 1.24 to 1.33 N on the CLT-floors with additional plasterboards (F3.0, F4.0 and F5.0). Correspondingly, the impulses were 0.64–0.69 Ns and 0.62–0.67 Ns on the floor F1.0 and on the floors F3.0, F4.0 and F5.0, respectively. Thus, the impulses were a little above the geometrical mean value and the differences between the results at different source positions were minor. The results imply that in case of massive wooden plates the impact force excitation generated by the ISO tapping machine is quite independent on the position of the apparatus.

In case of the rib slab floors (F6.0, F8.0, F9.0 and F10.0), the effect of the thin wooden deck and the ribs on the force was prominent. When the source position was above the rib or in the vicinity of it (at S1 or S3), the force spectra had higher values than at the other source positions. This occurred especially on the floors F6.0 and F8.0, but the differences diminished when the floor included at least two layers of plasterboards (floors F9.0 and F10.0). On the floor F6.0, the shape of the spectra measured at the source positions between the ribs (S2, S4 and S5) resembled the spectra measured on the floors equipped with the floor coverings. In the low-frequency range the force spectra had values 1.04–1.39 N on the floor F6.0, and values 0.9–1.31 N on the floors F8.0, F9.0 and F10.0. Respectively, the impulses exerted by the hammer ranged from 0.52 to 0.70 Ns and between 0.46 and 0.66 Ns, on these floors. These variations correspond to the force level difference of even 3 dB of the force input in the low-frequency range. This kind of behaviour was prominent also in the results presented by Gudmundsson [15], where the measured force level spectrum was lower even in the low-frequency range when the floating floor was a lightweight structure in comparison with concrete floating floors. Therefore, it seems justified to recommend more impact source positions in addition to the minimum number of positions when measuring the impact sound insulation of rib slab floors, cf. [2]

When the surface structure was the bare floating floor (floors F2.0 and F7.0), the results were rather uniform and independent of the source position. The force spectra ranged from 0.93 to 1.01 N in the low-frequencies and started to decrease around 500 Hz. In correspondence with the low-frequency results, the impulses varied from 0.47 to 0.50 Ns. Therefore, the impact of the hammer upon these floors could be regarded as nearly inelastic. This is one reason why the secondary impacts occurred on the floor F7.0, as discussed in Section 2.5. The minor differences between the results for the floors F2.0 and F7.0 imply that the bearing structures below the floating floors did not affect the force generation on the floating floors differently.

When the floor coverings were installed on the CLT-floors, the low-frequency values of the force spectra and the impulses decreased. This phenomenon did not occur on all the rib slab floors. Interestingly however, installing the floor coverings on the floating floor structures increased these values.

When the floor covering was the multilayer parquet with the underlayment (floor types Fx.1), the shapes of the force spectra were similar on the respective source positions. The force spectra began to decrease around 100 Hz and reached their first local minima in the frequency range from 500 to 800 Hz depending on the source position. In the low-frequency range, the force spectra had values 0.96–1.29 N. Correspondingly, the impulses were between 0.48 Ns (nearly inelastic impact) and 0.64 Ns (near the geometrical mean value of the impulse). However, the differences between the results on the same floor corresponded to the level difference of at most 1.3 dB of the force input in the low-frequency range. The differences between the different source positions presumably originated from the different distances between the respective source position and the tongue-and-groove joint of the parquet. The resemblance of the results at the corresponding source positions was also prominent in the individual force pulses (see Appendix 3 of the supplementary material). The force pulses had often two local maxima, which probably occurred due to the behaviour of the surface structure under the hammer. When the hammer first hit the floor, the first local peak occurred. After this moment, the parquet shortly bended and during this the hammer and the floor were in contact. When the bending stopped, the second local maximum followed. The results imply that the structure under the multilayer parquet with the underlayment has little effect on the force input of this floor type, but the local behaviour of the parquet determines the driving force of the floor.

When the cushion vinyl was the floor covering (floor types Fx.2), the behaviour of the force spectra was similar to that of the floor types Fx.1 discussed above. The force spectra began to decrease around 100 Hz as with the parquet. However, the first local minima occurred at higher frequencies than on the floors Fx.1, at above 800 Hz. In the low-frequency range the force spectra had values between 0.98 and 1.23 N. Respectively, the impulses ranged from 0.49 Ns (nearly inelastic impact) to 0.62 Ns (near the geometrical mean value of the impulse). When the substructure under the cushion vinyl was the CLT-slab (floor F1.2) or the floating floor (floors F2.2 and F7.2), the differences between the impulses on different source positions were minor, and less than with the floor types Fx.1. In case of the floor F6.2, where the load bearing floor was the rib slab, the differences between the spectra and the impulses on different source positions were greater because of the different distance between the source positions and the ribs.

4.2. The time dependency of the impact force

The standards [1,2] state that the impact sound pressure levels can reveal time dependency after the tapping is started. Hence, the time dependency of the impact force excitation was also studied. According to the measurement results the impact force did not seem to vary over time. This is evident from the results of the individual force pulses presented in the Appendix 3 of the supplemental material (see also Fig. 7) and from the standard deviations of the force impulses (Table 2). This suggests that in case of the measured wooden floors the overall spectrum of the force excitation can be determined based on the first few impacts upon the floor after rather steady impacting conditions have been achieved. This

implies that the process of excitation of the wooden floors was not transient. Thus, the vibration of the measured wooden floors did not significantly affect the excitation force generated by the ISO tapping machine and a transient force model, such as presented in [11], might not be necessary to describe the impact force excitation on wooden floors.

5. Conclusions

This paper presented a procedure for measuring the impact force excitation generated by the ISO tapping machine and showed measurement results on 24 wooden floors. Such a wide experimental evidence has not been published previously in this field. The experiments were carried out with an instrumented ISO tapping machine, which measured the force generated in the impacts of the hammer upon the floor. With the described post-processing method, the impact force excitation driving the floor was determined. The measurement results were shown for the magnitude of the amplitude spectrum of the force and for the impulse generated in the collision of the hammer and the floor. Additionally, the average peak values and the duration of the force pulses were presented.

The differences between the force spectra on different wooden floors were prominent especially at frequencies above 500 Hz. Comparing the results with the spectra measured on concrete and steel structures shown in the literature revealed essential differences between the impact force excitation of wooden and concrete floors. At the frequencies below 100 Hz, the variation of the results was minor in comparison with the high frequencies. However, the variation in the low-frequency range corresponds to the level difference of over 3 dB of the force input. It was also noticed that the geometrical mean value of the impulse does not represent the actual value of the impulse exerted by the hammers on wooden floors.

The results for the force spectra and the impulses implied that the force driving the bare CLT-floors was rather independent on the position of the apparatus. However, in case of the rib slab floors, differences between the source positions were evident. This occurred due to the different distances between the source positions and the ribs. Adding plasterboards on the structure seemed to reduce the difference of the results between the source positions.

The force input on the bare floating floors and on the multilayer parquet with the underlayment was little influenced by the structure under these surface structures. This suggests that mostly the information of the floating structure and its material parameters are needed in order to evaluate the impact force excitation of these structures. Moreover, it was discovered that results on the floating floor did not depend on the source position. When the floor covering was the parquet, it was presumed that the differences between the source positions were caused by the different distances between the respective source position and the closest tongue-and-groove joint of the parquet.

When the floor covering was the cushion vinyl, the results were dependent on the source position only when the bearing structure was the rib slab. When the source position was between the ribs, the thin wooden deck behaved flexibly under the hammer, thus producing a lower force spectrum than at the position placed on the rib. On the other floors, the differences between the results of the source positions were minor.

According to the standards [1,2], the impact sound pressure levels can reveal time dependency after the tapping is started. The results of this paper showed that the process of excitation with the ISO tapping machine was not transient for the structures studied. Thus, no time dependency was detected, and the vibration of the measured wooden floors did not seem to influence the excitation force. This implies that a transient force model, such as presented in [11], might not be needed to describe the impact force excitation on wooden floors.

Declaration of Competing Interest

The authors declare that they have no known competing financial interests or personal relationships that could have appeared to influence the work reported in this paper.

Acknowledgements

The authors would like to thank Dr. Valtteri Hongisto and Mr. Ville Kovalainen for their constructive comments during the preparation of this manuscript. In addition, the authors would like to acknowledge Christian Berner Oy, Saint-Gobain Finland Oy, Stora Enso Oy and Upofloor Oy for donation of construction materials for this project.

Appendix A. Supplementary material

Supplementary data to this article can be found online at https://doi.org/10.1016/j.apacoust.2020.107821.

References

[1] ISO 10140–5. Acoustics – Laboratory measurement of sound insulation of building elements – Part 5: Requirements for test facilities and equipment. Geneva: International Organization for Standardization; 2010.
[2] ISO 16283–2. Acoustics – Field measurement of sound insulation in buildings and of building elements – Part 2: Impact sound insulation. Geneva: International Organization for Standardization; 2015.
[3] Rasmussen B, Machimbarrena M. Building acoustics throughout Europe—Volume 1: towards a common framework in building acoustics throughout Europe, COST Action TU0901, Brussels, 2014.
[4] Brunskog J, Hammer P. The interaction between the ISO tapping machine and lightweight floors. Acta Acust United with Acust 2003;89:296–308. , https://www.ingentaconnect.com/contentone/dav/aaua/2003/00000089/00000002/art00013.
[5] Cremer L, Heckl M, Petersson BAT. Structure-borne sound. 3rd ed. Berlin Heidelberg: Springer-Verlag; 2005.
[6] Heckl M, Rathe EJ. Relationship between the transmission loss and the impact-noise isolation of floor structures. J Acoust Soc Am 1963;35:1825–30. https://doi.org/10.1121/1.1918830.
[7] Cremer L, Heckl M, Ungar EE. Structure-borne sound. Berlin Heidelberg: Springer-Verlag; 1973.
[8] Vér IL. Impact noise isolation of composite floors. J Acoust Soc Am 1971;50:1043–50. https://doi.org/10.1121/1.1912726.
[9] Scholl W, Maysenhölder W. Impact sound insulation of timber floors: interaction between source, floor coverings and load bearing floor. Build Acoust 1999;6:43–61. https://doi.org/10.1260/1351010991501266.
[10] Lindblad S. Impact sound characteristics of resilient floor coverings. Lund Institute of Technology, Division of Building Technology, Bulletin 2, Lund, Sweden, 1968.
[11] Rabold A, Buchschmid M, Düster A, Müller G, Rank E. Modelling the excitation force of a standard tapping machine on lightweight floor structures. Build Acoust 2010;17:175–97. https://doi.org/10.1260/1351-010X.17.3.175.
[12] Wittstock V. On the spectral shape of the sound generated by standard tapping machines. Acta Acust United with Acust 2012;98:301–8. https://doi.org/10.3813/AAA.918513.
[13] Amiryarahmadi N, Kropp W, Bard D, Larsson K. Time-domain model of a tapping machine. In: Proc. Forum Acusticum 2011, Aalborg, Denmark, 2011, p. 1713–18.
[14] Coguenanff C, Guigou-Carter C, Jean P, Desceliers C. Probabilistic model of the impact force spectrum for the standard ISO tapping machine. In: Proc. 22nd Int. Congr. Sound Vib. ICSV 2015, Florence, Italy, 2015. p. 5551–58.
[15] Gudmundsson S. Sound insulation improvement of floating floors. A study of parameters. Lund Institute of Technology, Department of Building Acoustics, Report TVBA-3017, Lund, Sweden, 1984.
[16] Olsson J, Linderholt A. Force to sound pressure frequency response measurements using a modified tapping machine on timber floor structures. Eng Struct 2019;196:109343. https://doi.org/10.1016/j.engstruct.2019.109343.
[17] Jeon JY, Ryu JK, Jeong H, Tachibana H. Review of the impact ball in evaluating floor impact sound. Acta Acust United with Acust 2006;92:777–86. , https://www.ingentaconnect.com/content/dav/aaua/2006/00000092/00000005/art00014.

[18] Amiryarahmadi N, Kropp W, Larsson K. Identification of low-frequency forces induced by footsteps on lightweight floors. Acta Acust United with Acust 2016;102:45–57. https://doi.org/10.3813/AAA.918923.
[19] Brunskog J, Hammer P. Prediction model for the impact sound level of lightweight floors. Acta Acust United with Acust 2003;89:309–22. , https://www.ingentaconnect.com/contentone/dav/aaua/2003/00000089/00000002/art00014.
[20] ISO 9052–1. Acoustics – Determination of dynamic stiffness – Part 1: Materials used under floating floors in dwellings. Geneva: International Organization for Standardization; 1989.
[21] Ljunggren F, Simmons C, Hagberg K. Correlation between sound insulation and occupants' perception - Proposal of alternative single number rating of impact sound. Appl Acoust 2014;85:57–68. https://doi.org/10.1016/j.apacoust.2014.04.003.
[22] Ljunggren F, Simmons C, Öqvist R. Correlation between sound insulation and occupants' perception – Proposal of alternative single number rating of impact sound, part II. Appl Acoust 2017;123:143–51. https://doi.org/10.1016/j.apacoust.2017.03.014.

PUBLICATION II

Simulation of impact force generated by an ISO tapping machine on a wooden slab using explicit dynamics analysis

Jesse Lietzén, Juho Sormunen, Sami Pajunen, Mikko Kylläinen

Engineering Structures 270, article 114855
https://doi.org/10.1016/j.engstruct.2022.114855

Engineering Structures 270 (2022) 114855

Contents lists available at ScienceDirect

Engineering Structures

journal homepage: www.elsevier.com/locate/engstruct

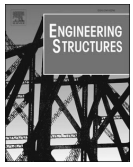

Simulation of impact force generated by an ISO tapping machine on a wooden slab using explicit dynamics analysis

Jesse Lietzén *, Juho Sormunen, Sami Pajunen, Mikko Kylliäinen

Tampere University, Faculty of Built Environment, Unit of Civil Engineering, Korkeakoulunkatu 5, P.O.Box 600 , 33014 Tampere University, Finland

ARTICLE INFO

Keywords:
Impact sound insulation
Impact force
FEM
Explicit time integration
LS-DYNA
Tapping machine
Wooden floor
CLT

ABSTRACT

Application of simulation tools to compute impact sound insulation properties of wooden floors has raised interests in recent decades. To achieve accurate results from the prediction models, information from force excitation generated by impact sound sources is required. The purpose of our study was to present a validated procedure to determine the non-linear impact force excitation generated by an ISO tapping machine. The method comprised use of finite element method (FEM) and explicit time integration to compute impact force pulse generated by a hammer of the tapping machine. With a post-processing procedure, the force pulses can be converted to present point forces describing the continuous operation of the tapping machine on the floor. To demonstrate the applicability of the method, the finite element model was applied to imitate an experimental situation on a cross-laminated timber (CLT) slab. The model validation showed that the computational model closely predicts the force pulse generated on the CLT slab. Findings from a sensitivity analysis revealed that local properties of the slab were the most important to the simulated impact force pulse. The findings of the analysis are helpful for those developing simulation tools to compute the impact force generated by the tapping machine on wooden floors.

1. Introduction

In the recent decades, the use of finite element method (FEM) and other simulation tools to compute impact sound insulation (ISI) of wooden floors has raised interests [1–5]. In a classic description, the prediction models have been divided in three parts: the excitation, the system, and the response. In this respect, the simulation tools make no exception when the ISI of the floor is of interest. In other words, the whole chain must be modelled correctly to achieve results corresponding the real equivalent. When focusing on the excitation, the force driving the structure must be known.

Requirements for the most widely used standardized impact sound source, the ISO standard tapping machine (STM), have been presented in the standards ISO 10140–5 [6] and ISO 16283–2 [7]. The STM has five steel hammers (mass of 500 g) which have spherical impact surfaces with curvature radius of 500 mm. The hammers are repeatedly dropped from 40 mm height one at the time on to the floor two times per second. This results in a total repetition rate of 10 Hz and the rate is 2 Hz for a single hammer. An essential feature of the STM is that the produced impact force depends on the interaction between the hammers and the floor [8,9]. The force spectrum produced by the apparatus, in terms of the magnitude spectrum, is constant on bare concrete slabs whereas on wooden floors the spectrum depends on the floor configuration [10]. The theoretic range of level difference of the spectrum is 6 dB in the low-frequency range, and the difference rapidly expands with the increasing frequency [8].

Several analytical models describing the impact force excitation generated by the STM have been presented in the literature. The models could roughly be divided into two categories based on their applicability for different types of structures: the simple models for stiff and heavy floor systems, such as concrete floors, and the general models applicable also for elastic floors. The simple models were presented by Heckl and Rathe [11], Lindblad [12], Vér [13], Cremer et al. [14], and Scholl and Maysenhölder [15]. Later on, the models of Lindblad [12], and Vér [13] have been further developed by Brunskog and Hammer [8], and Griffin [16], respectively. The general models were derived by Brunskog and Hammer [8], Rabold et al. [17], Wittstock [18] and Amiryarahmadi et al. [19]. Coguenanff et al. [20] presented a probabilistic model of the impact force generated by the STM. Thorough comparisons between some of the models can be found for example in refs. [8,17].

* Corresponding author.
E-mail address: jesse.lietzen@tuni.fi (J. Lietzén).

https://doi.org/10.1016/j.engstruct.2022.114855
Received 11 April 2022; Received in revised form 20 July 2022; Accepted 17 August 2022
Available online 2 September 2022

The simple models [11–14,16] assume a hard slab surface and a large driving-point impedance of the slab compared to the mass impedance of the hammer. Thus, these models are mainly suitable in describing the interaction between the STM and concrete floors. Even though the model of Scholl and Maysenhölder [15] represents the effect of the floor on the interaction by the mass of the floor, the model does not fully describe the interaction between the STM and wooden slabs [8]. In addition to bare concrete slabs, the models [12,13,15,16] can consider the effect of resilient floor coverings on the impact force on concrete slabs. In [8] these properties of the model of Lindblad [12] were applied by using the stiffness in the model to describe the local deformation of the slab and the resistance part to represent the energy transportation within the slab. In this manner, the model [8,12] has been used, e.g., by Mosharrof et al. [21] for wooden slabs.

The general models [8,17,18] can consider complex features of the floors making them better suitable for describing the interaction between the STM and the wooden floors. The model by Brunskog and Hammer [8] has been defined in frequency domain and it divides the frequency-dependent mobility of the slab into local and global parts. This division has also been used by Rabold et al. [17] where they presented models both in time and frequency domains taking into account a transient process of the relative velocities between the hammer and the slab. Thus, their models [17] suggest that the force excitation changes in time until reaching the steady state. The model of Wittstock [18] describes the contact between the hammer and the floor with a frequency-independent stiffness and a loss factor, and the global effects by driving-point mobility of the plate. The models [8,17] were developed for the needs of the ISI calculation of wooden floors, whereas Wittstock [18] was characterising the interaction between the hammers of the STM and an infinite reception plate, thus making his model better suitable for this special case.

The models [8,17], however, have few shortcomings regarding their use in the ISI simulations of the wooden floors. First, the models [8,17] require detailed information from the floor, such as the local and global driving-point mobilities, as input data to determine the impact force driving the floors. In a general situation of a complex wooden floor this means that, e.g., finite element models of the floor are required to model the sole excitation. Secondly, considering the temporally variable excitation process, as in [17], makes the calculation of the impact force tedious in comparison with the other models. According to a recent study [10], considering this kind of behaviour is not needed to describe the impact force excitation on wooden floors. Thirdly, the models [8,17] do not consider the geometric non-linearity caused by the spherical impact surfaces of the hammers. This effect is taken into account by Amiryarahmadi et al. [19] who modelled the contact force in time domain by applying non-linear Hertzian contact theory. However, using Boussinesq expression to describe the stiffness due to the local deformation [19] does not fully correspond to the behaviour of a wooden slab near the point of excitation [8].

An interesting and elaborate technique to compute the impact force excitation would be to simulate the impact itself by using a FEM tool. First benefit from this is that the method can be implemented as a part of the simulation process. Secondly, modern FEM tools allow to consider the non-linear behaviour of the contact between the hammers and the floor. Third, the floor could be modelled using complex material models and geometries with very few practical restrictions. In this study, we apply the techniques used in the field of *computational impact mechanics* to simulate the impact force generated by the STM. The field uses explicit time integration and FEM (later briefly called *explicit dynamics analysis*) for impact studies [22,23]. The use of explicit dynamics analysis can be justified with its applicability to compute short and complex non-linear impacts.

The object of this study is to present a procedure to determine the impact force excitation generated by the STM on a wooden floor by explicit dynamics analysis. With a post-processing procedure, the results from the analysis can be used to determine the point forces driving the simulation models in time and frequency domains. To demonstrate the use of the explicit dynamics analysis, simulations have been performed for a wooden cross-laminated timber (CLT) slab by imitating an experimental measurement situation. The second purpose of this study was to investigate how to model a CLT slab in sufficient detail and which parameters are most important to the results. This is an essential matter from acoustical engineers' and researchers' point of view when they are dealing with developing mathematical models predicting the ISI of wooden floors. The latter has been investigated by means of a sensitivity analysis.

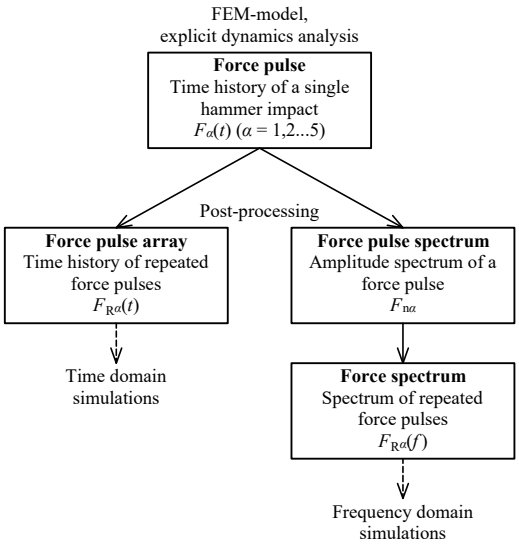

Fig. 1. Flowchart of the procedure for determining the point force generated by the STM.

2. Materials and methods

2.1. Procedure for determining the force generated by the STM

Impact force excitation generated by the STM on floors can be determined by a two-stage procedure illustrated in Fig. 1. The procedure aims to define the point force driving the floor both in time and frequency domains. These again can be utilized in ISI prediction models. First, the force pulse exerted by each of the five hammers must be known. At this stage, explicit dynamics analysis (FEM) is applied since it cost-efficiently enables describing the non-linear behaviour of the impact between the hammer and the floor. The second stage involves post-processing separately for time and frequency domain simulations. In the post-processing, the force pulses are converted into force quantities describing continuous operation of the STM.

Force pulse simulations are carried out within the time of contact, and when the hammer and the floor are disconnected no force driving the floor occurs. Thus, time history of the force $F_\alpha(t)$ of a single hammer α can be formulated extending the pulse signal with zeroes until the end of the period $T_r = 0.5$ s. In time domain, the excitation describing the continuous behaviour of the STM is a time history of repeated force pulses [8]. In frequency domain, the continuity is described with a Fourier spectrum for the repeated force pulses [8,18]. The force pulse array $F_{R\alpha}(t)$ and the force spectrum $F_{R\alpha}(f)$ can be determined for hammer α ($\alpha = 1,2\ldots5$) as follows:

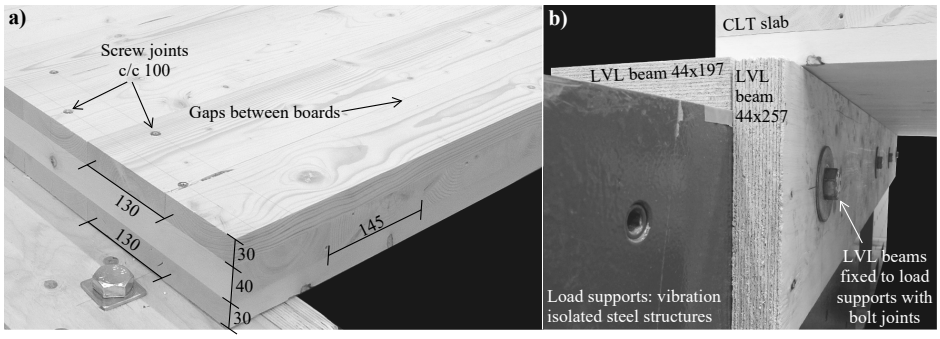

Fig. 2. CLT slab from a corner view (a) and supporting structures below another supported edge of the slab (b). Dimensions are presented in millimetres.

$$F_{R\alpha}(t) = \sum_{n=-\infty}^{\infty} F_{\alpha}(t - nT_r(1+k)) \tag{1}$$

$$F_{R\alpha}(f) = \sum_{n=-\infty}^{\infty} F_{n\alpha}\delta(f - nf_r) \tag{2}$$

where the constant k depends on the order of the hammer fall, $F_{n\alpha}$ is the amplitude of discrete frequency components, $f_r = 1/T_r$ is the repetition rate for a single hammer, $\delta(\bullet)$ denotes the Dirac delta function, and $i = \sqrt{-1}$ represents the imaginary unit [8,18]. When the impact order of the hammers is 1 – 3 – 5 – 2 – 4, k gets values:

$$k = \begin{cases} 0, if\alpha = 1 \\ 1/5, if\alpha = 3 \\ 2/5, if\alpha = 5 \\ 3/5, if\alpha = 2 \\ 4/5, if\alpha = 4 \end{cases} \tag{3}$$

The amplitude spectrum for a force pulse can be determined with a Fourier transform:

$$F_{n\alpha} = \frac{1}{T_r}\int_0^{T_r} F_{\alpha}(t - nT_r(1+k))e^{-2\pi ni/T_r}dt \tag{4}$$

which represents a two-sided presentation of the amplitude spectrum of the force $F_{\alpha}(t)$ [8]. The shift of the pulse signal leads to a phase shift of the force for all but the first impacting hammer [18]. For simulation purposes, we are interested of the single-sided amplitude spectrum of the force. This can be achieved by taking the positive side of the complex two-sided spectrum and multiplying it by a value of two.

As seen from **Eqs. (1–2)**, the only unknown is the time history of the force $F_{\alpha}(t)$ of a single hammer. A simulation procedure to determine the force pulse has been shown in Section 2.3. The simulations imitate the experiments presented in Section 2.2.

2.2. Experiments

The impact force excitation generated by the STM was investigated by experiments with an instrumented STM on a CLT slab [10]. The centre hammer of the apparatus was modified and equipped with a force sensor which was used to determine the impact force input into the floor. The force sensor lied between the hammer body and the modified hammer head. The hammer together with the equipment fulfilled the requirements for the tapping machines presented in the standards [6,7]. Since the force driving the floor $F_{floor}(t)$ was of interest but the force was measured between the hammer body and the hammer head, the sensor force signal $F_{sensor}(t)$ was corrected based on the mass difference of the total hammer and its body:

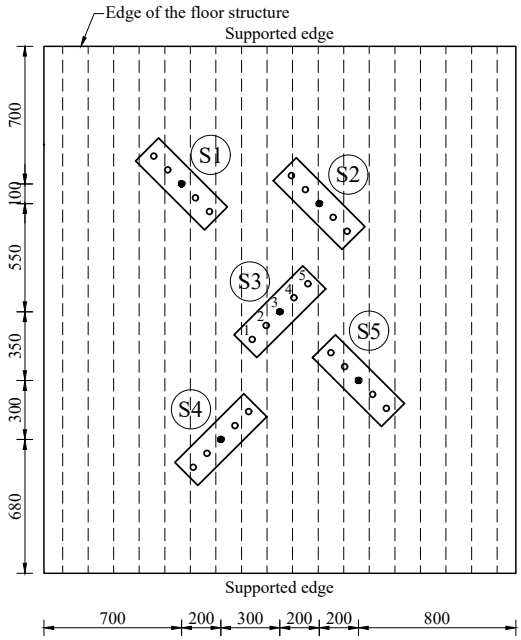

Fig. 3. Source positions S1–S5 on the floor structure (black circles). The rectangular boxes and the circles illustrate the orientation of the ISO tapping machine and the other hammers, and the dotted lines the board edges of the outer lamellae. Hammers for the tapping machine at source position S3 are numbered. Dimensions are presented in millimetres.

$$F_{floor}(t) = \frac{m_h}{m_h - m_c}F_{sensor}(t) = 1.061 \cdot F_{sensor}(t) \tag{5}$$

where m_h is the total mass of the instrumented hammer (503 g), and m_c denotes the mass of the hammer head (29 g). For more information from the hammer instrumentation and the experiments, see [10].

2.2.1. Floor slab

The floor slab under study was a 100 mm thick 3-layered CLT slab which had lamellae of thicknesses 30, 40, and 30 mm as depicted in Fig. 2**a**. Individual boards of the slab were attached to each other only from their broader sides, i.e., the narrow sides of the boards were unglued. Therefore, slight gaps between the boards were present and their

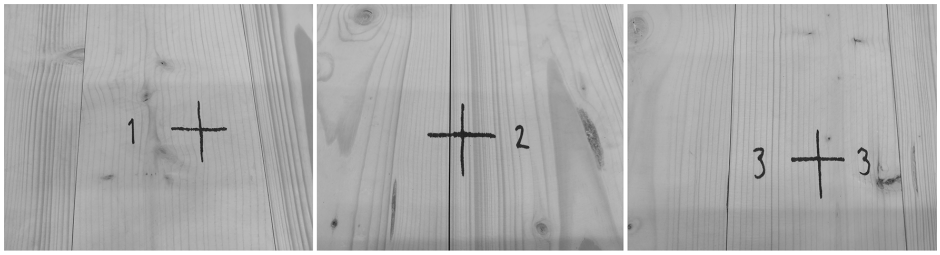

Fig. 4. Locations of the source positions S1, S2, and S3 and their distances from the board edges.

Table 1
Distances of the source positions S1–S5 from the board edges. The values follow the slab orientation depicted in Fig. 3.

Source position	Distance from the board edges [mm]	
	Left	Right
S1	85	45
S2	5	125
S3	65	65
S4	25	105
S5	75	55

maximum width was 1 mm [24]. Main widths of the boards in the outer lamellae and in the centre of the slab were 130, and 145 mm, respectively. Fig. 2**a** illustrates the CLT slab from its corner, where most of the abovementioned features can be seen.

Span of the CLT slab was 2.68 m and the outer layers of the slab ran parallel to this bearing direction. The width of the slab was 2.4 m. The slab was supported from its both ends to stiff laminated-veneer-lumber (LVL) beams with screw joints (Fig. 2**a**). The long sides of the slab were unsupported. The LVL beams were fixed into vibration isolated steel structures placed on the floor of the laboratory (Fig. 2**b**). This was done to prevent the possible vibrational background noise caused in the surroundings of the experiments. For more information on the structures and their installations, see [10]. As illustrated by Fig. 2, major part of the slab was constructed from timber sawn near the pith of the tree. Thus, the lamellae mainly consisted of heartwood where annual rings of the trees were visible.

2.2.2. Measurement positions

The force measurements were carried out at five source positions S1–S5 on the floor (Fig. 3). At each source position, the STM was oriented at a 45° angle to the bearing direction of the CLT slab. The position S3 was located at the centre of the floor structure. During the measurements, the STM operated normally on the floor and the time history of the impact force subjected to the sensor was recorded. The measurement duration at each position was approximately 30 s and the sampling frequency was 12800 Hz. Because the tapping machine drops its hammers two times per second, the number of full impacts generated by the hammer at the source positions was 60 or 61.

Fig. 4 shows an example of the location of the source positions S1, S2, and S3 and their distances from the closest board edges. The position S3 lied in the centre of the board and the S2 was in the furthermost location from the centre; the other positions lied between these extremes. The distances from all the source positions to the closest board edges have been shown correspondingly in Table 1.

2.3. Simulations

The force pulse generated by a hammer of the STM was simulated applying explicit dynamics analysis. Simulations were performed using a FEM program Ansys LS-DYNA (smp s R10.1.0 Revision: 123264).

2.3.1. Governing equations

Collision of two bodies (a hammer and a slab) can be described by a mathematical model in which the time-dependent motion of two structural domains Ω_{hammer} and Ω_{slab} causes contact between them. The domains are separate and their respective boundaries $\partial\Omega_{hammer}$ and $\partial\Omega_{slab}$ do not intersect during the collision since the deformed bodies cannot penetrate. Thus, their equations of motions remain uncoupled [25].

For brevity, the system and its finite element formulation is shown for a general domain Ω enclosed by its boundary $\partial\Omega$. The partial differential equation of motion describing the system inside the domain Ω is:

$$\nabla\cdot\boldsymbol{\sigma}+\rho\boldsymbol{f}=\rho\ddot{\boldsymbol{x}} \tag{6}$$

where $\boldsymbol{\sigma}$ is the Cauchy stress tensor, ρ is the density, $\boldsymbol{f}$ is the body force density, and $\ddot{x}$ is the acceleration (second-order time derivative of displacement) [23,25]. The equation must satisfy the boundary conditions for traction, displacement, and contact discontinuity on boundaries $\partial\Omega_1$, $\partial\Omega_2$, and $\partial\Omega_3$, respectively. These boundary conditions are:

$$\boldsymbol{\sigma}\cdot\boldsymbol{n}=\boldsymbol{t}(t) \tag{7}$$

$$\boldsymbol{x}(X_\alpha,t)=\boldsymbol{D}(t) \tag{8}$$

$$(\boldsymbol{\sigma}^{+}-\boldsymbol{\sigma}^{-})\cdot\boldsymbol{n}=0 \tag{9}$$

where $\boldsymbol{n}$ represents a unit outward normal to a boundary on $\partial\Omega$, $\boldsymbol{t}$ is the applied traction load, $\boldsymbol{D}$ is the specified displacement [23,25].

The deformation is expressed in terms of the convected coordinates [25]:

$$x_i=x_i(X_\alpha,t) \tag{10}$$

where $X_\alpha(\alpha=1,2,3)$ represents a point in undeformed geometry and $x_i(i=1,2,3)$ a moved point in the same fixed rectangular cartesian coordinate system. At time $t_0=0$, the given initial displacement $\boldsymbol{X}^0$ and velocity $\boldsymbol{V}^0$ inside the domain Ω are, respectively [25]:

$$x_i(\boldsymbol{X},0)=X_i^{\,0} \tag{11}$$

$$\dot{x}_i(\boldsymbol{X},0)=V_i^{\,0}(\boldsymbol{X}) \tag{12}$$

After a few mathematical operations, the weak integral form of the equilibrium equation becomes:

$$\int_\Omega\rho\ddot{\boldsymbol{x}}\delta\boldsymbol{x}d\Omega=-\int_\Omega\boldsymbol{\sigma}\delta\boldsymbol{x}d\Omega+\int_\Omega\rho\boldsymbol{f}\delta\boldsymbol{x}d\Omega+\int_{\partial\Omega_1}\boldsymbol{t}\delta\boldsymbol{x}ds \tag{13}$$

where $\delta\boldsymbol{x}$ denotes the variation of displacement, c.f. principle of virtual work [25]. By applying an approximation for the displacement field, we superimpose a mesh of finite elements [25]:

$$x_i(X_\alpha,t)=x_i(X_\alpha(\xi,\eta,\zeta),t)=\sum_{j=1}^{k}N_j(\xi,\eta,\zeta)x_i^{\,j}(t) \tag{14}$$

where N_j are shape functions describing the displacement field within the elements. The finite element formulation of the problem is:

$$\sum_{m=1}^{n}\int_{\Omega}\rho N_m^T N_m \boldsymbol{a} d\Omega = \sum_{m=1}^{n}\left(-\int_{\Omega}\boldsymbol{B}_m^T\boldsymbol{\sigma}d\Omega + \int_{\Omega}\rho N_m^T\boldsymbol{b}d\Omega + \int_{\partial\Omega_1}N_m^T\boldsymbol{t}ds\right) \quad (15)$$

where $\boldsymbol{a}$ is the nodal acceleration vector, $\mathbf{B}$ is the strain–displacement matrix, and $\boldsymbol{b}$ is the body force load vector [25]. This equation can be recognized as one form of Newton's second law in matrix presentation [23,25]:

$$\mathbf{M}\boldsymbol{a}^n = \mathbf{F}^n \quad (16)$$

The dynamics of the system, i.e., the nodal acceleration, velocity and displacement vectors $\boldsymbol{a}$, $\boldsymbol{v}$, $\boldsymbol{u}$ in time domain, respectively, is solved by applying explicit time integration. The commonly used central difference time integration method is also implemented in LS-DYNA [25]. The method allows direct calculation of the nodal acceleration vector:

$$\boldsymbol{a}^n = \mathbf{M}^{-1}\mathbf{F}^n \quad (17)$$

$$\boldsymbol{v}^{n+1/2} = \boldsymbol{v}^{n-1/2} + \boldsymbol{a}^n\Delta t^n \quad (18)$$

$$\boldsymbol{u}^{n+1} = \boldsymbol{u}^n + \boldsymbol{v}^{n+1/2}\Delta t^{n+1/2} \quad (19)$$

where.

$$\Delta t^{n+1/2} = (\Delta t^n + \Delta t^{n+1})/2 \quad (20)$$

Because the mass matrix $\mathbf{M}$ is diagonal, instead of inverting the mass matrix, the nodal acceleration $\boldsymbol{a}$ in each time step is calculated by a simple division. After solving the nodal displacement vector $\boldsymbol{u}$, the initial geometry is updated, and the force matrix $\mathbf{F}$ is recalculated. This loop is repeated until the time of interest is reached. [23,25].

As seen from the above, the diagonal mass matrix $\mathbf{M}$ increases the efficiency of the time integration. This is one of the main features of the explicit dynamic method and means that the system consists of lumped elements, which are calculated separately. The diagonal mass matrix can be used since there is no loss of accuracy in comparison with the use of the consistent mass matrix [23,26]. Moreover, this leads to a requirement that the sound wave cannot travel to the other side of the element within the time step Δt. Therefore, to ensure a stable solution, the time step must be set below the critical time step:

$$\Delta t_{crit} = 2/\omega_{max} \quad (21)$$

where ω_{max} denotes the largest elemental natural frequency of the structure in consideration. However, to increase the accuracy of the model, it is beneficial to use smaller time steps (or reduce the element sizes) [23].

The contact between the two domains Ω_{hammer} and Ω_{slab} is primarily modelled as frictional using a Coulomb formulation [25]. Thus, the frictional force at time n ($\boldsymbol{f}_n$) can be calculated, when the frictional coefficient μ, and the tangential contact force F_y are known:

$$F_y = \mu|\boldsymbol{f}_n| \quad (22)$$

where

$$\mu = \mu_d + (\mu_s - \mu_d)e^{-c|\boldsymbol{v}|} \quad (23)$$

where μ_s denotes the static and μ_d the dynamic frictional coefficients, and $\boldsymbol{v}$ is the relative velocity between the element nodes in contact.

2.3.2. Model settings and geometry

For the contact problem between the hammer and the CLT slab, imitating the experiments (see Section 2.2), the terms including the effects of both the body force loads $\boldsymbol{b}$ and the tractions on the boundary $\boldsymbol{t}$ in

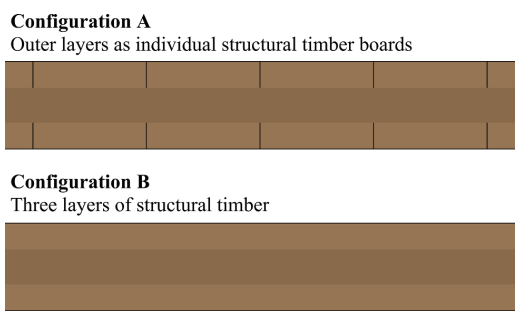

Fig. 5. Slab modelling configurations. Configuration A has primarily been applied in the simulations.

Eq. (11) were regarded insignificant. Thus, the gravitational forces and the load from the legs of the STM to the slab were neglected in the simulations. The vertical displacements on the supported edges (see Fig. 3) were set to 0 mm. The FEM-model was built by using linear 8-node hexahedron solid elements of type −2 (LS-DYNA) with modified Jacobian matrix to prevent locking of elements during the impact [25].

In the experiments [10], it was found out that there was little temporal variation in the measured impact force pulses. It was concluded that the vibration of the slab did not significantly contribute to the force pulses [10]. Because of this, initially the CLT slab was at rest in the simulations. The hammer of the STM was dropped from a height of 40 mm to the CLT slab. Hence, the initial velocity of the hammer $\boldsymbol{V}^0$ was 0.886 m/s and the $\boldsymbol{X}^0$ of the CLT slab was zero (c.f. **Eqs. (11–12)**). The simulations for the model validation were carried out at each source position S1–S5 (Fig. 3).

The contacts between the hammer and the slab were modelled by using a penalty method (LS-DYNA keyword: *CONTACT_AUTOMATIC_SINGLE_SURFACE [27]) and the contact forces were read with a force transducer contact (*CONTACT_FORCE_TRANSDUCER_PENALTY [27]). Both the static and the dynamic frictional coefficients μ_s and μ_d were set to a value 0.5. Hence, according to **Eq. (23)** the frictional coefficient μ reduces to $\mu = \mu_d = 0.5$. The hammer of the STM represented a simplified model of the instrumented hammer used in the experiments (see Section 2.2). The impacting head of the hammer was modelled to represent closely the real hammer head in the measurements, but the body with the sensors and additional parts of the hammer was modelled as a simplified cylinder with diameter of 20 mm. The height of the cylinder was adjusted so that the total mass of the modelled hammer corresponded to m_h = 503 g [10]. In the analyses the hammer was treated as an ideal impact source and, thus, all the possible imperfections of the STM [6,18], such as the possible variation in velocity at impact, were neglected.

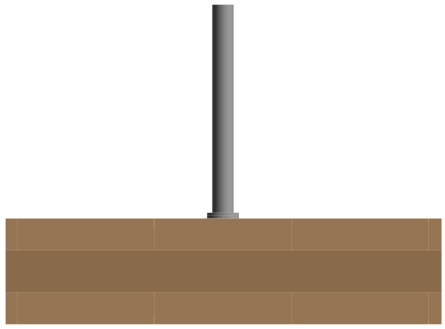

Fig. 6. Geometry of the model near the impact area.

Table 2
Material parameters describing the linear isotropic elastic behaviour of the hammer. The bolded values are the average parameters presented by the standards EN 1993–1-1 and EN 1993–1-4 [29,30].

Material parameter	ρ [kg/m^3]	E [MPa]	ν [-]
Steel hammer	7 641	**205 000**	**0.3**

The simulations were carried out for two slab modelling configurations (Fig. 5) where the structural timber layers were meshed together. Thus, it has been assumed that glue layers between structural timber layers are very thin and the glue perfectly connects the timber layers. In the configuration A, the outer lamellae of the CLT slab were modelled as individual structural timber boards. In this configuration, no contacts were defined between the narrow sides of the lamellae. Note, however, that this procedure prevents the boards from contacting adjacent boards. In the configuration B, the CLT slab was modelled with three continuous structural timber layers. In both configurations the direction of the boards determined the principal axes of the lamellae. Since the configuration A presents the slab in the experiments in a more detailed way, this configuration has primarily been applied in the simulations. The slab configuration B was used in the sensitivity analysis.

Fig. 6 shows the geometry of the model near the impact area when the hammer was at the source position S3 in the centre of the CLT slab's surface. In the beginning of the simulation, the tip of the hammer head was in contact with the slab in a single point and the hammer was just dropped to the slab.

2.3.3. Material parameters

The hammer of the STM was modelled as linear isotropic elastic material (*MAT_ELASTIC [28]), and the boards of the slab as linear orthotropic elastic material (*MAT_ORTHOTROPIC_ELASTIC [28]). Table 2 shows the material parameters used to describe the behaviour of the steel hammer. Density of the hammer head was determined based on its mass (29 g) and known volume. The density of the whole hammer was assumed to be the same. Modulus of elasticity E, and the Poisson's ratio ν of the hammer were not known but they were presumed to correspond with the average parameters of structural and stainless steels [29,30].

According to the European Technical Assessment for the CLT slab [24], the wood species used in the product was European spruce or equivalent softwood. In this study, it has been presumed that the wood species used in the lamellae was European (or Norway) spruce (*Picea abies* (L.) Karst.) and no other wood species was present to a significant extent. The individual boards of the CLT slab may be described as a linear orthotropic elastic material whose three principal axes are longitudinal (L), radial (R), and tangential (T) axes with respect to the fibre direction and annual rings of the timber [31]. In major part of the simulations, these axes were assumed to correspond the local coordinate axes of the CLT lamellae in a cartesian coordinate system. However, in a part of the sensitivity analysis, the material parameters were partly in a cylindrical coordinate system by locally rotating the system. Strength class of the boards according to standard EN 338 [32] was mainly C24 but 10 % of the material could be included from the class C16 [24]. In addition to the density ρ of the material, the standard EN 338 presents three of the nine independent constants describing the orthotropic behaviour of the boards: moduli of elasticity E_L and E_T, and shear modulus G_{LT}. These parameters present mean characteristic values for structural timber made from softwood in corresponding strength classes [32].

Values for all the parameters needed to completely describe the linear orthotropic elastic material have not been presented by the standard EN 338. The remaining six constants E_R, G_{LR}, G_{RT} and the Poisson's ratios ν_{LR}, ν_{LT}, and ν_{TR} have been derived from the measurement results for the Norway spruce presented by Keunecke et al. [33]. This has been carried out by scaling the results presented by the study [33] for the modulus of elasticity E_R and the shear moduli G_{LR}, and G_{RT} with respect to the values of E_L and G_{LT} presented by the standard EN 338, respectively. The Poisson's ratios have been adopted straight from [33] by presuming their dependence on the strength classes insignificant. This approach was used to determine the material parameters for the European (or Norway) spruce in strength classes C24, C16, and C30 (Table 3). The values for C24 have primarily been used to describe the behaviour of the individual boards of the CLT slab under study. The values for C16, and C30 have been used in the sensitivity analysis.

2.4. Calculation results for the force pulses

The contact force pulse $F(t)$ during the impact was derived from the simulations by filtering the result with a Butterworth filter of which cut-off frequency was 6000 Hz (in building acoustics, the most interesting frequency range is 20–5000 Hz). In addition to the time history, a two-sided amplitude spectrum of the force F_n (**Eq. (4)**), a mechanical impulse I, i.e., change in the momentum, and a low-frequency force F_{lf} were calculated. The relation between the mechanical impulse I, and low-frequency force F_{lf} is:

$$F_{lf} = \frac{1}{T_r} I = \frac{1}{T_r} \int_0^{T_r} F(t)dt \tag{24}$$

when the low-frequency force corresponds to the limit value of F_n, when frequency f approaches 0 Hz [8]. To achieve comparable scalars describing the magnitude and the duration of the force pulse $F(t)$, the peak value of the force (F_{peak}) and the length of the pulse (T_{pulse}) were also determined.

2.5. Model validation and sensitivity analysis

The finite element model was validated by comparing the simulation results with the measurement results from the experiments (see Section 2.2). In the model, the strength class of the CLT slab was C24 (see Section 2.3.3), and the simulations were done applying the slab modelling configuration A (Fig. 5). The modelling process was carried out in two steps: first, the element mesh was determined based on a mesh convergence study; secondly, the chosen mesh was used in the calculations. The simulation results were received from the body interaction contact between the hammer and the slab imitating the experimental situation [10]. The validated model was further applied for sensitivity analysis. Purpose of this analysis was to investigate which parameters are the most important or sensitive to the results and how to model a CLT slab in sufficient detail. Moreover, the validated model was applied to compute force results for all hammers in an example situation. These results were post-processed to reach input values applicable for time and frequency domain simulations as illustrated in Section 2.1.

Table 3
Material parameters describing the linear orthotropic elastic behaviour of European (or Norway) spruce in strength classes C24, C16, and C30. The bolded values are the parameters presented by the standard EN 338 [32]. The remaining values have been derived from the measurement results presented by Keunecke et al. [33].

Strength class	ρ [kg/m^3]	E_L [MPa]	E_R [MPa]	E_T [MPa]	ν_{LR} [-]	ν_{LT} [-]	ν_{TR} [-]	G_{LR} [MPa]	G_{LT} [MPa]	G_{RT} [MPa]
C24	**420**	**11 000**	537	**370**	0.36	0.45	0.21	725	**690**	62
C16	**370**	**8 000**	391	**270**	0.36	0.45	0.21	526	**500**	45
C30	**460**	**12 000**	586	**400**	0.36	0.45	0.21	788	**750**	68

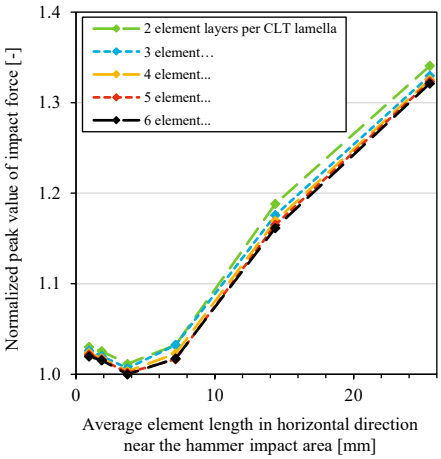

Fig. 7. Mesh convergence study at source position S3.

3. Results

3.1. Validation results

As discussed in Section 2.3.1, it is important to have a valid mesh to get relevant results from the explicit dynamics analysis. Thus, the model validation began with a mesh convergence study carried out at the source position S3. In the study, the element mesh of the CLT slab was varied in two different ways. First, the number of element layers through one CLT lamella ranged between two and six. Secondly, the average element length in horizontal direction near the impact area was reduced in steps from 25 mm to 1 mm. Outside the impact area, the element length in the horizontal direction was set to approx. 28 mm. The mesh of the hammer was kept constant in the convergence study with element lengths between 1.4 and 3.0 mm and 2.4 to 8.6 mm for the hammer head and body, respectively.

Fig. 7 shows the results of the mesh convergence study by normalizing the determined peak values of impact force with the lowest result of the study. The figure illustrates how the element mesh affects the results: when the mesh is coarse, the CLT slab is overly stiff and leads to overestimated impact force; when the element length is decreased, there exists an element dimension after which a denser mesh does not

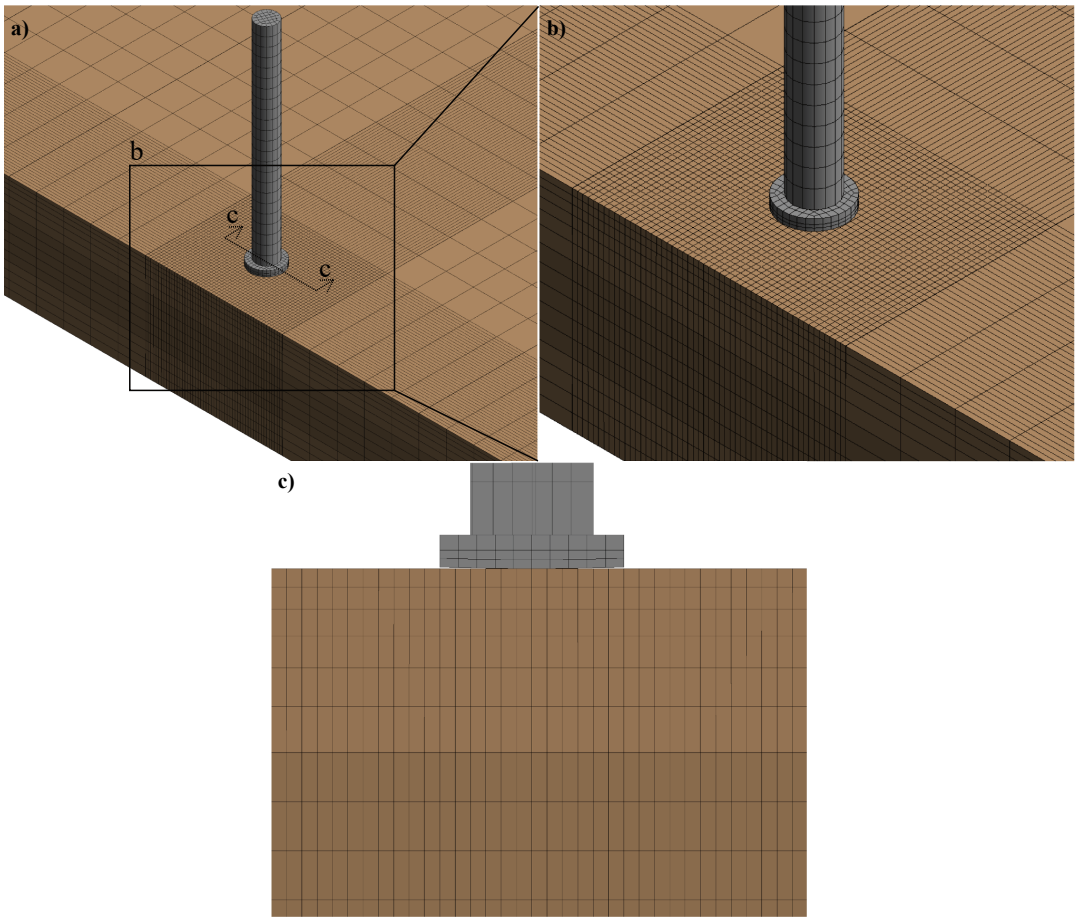

Fig. 8. Element mesh of the hammer and the slab: a) hammer and impact area, b) impact area magnified, c) cross section of impact area. Note that the elements on the left side of the Fig. 8a and 8b have been hidden to highlight the mesh in the sectional direction.

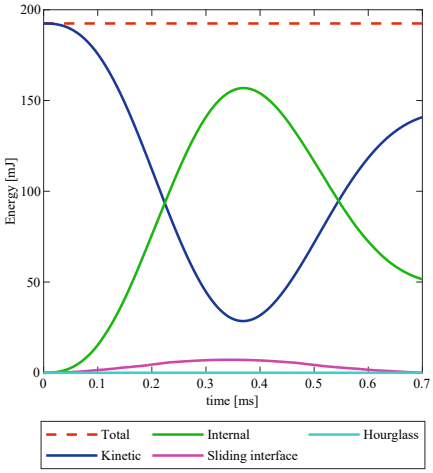

Fig. 9. Energy balance of the simulation.

drastically improve the accuracy of the model. Furthermore, the figure shows that the convergence decelerates with shorter horizontal element lengths. This is probably influenced by the size and aspect ratios of the elements of the hammer and the CLT slab further away from the impact area.

Based on the results of the mesh convergence study (Fig. 7), the mesh used in the analysis was constructed from elements of average length 2.5 mm near the impact area. Elsewhere the mesh was coarser, and the element length was set to approx. 28 mm. Furthermore, the upper CLT lamella was formed from six, the centre lamella from five, and the lowest lamella from four elements through the thickness of the layer. This criterium was kept for the whole slab as in the mesh convergence study. For the whole model at the source position S3, the number of elements was 267,724 and the number of nodes 313244. Fig. 8 illustrates the element mesh near the impact area including the hammer and the slab.

Due to the collision of the hammer and the CLT slab, kinetic energy transfers into the slab, and the energy balance is a function of time. An example of this has been shown in Fig. 9 by using the model described above (source position S3). The total energy of the system was 192.5 mJ, which initially consisted of kinetic energy only. Since energy cannot transfer outside the modelled system, the total energy stays at this constant level. During the interaction of the hammer and the slab kinetic energy transfers into internal energy and into the energy of the sliding interface. The change in the kinetic energy before and after the collision represents energy dissipation. Hourglass energy during the impact is zero because of the chosen element type (see Section 2.3.2). Nonzero hourglass energy would imply nonphysical behaviour of the model.

Fig. 10 depicts the comparison of the simulated and measured force pulses in time and frequency domains. The figure shows the measured and the simulated contact force pulses $F(t)$ and magnitudes of their amplitude spectra F_n at the source positions S1…S5. To ease comparison, the measured force pulses have been centred according to the peak values of the simulation results. Hence the nonzero values before t_0. The peak value of the force F_{peak}, the low-frequency force F_{lf}, the mechanical impulse I, and the length of the pulse T_{pulse} have been presented in Table 4 for the measured and simulated force pulses. The measurement results presented in Fig. 10 and Table 4 have been reproduced from [10] by using a correction factor as in **Eq. (5)**.

Fig. 10 and Table 4 indicated reasonable equivalency of the measurement and simulation results. Thus, the simulation model was regarded valid. However, it is noticeable that the computational model led to minor spatial variation in comparison with the measurement results. The simulation seemed to closely predict the measured peak value of the force F_{peak} at the source positions S3, and S5. Additionally, the low-frequency force F_{lf}, and the mechanical impulse I of the simulation results were near equivalent with the measurement result at the source position S4. Minor discrepancies between the measurement and simulation results at the source positions S1, and S2 were prominent. Moreover, the lengths of the simulated force pulses were shorter than the measured values at all the source positions. This can be explained with the low time resolution of the measurements in comparison with the simulations [10]. The magnitude spectra of the simulation results resembled the measured spectra closely and minor differences were prominent at frequencies above 2000 Hz. In the low-frequency range, discrepancies between the measured and the simulated F_{lf} results correspond with a 0.7 dB level difference at the source position S2 [8]. At other positions differences were smaller.

The simulations produced results near the measured maximum both in time and frequency domains. As can be seen, there was little spatial variation in the simulation results whereas the measured results varied greater (Table 4). The source positions S3, and S5, where the maximum peak value of the force F_{peak} was measured, lied near the centre of the boards (Table 1). At these positions, the F_{peak} of the simulated force pulses also reached their maximum values. Moreover, the source position S2 lied at the furthermost location from the centre of the board. At this position, both the measured and simulated force pulses got their lowest values for F_{peak}. This behaviour suggests that the local properties of the CLT slab affect the impact force.

To study the importance of the local properties to the impact force pulse, deformation process of the slab under the hammer has been illustrated in Fig. 11. As an example, the figure depicts the total (elastic) deformation of the CLT slab during the impact from 0.1 to 0.7 ms at the source positions S1, S2, and S3. The results show that the maximum deformation occured straight under the tip of the hammer head and when the impact force pulse was near its peak value (cf. Fig. 10). Furthermore, only a minor part of the slab was deformed during the impact, which suggests that for a short impact the global behaviour of the slab is not of importance from the point of view of the single impact force pulse. Additionally, the non-linear interaction between the hammer and the slab can be seen from Fig. 11 since the contact surface between the hammer and the slab is a function of time. The effect of the local and global properties to the impact force and reasons causing the differences between the measurement results at different source positions were studied with the sensitivity analysis.

3.2. Sensitivity analysis

The sensitivity analysis was carried out in six phases. For the sake of simplicity, the sensitivity of different parameters on the simulation results have been shown by comparing the results for the peak values of the force F_{peak}. First, to study the effect of the global source position on the impact force, simulations with the validated model were repeated applying the slab configuration B (Fig. 5). The configuration ignores the gaps between the boards of the CLT slab but otherwise the computational model was created similarly than the model in validation. The simulations were carried out at all the source positions S1–S5, and the comparison of the F_{peak} with the measurement results and the results from the validated model have been shown in Fig. 12. According to the simulation results for the configuration B, the maximum change in the F_{peak} was 2.9 N between source positions S1 and S3, when the lowest levels occurred at S3. The results imply that the impact force pulse is insensitive to the global position of the hammer on the slab, but the local properties of the CLT must explain spatial variation in the measurement results. The sensitivity analysis was continued with the slab modelling configuration A and the analyses were performed at the centre of the CLT slab, c.f. the source position S3.

To further study the effect of the global properties on the impact force, the sensitivity analysis was continued in the second phase by

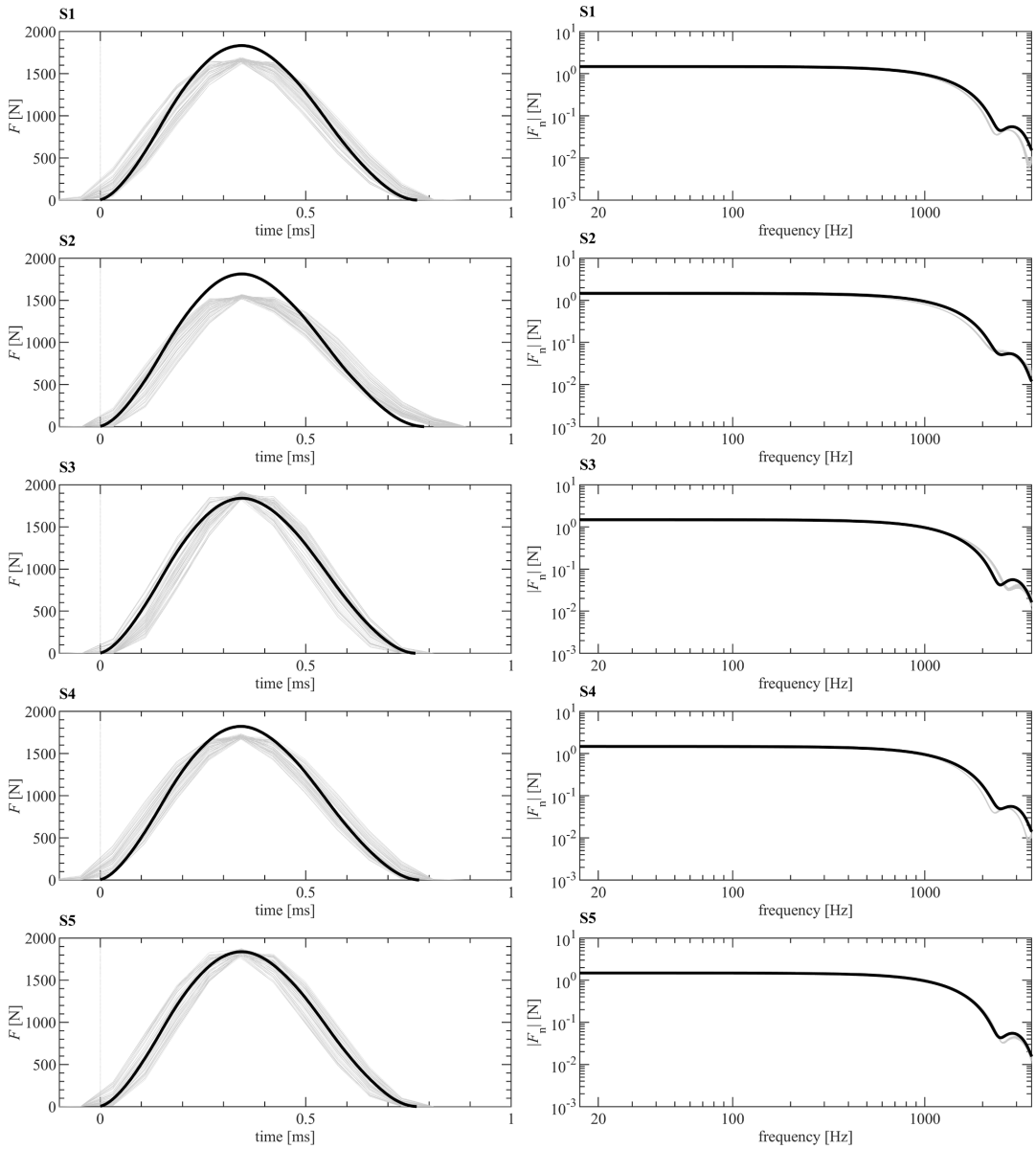

Fig. 10. Simulated contact force pulses $F(t)$ and magnitudes for their two-sided amplitude spectra F_n at the source positions S1…S5 (black lines) and the corresponding measurement results from the experiments [10] (thin grey lines). Note the overlapping of the results.

varying the CLT slab size (or the boundary conditions) by shortening the length and the width of the slab in 200 mm steps. The results of the study show that the floor size has minor effect on the peak value of the force and reducing the size of the floor does not significantly decrease the accuracy of the simulation results (Fig. 13). This occurred probably due to the short duration of the impact (less than 1 ms, see Table 4) when the reflecting stress wave did not reach from the boundaries of the CLT slab to the contact position within the time of impact even if the floor size was diminished. Thus, in the modelled situation it is justified to simulate the contact force pulse by reducing the size of the floor. The sensitivity analysis was proceeded with a CLT slab of size 1000 mm × 1000 mm to reduce calculation time.

Thirdly, the effect of the friction between the colliding bodies on the results was studied by changing the friction coefficients exaggeratedly from 0.5 to 0 and 1. The main motivation for the analysis was to find out if the friction coefficient is an important parameter for the analysis since exact values for different structures are not necessarily known. Fig. 14 shows the peak values of the force when the friction coefficients (both static and dynamic) between the hammer and the slab are 0, 0.5, and 1. The results indicate that the friction affects the results minorly. This

Table 4
Scalar values determined for the measured and simulated force pulses. Measured values show the average results based on all the measured force pulses at the corresponding source position.

Source position	Measured (M)/ Simulated (S)	F_{peak} [N]	F_{lf} [N]	I [Ns]	T_{pulse} [ms]
S1	M	1662.5	1.42	0.71	0.99
	S	1833.4	1.48	0.74	0.77
S2	M	1546.3	1.36	0.68	1.02
	S	1813.3	1.47	0.74	0.79
S3	M	1878.5	1.40	0.70	0.91
	S	1839.3	1.48	0.74	0.77
S4	M	1699.4	1.47	0.74	1.01
	S	1822.2	1.48	0.74	0.78
S5	M	1832.8	1.45	0.73	0.94
	S	1838.2	1.48	0.74	0.77

occurred probably due to the normal incidence of the hammer relative to the surface of the slab. The sensitivity analysis was continued with the friction coefficients 0.5.

The impact force is affected by local properties in the horizontal direction of the slab, as shown by Figs. 10–12. Because of this, the local effects in the sectional direction of the CLT slab were studied with two analyses. First, the effect of the strength class of the centre lamella on the results was analysed by varying it from C24 to C16 and C30 while the upper and the lower lamellae were C24. Secondly, the effect was analysed with introducing imaginary materials to the analysis by increasing the stiffness parameters of the lamellae so that the moduli of elasticity and the shear moduli were magnified tenfold (material X10). Physically this could represent material of a hard tree knot, but the intention was to consider the effect of a drastic change in stiffness of the material. The results of these analyses have been shown in Fig. 15. According to the results, the strength class of the centre lamella has a minor effect on the impact force, but drastic changes in the stiffness properties can have a major effect on the impact force especially if the upper lamellae changes (c.f. tree knots near the impact area).

The material parameters of real wood are not constant but vary depending on the tree and between the specimens [33]. Because of this, the effect of the material parameters of the boards on the impact force was studied. The motivation for the analysis was to find out if the differences of the material parameters would explain the discrepancies between the simulation and the measurement results and especially the variation between the measurement results between source positions. In the study, the calculations were conducted by varying a single material parameter at a time. The varied material parameters were the density ρ, moduli of elasticity E_L, E_R, and E_T, Poisson's ratios (ν_{LR}, ν_{LT}, and ν_{TR} simultaneously), and the shear moduli G_{LR}, G_{LT}, and G_{RT}. The range of the material parameters was such that the lower values correspond to the material parameters for spruce in the strength class C16 and the higher values to the parameters for spruce in the class C30 (see Table 3). The results for the analysis (Fig. 16) depict that the modulus of elasticity E_R, the shear modulus G_{LR}, and the density ρ have the greatest effect on the peak value of the force.

The CLT slab used in the measurements was mainly made from heartwood near the location of the pith (see Fig. 2). The boards were oriented so that the broad side closer to the pith could lay on either upwards or downwards in the slab. Thus, using the cartesian coordinate system describing the material of the timber boards is a simplification of the real situation. The effect of this simplification and the use of heartwood and sapwood on the results was analysed by replacing the cartesian coordinate system of the impacted upmost timber board with a locally rotated cartesian coordinate system with different origins from the pith. From the point of view of the boards, this corresponds to a cylindrical coordinate system. Boards from four different locations relative to the distance from the pith perpendicularly from the centre of the lower edge of the lamellae were studied: A) heartwood, distance from the pith 0 mm, B) heartwood of a large log, distance from the pith 100 mm, C) sapwood of a medium-sized log, distance from the pith 150 mm, D) sapwood of a large log, distance from the pith 500 mm (Fig. 17). In all the configurations, the radius from the origin pointed upwards in the normal direction of the board.

The analysis was carried out with a symmetrical half model with respect to the transverse direction of the top and bottom lamellae. The impact simulations were performed in 10 mm steps from the edge of the board (centre distance from the edge was 15 mm, cf. the radius of the hammer head) to the centre of the board. The results of the analysis have been depicted in Fig. 18 with different distances from the nearest board edges, the centre distance of the board being 65 mm. To ease comparison with the measurements and previously presented simulation results, the figure also shows the results for the source positions S1–S5 (see Fig. 12), and a polynomial trend line of order two for the measurement results (assumed symmetry of the results around the centre axis). The results clearly indicate that the differences in the measurement results can be explained with the presence of heartwood in the CLT slab. Hence, using rotated cartesian coordinate system improves the correlation between the measurement and the simulation results.

The sensitivity analysis confirms the insignificance of the global and importance of the local properties to the single impact force pulse. Additionally, the results of the analyses give reasons for the differences between the measurement results and the simulation results from the validated model.

3.3. Post-processed force results

To use the simulated force pulses as inputs for point forces in time or frequency domain ISI simulations, the results must be post-processed to describe the continuous operation of the STM. To demonstrate this procedure, the validated model was applied to compute the force pulse for each of the five hammers of the STM on the CLT slab at the source position S3. The simulated force pulses were post-processed according to Section 2.1. The post-processed force results have been depicted in Fig. 19 both for time and frequency domain simulations. The figure shows the force pulse array $F_{R\alpha}(t)$ for the two first pulses, and the single-sided force spectrum $F_{R\alpha}(f)$ for individual hammers at the source position. The time shift of the force pulses causes phase shift to the force spectra which can be seen as fluctuation of real and imaginary parts of the force spectra.

4. Discussion

4.1. Model applicability and findings

The model validation shows that the explicit dynamics analysis is applicable in predicting the impact force generated by the STM on a wooden slab (Fig. 10, and Table 4) when the calculation mesh is appropriate (Fig. 7) and the values for material parameters represent the behaviour of the slab. Comparison of the simulation and experimental results for the CLT slab indicated that in time domain, the measured force pulses vary more than the simulated ones with respect to the source position (Fig. 10). However, the finite element model seemed to closely predict the maximum force pulse regardless, which is a desirable effect considering ISI calculations (e.g., computing the normalized impact sound pressure level L_n) of wooden floors using the FEM. Discrepancies between the measurement results of different source positions can partly be explained with the different distances from the closest board edges. The differences between the simulated and measured values were, however, minor in the low-frequency range. Reasons explaining the differences between the measurement and simulation results, and the minor spatial variation of the simulation results (Fig. 10, and Table 4) were found in the sensitivity analysis. First, the material properties in the sectional direction of the CLT slab were found important, and properties of the uppermost lamella seemed to

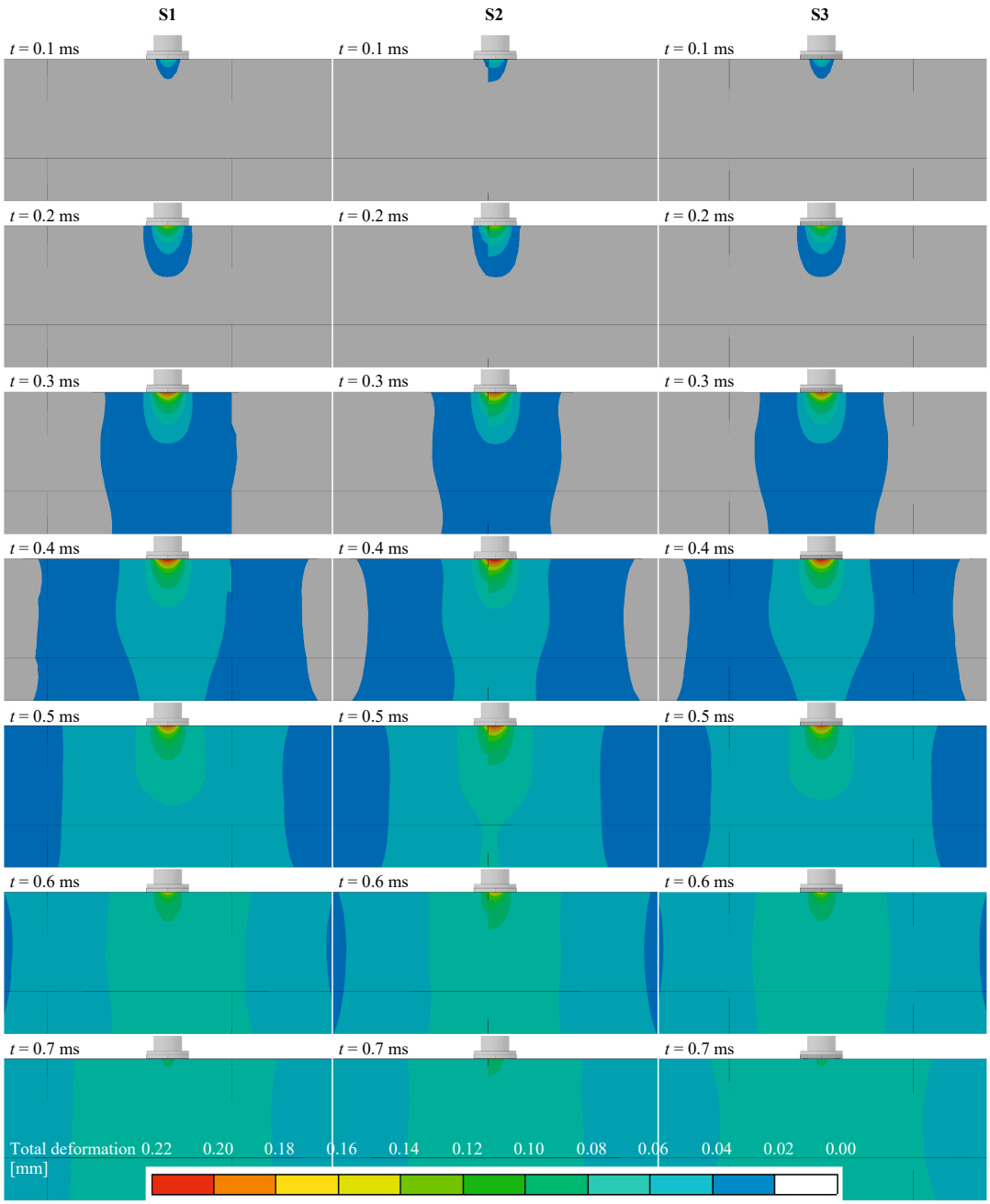

Fig. 11. Total (elastic) deformation process of the CLT slab during the impact at the source positions S1, S2, and S3.

affect the most significantly the impact force (Fig. 15). Furthermore, the force was slightly affected if the strength class of the centre lamella was changed, and major changes in the stiffness of the lower lamellae lead to greater influence on impact force. The former result also justifies the assumption of very thin and perfectly connecting glue layers between lamellae: if the thin glue layers would be modelled, probably the effect on the impact force would be minor, too. The most important material parameters for the impact force were found to be the modulus of elasticity E_R, the shear modulus G_{LR}, and the density ρ of the slab (Fig. 16). In the sensitivity analysis, the values of material parameters were varied one at a time. Thus, it is likely that the real material changes affect the impact force even more. Thirdly, the presence of the heartwood in the

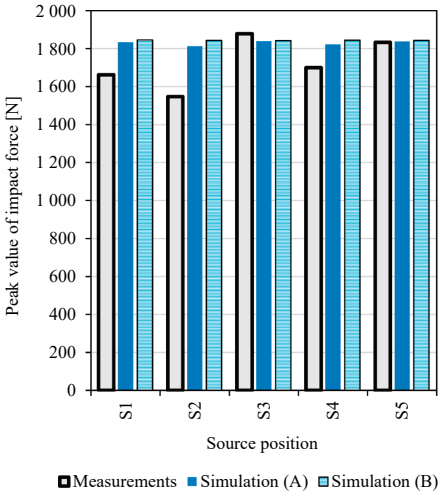

Fig. 12. Peak values of the force: comparison of the measurement and simulation results (slab configurations A and B).

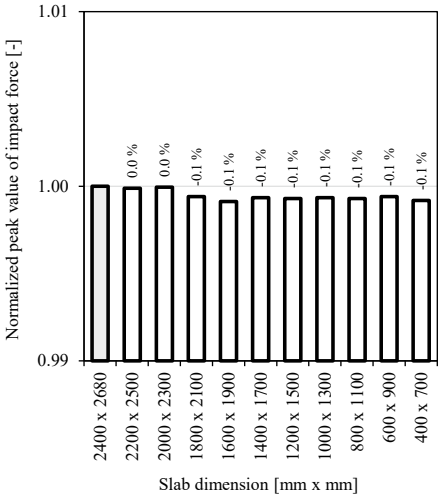

Fig. 13. Sensitivity of slab dimension on the peak value of the impact force (normalized to the result of the model in validation, in grey colour).

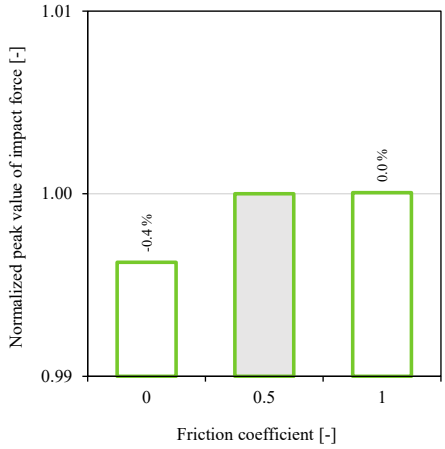

Fig. 14. Sensitivity of friction coefficients on the peak impact force (normalized to the result in grey colour).

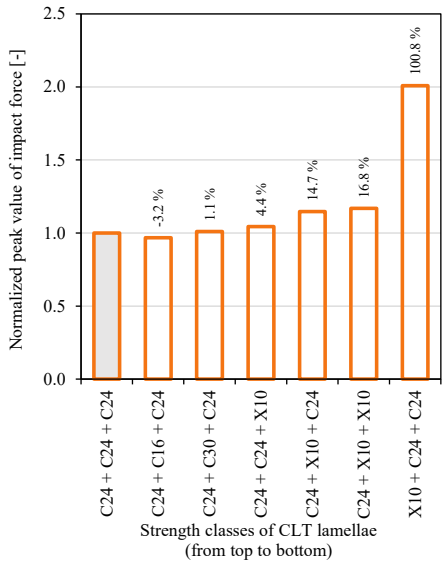

Fig. 15. Sensitivity of the lamellae's strength class on the peak impact force (normalized to the result in grey colour).

impacted part of the slab was found to be a significant feature explaining the differences in the force pulses at different distances from the board edges (Fig. 18). If the annual rings of wood are evident and the specimen is well known, the use of rotated cartesian (or cylindrical) coordinate system is justified for improving the computational accuracy.

The abovementioned findings indicate that the local properties of the CLT slab close to the impacted area are important to the impact force. However, the friction between the hammer and the slab did not affect the force (Fig. 14). This can be regarded important since exact friction coefficients between the hammer and the floors are not necessarily known. In addition, it was found that the impact force was insensitive to the global position of the hammer on the CLT slab (Fig. 12), and to the slab size or boundary conditions (Fig. 13), i.e., the global properties of the slab. These findings support modelling only a part of the slab around the impact area to still compute the impact force pulse accurately. This occurs because the stress waves caused by the impact to the slab cannot reach the impact area from the boundaries during the time of contact (Fig. 11).

The results of the sensitivity analysis imply possibilities to develop computational models for engineers and researchers. First, the need to model only a part of the impacted floor to reach accurate results provides a route to efficient tools for acoustical engineers' and researchers' purposes even when large structures are studied. Second, to compute the impact force results reaching for values on the safe side, i.e., close to the maximum, modelling the timber boards as linear orthotropic elastic material with principal axes in cartesian coordinate system and as continuous layers can offer a solution. For research purposes, it must be

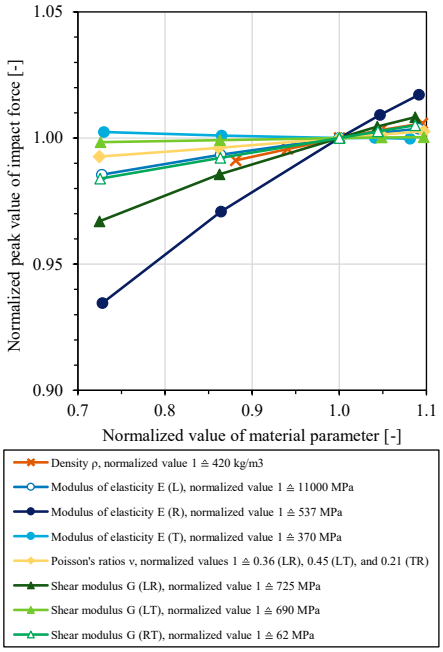

Fig. 16. Sensitivity of material parameters of the CLT slab on the peak impact force.

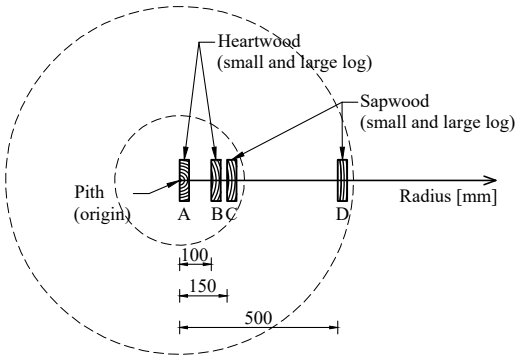

Fig. 17. Studied locally rotated coordinate systems.

noted that changes in material properties affect the results and lead to spatial variation even on CLT slabs. To take this into account, the slabs must be modelled in detail and accurate information from the material parameters is needed. If the presented techniques for modelling impact force pulses generated by the hammers of the STM are used to compute point forces driving the floor for ISI prediction models, the post-processing procedure can be implemented in simulation tools as illustrated in Section 2.1 and Fig. 19. Note that the findings from the sensitivity analysis should be verified case by case if other floors are studied with the presented procedure.

4.2. Limitations and need for further research

As with all models, it should be noted that the finite element model

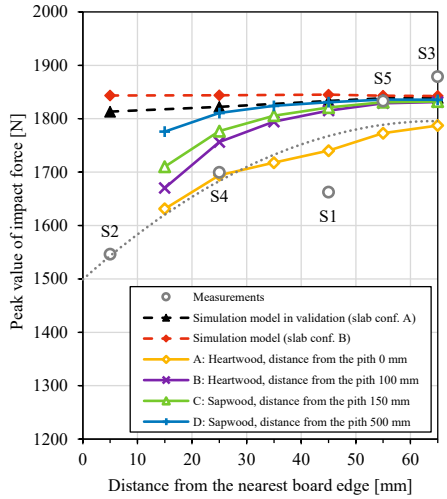

Fig. 18. Effect of the heartwood and sapwood on the peak impact force: comparison of measurement and simulation results. The average measurement results at different source positions have been indicated with labels S1–S5 and with a polynomial trend line of order two (dotted (:) grey line).

presented in this paper was used under a few assumptions. First, the CLT slab was initially at rest in the simulations. This initial state is based on the findings from the experimental study [10] as noted in Section 2.3.2. Because of this, the finite element model was used to compute the force pulse generated by a single hammer drop. It would be interesting if in further research the effect of the vibration of the slab on the impact force would be studied in detail with simulations. One possible way for this is to connect implicit finite element analysis describing the vibration behaviour of the slab to the impact force analysis. Secondly, the finite element model did not include material damping since the model was used to simulate only a very short collision between the bodies. For further studies, Rayleigh damping, especially the β damping factor (stiffness matrix damping multiplier), could be incorporated if the effect of the damping on the impact force is of interest. However, according to our knowledge and experience, damping would only minorly affect the impact force results shown in this paper. Thirdly, a regular contact-impact algorithm was used in the finite element model to simulate the collision between bodies. For engineering and research purposes, it would be interesting to study the possible benefits of using a SMOOTH option (surface fitting algorithm) [27] for the contact. The SMOOTH contact can provide a more accurate presentation of the curvature of the hammer head and produce smoother results with coarser meshes [27]. Thus, using SMOOTH contact could improve the mesh convergence.

5. Conclusions

This paper presented a method to simulate the impact force pulse generated by a hammer of the STM on a wooden slab by using explicit dynamics analysis. According to the model validation and sensitivity analysis, the method is applicable in computing the non-linear behaviour of the contact between the hammer and the slab. The validated model predicted closely the maximum impact force measured on the CLT slab both in time and frequency domains. Local properties of the CLT slab were discovered to be important to the results. The discrepancies between the simulation and the measurement results were suggested to be affected by the local material properties of the CLT slab: both material parameters and the use of heartwood explained the differences. On the other hand, the global properties such as the location of

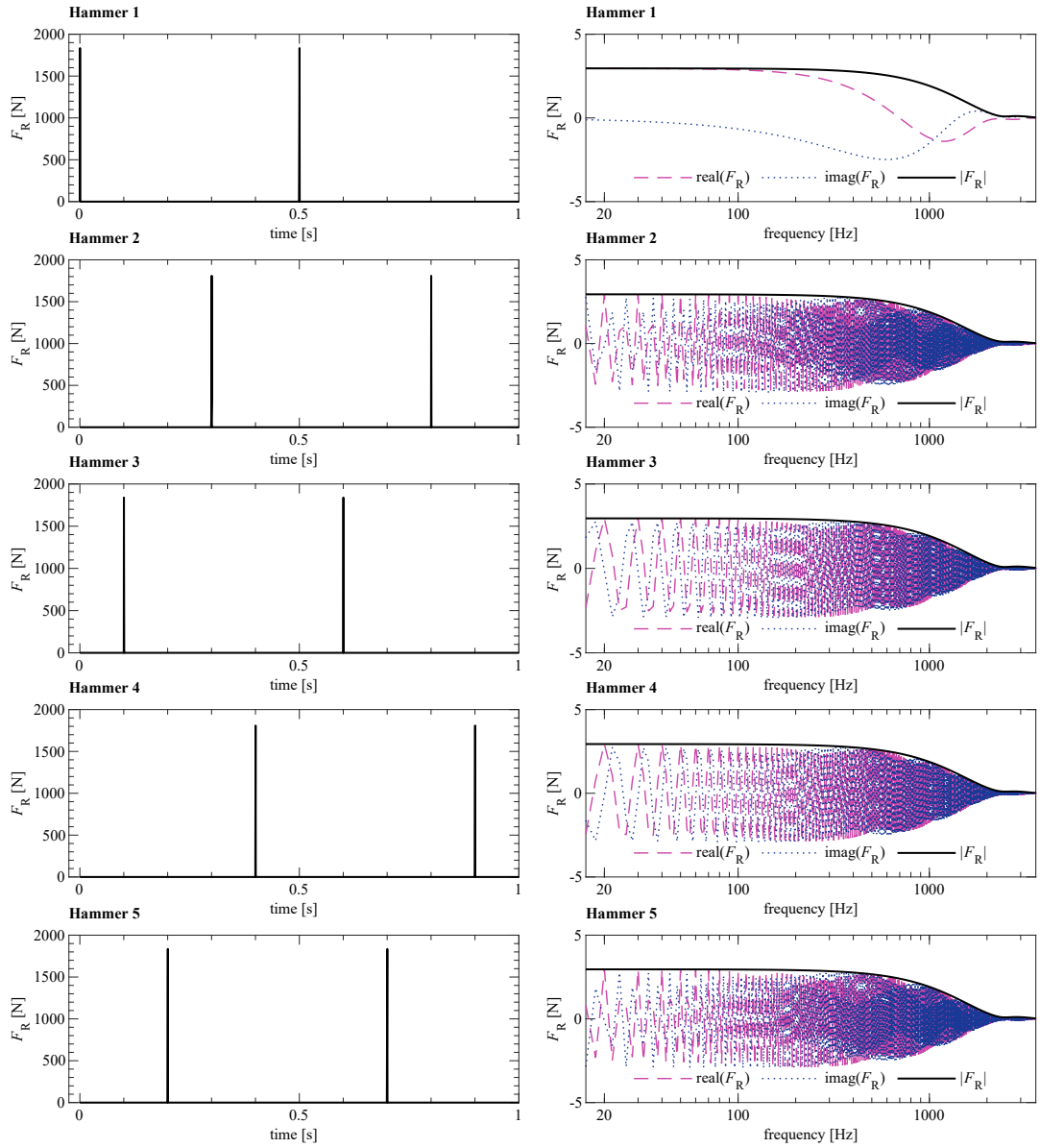

Fig. 19. Post-processed impact force results for time domain simulations (left), and for frequency domain simulations (right). For the frequency domain results, the magnitude (solid black line), the real part (dashed (–) magenta line), and the imaginary part (dotted (:) blue line) of the force spectrum $F_R(f)$ has been presented.

the hammer on the slab and the slab size were found to be insignificant to the simulated impact force pulses. The findings from the sensitivity analysis offer possibilities to develop tools predicting the excitation force for both engineering and research purposes. The post-processing procedure can be implemented in these tools to achieve point forces describing the continuous excitation generated by the STM in time and frequency domains.

The simulations were performed for a CLT slab, but the authors see no reason to restrict the use of the presented techniques to CLT or other massive wooden slabs only. The mathematical presentation of the model is valid on floor structures in general. Hence, the structures can include other types of wooden floors and, e.g., surface structures such as additional layers, floating floors, or floor coverings, if only their properties are known. However, there is a need for further sensitivity analyses when developing corresponding simulation models for other types of floors.

Declaration of Competing Interest

The authors declare that they have no known competing financial

interests or personal relationships that could have appeared to influence the work reported in this paper.

Acknowledgements

This paper was written within the Doctoral School in Industrial Timber Construction of Tampere University.

References

[1] Rabold A, Düster A, Rank E. FEM based prediction model for the impact sound level of floors. Proc Acoust '08 2008;123. https://doi.org/10.1121/1.2933931.
[2] Kohrmann M, Buchschmid M, Schanda U, Müller G. A FEM-based planning tool for the vibro-acoustic design of wooden floors at low frequencies. Proc. INTER-NOISE 2016 - 45th Int. Congr. Expo. Noise Control Eng. Towar. a Quieter Futur., Hamburg, Germany: 2016, p. 3743–51.
[3] Bard D, Negreira J, Guigou Carter C, Borello G, Kouyoumji J, Speranza A, et al. Modelling prerequisites – FEM/SEA Impact and Airborne Sound. Silent Timber Build, repor no STB01 WG1. 2017.
[4] Qian C, Ménard S, Bard-Hagberg D, Kouyoumji JL, Negreira J. Calibration of the ISO tapping machine for finite-element prediction tool on a wooden-base floor. Build Acoust 2019;26:157–67. https://doi.org/10.1177/1351010X19855227.
[5] Wang P, Van hoorickx C, Lombaert G, Reynders E. Numerical prediction and experimental validation of impact sound radiation by timber joist floors. Appl Acoust 2020;162:107182.
[6] ISO 10140-5. Acoustics – Laboratory measurement of sound insulation of building elements – Part 5: Requirements for test facilities and equipment. Geneva: International Organization for Standardization; 2010.
[7] Iso. 16283–2. Acoustics – Field measurement of sound insulation in buildings and of building elements – Part 2: Impact sound insulation. Geneve: International Organization for Standardization; 2015.
[8] Brunskog J, Hammer P. The interaction between the ISO tapping machine and lightweight floors. Acta Acust United with Acust 2003;89:296–308.
[9] Cremer L, Heckl M, Petersson BAT. Structure-Borne Sound. 3rd ed. Berlin Heidelberg: Springer-Verlag; 2005.
[10] Lietzén J, Miettinen J, Kylliäinen M, Pajunen S. Impact force excitation generated by an ISO tapping machine on wooden floors. Appl Acoust 2021;175:107821.
[11] Heckl M, Rathe EJ. Relationship between the transmission loss and the impact-noise isolation of floor structures. J Acoust Soc Am 1963;35:1825–30. https://doi.org/10.1121/1.1918830.
[12] Lindblad S. Impact sound characteristics of resilient floor coverings. Sweden: Lund; 1968.
[13] Vér IL. Impact noise isolation of composite floors. J Acoust Soc Am 1971;50:1043–50. https://doi.org/10.1121/1.1912726.
[14] Cremer L, Heckl M, Ungar EE. Structure-Borne Sound. Berlin Heidelberg: Springer-Verlag; 1973.
[15] Scholl W, Maysenhölder W. Impact sound insulation of timber floors: interaction between source, floor coverings and load bearing floor. Build Acoust 1999;6:43–61. https://doi.org/10.1260/1351010991501266.
[16] Griffin D. Accuracy of prediction methods for the improvement of impact sound pressure levels using floor coverings. Proc. Internoise 2017, Hong Kong, China: 2017, p. 3805–13.
[17] Rabold A, Buchschmid M, Düster A, Müller G, Rank E. Modelling the excitation force of a standard tapping machine on lightweight floor structures. Build Acoust 2010;17:175–97. https://doi.org/10.1260/1351-010X.17.3.175.
[18] Wittstock V. On the spectral shape of the sound generated by standard tapping machines. Acta Acust United with Acust 2012;98:301–8. https://doi.org/10.3813/AAA.918513.
[19] Amiryarahmadi N, Kropp W, Bard D, Larsson K. Time-domain model of a tapping machine. Proc. Forum Acusticum 2011, Aalborg, Denmark: 2011, p. 1713–8.
[20] Coguenanff C, Guigou-Carter C, Jean P, Desceliers C. Probabilistic model of the impact force spectrum for the standard ISO tapping machine. Proc. 22nd Int. Congr. Sound Vib. ICSV 2015, Florence, Italy: 2015, p. 5551–8.
[21] Mosharrof MS, Brunskog J, Ljunggren F, Ågren A. An improved prediction model for the impact sound level of lightweight floors: Introducing decoupled floor-ceiling and beam-plate moment. Acta Acust United with Acust 2011;97:254–65. https://doi.org/10.3813/AAA.918405.
[22] Rao CL, Narayanamurthy V, Simha KRY, editors. Applied Impact Mechanics. Chichester, UK: John Wiley & Sons, Ltd; 2016.
[23] Wu SR, Gu L, editors. Introduction to the Explicit Finite Element Method for Nonlinear Transient Dynamics. Wiley; 2012.
[24] ETA-14/0349. European Technical Assessment. Austrian Inst Constr Eng 2014.
[25] LS-DYNA Theory Manual. r:8571. Livermore, California: Livermore Software Technology Corporation (LSTC); 2017.
[26] Wu SR. Lumped mass matrix in explicit finite element method for transient dynamics of elasticity. Comput Methods Appl Mech Eng 2006;195:5983–94. https://doi.org/10.1016/j.cma.2005.10.008.
[27] LS-DYNA Keyword User's Manual, Volume I (r:8752). Livermore, California: Livermore Software Technology Corporation (LSTC); 2017.
[28] LS-DYNA Keyword User's Manual, Volume II: Material Models (r:8944). Livermore, California: Livermore Software Technology Corporation (LSTC); 2017.
[29] EN 1993-1-1. Eurocode 3: Design of steel structures - Part 1-1: General rules and rules for buildings. Brussels: European Committee for Standardization; 2005.
[30] EN 1993-1-4. Eurocode 3: Design of steel structures - Part 1-4: General rules - Supplementary rules for stainless steels. Brussels: European Committee for Standardization; 2006.
[31] Wood Handbook – Wood as an Engineering Material. Madison, Wisconsin: U.S. Department of Agriculture, Forest Service, Forest Products Laboratory; 2010.
[32] EN 338. Structural timber – Strength classes. Brussels: 2016.
[33] Keunecke D, Hering S, Niemz P. Three-dimensional elastic behaviour of common yew and Norway spruce. Wood Sci Technol 2008;42:633–47. https://doi.org/10.1007/s00226-008-0192-7.

PUBLICATION III

Vibration level reduction by floor coverings installed on wooden slabs

Jesse Lietzén, Mikko Kylliäinen, Saveli Valjakka, Sami Pajunen

Building Acoustics 29(2), 221–237
https://doi.org/10.1177/1351010X221080613

Original Research

BUILDING ACOUSTICS

Building Acoustics
2022, Vol. 29(2) 221–237

DOI: 10.1177/1351010X221080613
journals.sagepub.com/home/bua


Vibration level reduction by floor coverings installed on wooden slabs

Jesse Lietzén[1], Mikko Kylliäinen[1], Saveli Valjakka[2] and Sami Pajunen[1]

Abstract

Effect of floor coverings on impact sound insulation can be described with a vibration level reduction (ΔL_a). In this study, tests with two floor coverings, eight wooden slabs and with a concrete mock-up slab were conducted by applying the method presented by Sommerfeld and the standard ISO 16251-1. The aim was to study the differences affecting the measured ΔL_a and the behaviour of the floor coverings installed on different slabs. The results suggest that the ΔL_a on concrete slabs do not correspond with the ΔL_a on wooden slabs. Thus, the floor coverings should be measured on wooden slabs when they are to be used within the timber construction industry. The results also show that the coverings should be measured on the wooden slabs where the products are expected to be used. In addition, a standardized test method for the wooden slabs corresponding the method of ISO 16251-1 should be developed.

Keywords

Impact sound insulation, vibration level reduction, floor coverings, wooden floors, tapping machine

Introduction

Typical floor coverings used in apartment buildings are cushion vinyls, wall-to-wall carpets, and multilayer parquets or laminates installed on an underlayment.[1] From an acoustic point of view, the purpose of a floor covering is to improve impact sound insulation between rooms by reducing force generated by impacts upon a bare intermediate floor (later briefly called *slab*). This relative improvement of impact sound insulation (ΔL) caused by the floor covering is a function of frequency and it can be determined by following two different standardized measurement procedures[2–5] using an ISO tapping machine as an impact sound source. To take real products into account in the assessment of the impact sound insulation, the measured ΔL of the floor coverings should be available and represent the behaviour of the floor covering on the corresponding slab. The measurement results should also be available because the exact modelling of the

[1]Faculty of Built Environment, Unit of Civil Engineering, Tampere University, Tampere, Finland
[2]AINS Group, Department of Acoustical Engineering, Tampere, Finland

Corresponding author:
Jesse Lietzén, Tampere University, Korkeakoulunkatu 7, Tampere 33720, Finland.
Email: jesse.lietzen@tuni.fi

floor covering, for example, by using finite element method (FEM), is often tedious due to the complexity of the floor covering (c.f. multi-layered resilient toppings or soft wall-to-wall carpets).

Traditionally, the ΔL of the floor covering is determined in a laboratory with impact sound insulation measurements between source and receiving rooms according to the laboratory standard ISO 10140 series.[2–4] The measurements are carried out on a reinforced massive concrete slab or on one of the three wooden rib slabs presented by ISO 10140-5.[4] An optional method for measuring the ΔL of a light floor covering on a concrete slab has been presented in the standard ISO 16251-1.[5] The standard method[5] is based on measuring the vibratory acceleration levels of a small concrete slab. The tests on the concrete mock-up slab are conducted with and without the floor covering specimen on the slab and the vibration level reduction (ΔL_a) is yielded from the acceleration level differences of these measurements. Since the concrete mock-up slab is 200 mm thick, the method involves measurements mainly above the coincidence frequency of the slab.

The method of ISO 16251-1[5] has been noted to yield results comparable to those gained with ISO 10140 series[2–4] on concrete slabs,[5–10] that is, for concrete floors, the ΔL_a can be regarded to correspond with the ΔL. The method in ISO 16251-1[5] is based on the study conducted by Sommerfeld,[6] where he tested the method both on a small concrete and on a wooden mock-up slab. The method[6] for the concrete mock-up slab was later standardized[5] and so far, a similar standardized measurement method for a wooden mock-up slab does not exist. However, the method using a wooden mock-up slab proved promising when compared with ISO 140-11[11] tests on a wooden slab, especially when they were conducted for the PVC, the carpet and the linoleum floor coverings.[6] In case of the laminate floor covering, minor discrepancies between the ΔL_a and the ΔL from the standard method[11] were discovered.[6]

The reason why the measurement method[6] for the wooden mock-up slab has not been standardized could have been driven by the simplicity of the wooden mock-up slab used in the study[6]: the wooden mock-up slab was small, and consisted of two wooden joists at the edges of the floor and a chipboard layer upon them. According to the recent research,[12] the impact force generated by the ISO tapping machine varies on a rib slab due to the different distances between the source positions and the ribs. Thus, a very essential behaviour of the slab could have been discarded by considering only the deck between the ribs in the measurements. Furthermore, it is possible that the laminate floor covering in Sommerfeld[6] acted as partially resonantly reacting floor covering when the size of the floor could effect on the results.

It is an acknowledged problem that the ΔL depends upon the bare slab.[4,13–15] This is also the reason why the wooden slabs and the wooden mock-up slab have been included in the standard ISO 10140-5.[4] Despite the possibility to measure on the wooden slabs, construction industry has made measurements of floor coverings mainly on concrete slabs. One reason for this is could be that the wooden slabs presented by the standard[4] do not represent the floors under the floor coverings used by the timber construction industry, see for example.[16,17] This is the situation for example in Finland.

Comparing the results of different laboratory measurement series presented in the literature[18–23] reveals that resilient floor coverings have a different ability to reduce impact sound on wooden and concrete slabs.[24] In fact, the differences between the ΔL results on these slabs are evident especially in the high frequency range from 1000 to 5000 Hz, where the ΔL levels are always lower on the wooden floors. However, these observations are based on individual measurements on resilient floor coverings on different slab types. According to the authors' knowledge there is a lack of a systematic study where the results of different floor coverings are compared on concrete and

Table 1. Properties of the floor coverings: thickness of the layer (h), mass per unit area (m') and dynamic stiffness per unit area (s').

ID	Floor covering	h (mm)	m' (kg/m^2)	s' (MN/m^3)
a	Multilayer parquet	14	7.73	–
	Soft underlayment	3	0.15	65.1
b	Cushion vinyl	3	1.66	2282.0

different type of wooden slabs. In addition to the resilient floor coverings, a parquet or a laminate installed on a resilient underlayment needs to be considered.

The purpose of this paper was to study the differences affecting the ΔL of the floor coverings when they are installed on wooden and concrete mock-up slabs. This has been done by applying the method of Sommerfeld[6] (presented currently in ISO 16251-1[5]) on wooden slabs with the difference that, in this study, the studied slabs were considerably larger than the mock-ups in Sommerfeld.[6] Studying the method itself was not of the main interest of this research. Instead of that, the authors were interested in studying the behaviour of the floor coverings on different types of slabs. In addition to the traditional wooden rib slab, a massive wooden slab (cross-laminated-timber, CLT) was studied. The influence of adding mass to these load-bearing wooden slabs was also investigated. For comparison, the measurements on the concrete mock-up slab were carried out according to ISO 16251-1.[5] Thus, the vibration level reduction ΔL_a for the wooden slabs and the concrete mock-up slab have been derived from the vibrational acceleration level differences on the corresponding floors. The research was done by conducting a series of experiments on eight different wooden slabs, concrete mock-up slab and with two floor coverings. The total number of the measured wooden floor constructions was 10, and the two on the concrete mock-up.

Materials and methods

Floor coverings

Two different floor coverings were studied: a 14 mm thick multilayer parquet on a 3 mm thick, soft underlayment (a), and a 3 mm thick cushion vinyl (b). Both materials are used especially in Nordic apartment houses and their weighted reductions in impact sound pressure level ΔL_w are ca. 20 dB on concrete slabs.[1]

The multilayer parquet was made of maple and equipped with tongue-and-groove joints. This was installed on an underlayment consisting of two thin polyethene layers with flexible polystyrene granules between them. Hence, the parquet on the underlayment formed a floating structure where the parquet acts as a plate on a resilient layer formed by the underlayment. In all the measurement situations, the parquet was installed in identical order on the wooden slabs.

The cushion vinyl was a soft 3 mm thick product especially used in apartment houses. In the measurement situations, the cushion vinyl was glued to the surface of the wooden slabs around the centre hammer of the ISO tapping machine at each source position. This was done due to the simultaneous impact force excitation measurements presented in Lietzén et al.[12] Otherwise, the cushion vinyl was installed loosely to the surface of the slab.

Table 1 shows the thickness (h) of the floor covering layers, and the mass per unit area (m') of the floor coverings and the dynamic stiffness per unit area (s') of the resilient products measured according to the standard ISO 9052-1.[25] Cross sections showing the floor covering materials installed on CLT slabs has been shown in Figure 1.

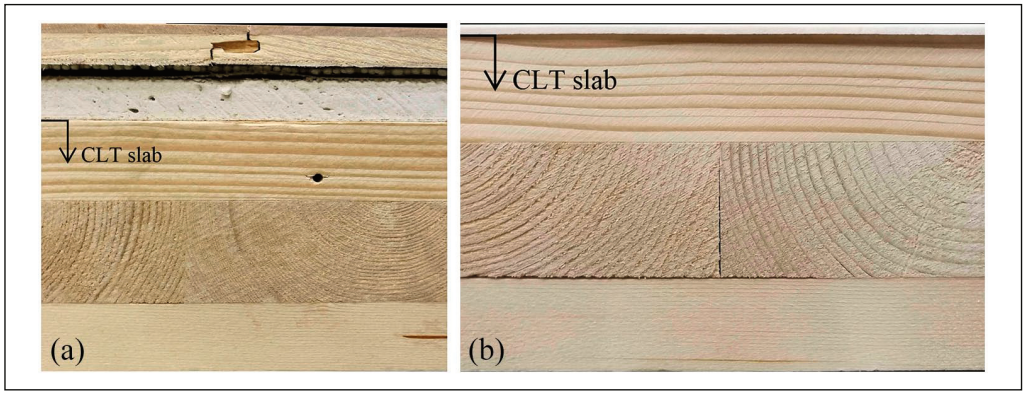

Figure 1. Cross sections of the multilayer parquet on the underlayment (a), and of the cushion vinyl (b) installed on different CLT slabs. Note that the figure (a) includes a single layer of 15 mm plasterboard attached to the surface of the CLT (see Section 2.2).

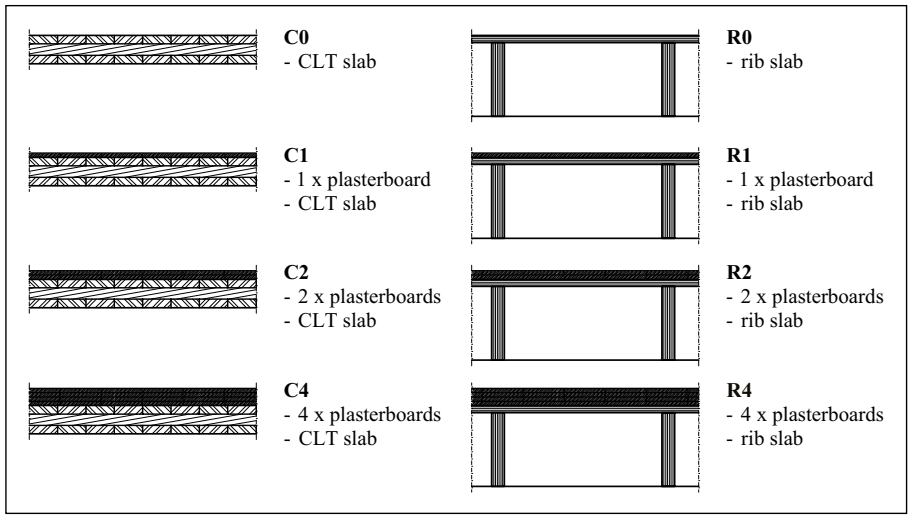

Figure 2. Wooden slabs.

Load-bearing slabs and additional layers

The floor coverings described in Section 2.1 were installed on eight different wooden slabs illustrated in Figure 2. The slabs comprised two different load-bearing wooden slabs and the slabs with additional plasterboards increasing the mass of the slab. The two load-bearing slabs were a 100 mm thick three-layered CLT slab (floors C0–C4) and a prefabricated rib slab (floors R0–R4) with 25 mm thick LVL panel deck and 45 mm × 260 mm LVL beams (c/c 578–600 mm). In addition to the load-bearing wooden slabs, the slabs C1–C4 and R1–R4 included one, two or four layers of additional plasterboards ($h = 15$ mm, m' = 15.4 kg/m^2). These plasterboards were attached to the surface of the slabs and were glued and screwed to each other.

To overcome the problems with the wooden mock-up slab in Sommerfeld[6] (see Section 1), the experiments on wooden slabs were carried out on larger floor constructions, in this study. The size

of the floor constructions was 2.4 m × 2.7 m with a span of 2.7 m. In the test setup, the CLT slab and the rib slab were fixed from their both ends to the load supports with screw connections. The supports were attached to vibration isolated steel structures. For further details of the wooden slabs and their installation procedures, see Lietzén et al.[12]

Procedures of experiments

In the present study, the vibration level reduction ΔL_a caused by the floor coverings (see Section 2.1) was studied both on the wooden slabs (see Section 2.2) and on the concrete mock-up slab. The aim of this was to find out how the results differ on wooden and concrete slabs, and the reasons for the possible discrepancies. First, the ΔL_a of the floor coverings were determined on the wooden slabs by adopting the measurement methods from Sommerfeld[6] presented in the standard ISO 16251-1.[5] Secondly, tests in accordance with the standard[5] were carried out for the same floor coverings on the concrete mock-up slab. The results for the ΔL_a were derived from the measured vibratory acceleration levels of the floors.

Probably because of the observations done by Sommerfeld,[6] the method presented in ISO 16251-1[5] is restricted to light, soft, flexible floor coverings placed on top of concrete slab. Such coverings behave locally on the floor when the size of the floor covering would not influence the results. The soft cushion vinyl (floor covering (b), see Section 2.1) studied in this paper obviously falls into this category. However, the parquet with the soft underlayment (floor covering (a), see Section 2.1) consists of a flexible underlayment and a floating layer upon it so the question is whether it behaves locally.

A similar floor covering, a parquet with an underlayment, was tested in accordance with the method[5] in Keränen et al.[10] and compared with results from ISO 10140[2–4] tests. In the study,[10] it was shown that there were no significant discrepancies between the results of the different standard methods. Therefore, the method of the standard ISO 16251-1[5] can be regarded to be suitable for testing the ΔL_a of the floor covering comprising the multilayer parquet on the soft underlayment, that is, the floor covering (a).

Both on the wooden slabs and on the concrete mock-up slab, the results for the ΔL_a were calculated from the measured vibratory acceleration levels L_a, in a similar manner according to ISO 16251-1.[5] The vibration level reduction $\Delta L_{a,t,i}$ [dB] for each accelerometer position i and tapping machine position t combination was the level difference

$$\Delta L_{a,t,i} = L_{a,without,t,i} - L_{a,with,t,i}, \tag{1}$$

where the $L_{a,\mathrm{without},t,i}$ [dB] is the background noise corrected[5] vibratory acceleration level of the bare slab and the $L_{a,\mathrm{with},t,i}$ [dB] denotes the background noise corrected acceleration level when the floor covering was on the slab, in the corresponding source and receiver positions. The total vibration level reduction ΔL_a was

$$\Delta L_a = \frac{1}{t \cdot i} \sum_t \sum_i \Delta L_{a,t,i} \tag{2}$$

where t runs from 1 to the total number of tapping machine positions and i from 1 to the total number of accelerometer positions.[5] All the results were determined for 1/3-octave band centre frequencies in the frequency range 50–5000 Hz.

Experiments on wooden slabs. The measurements were carried out using five tapping machine positions per wooden floor construction (Figure 3). The vibratory acceleration levels of the floors were

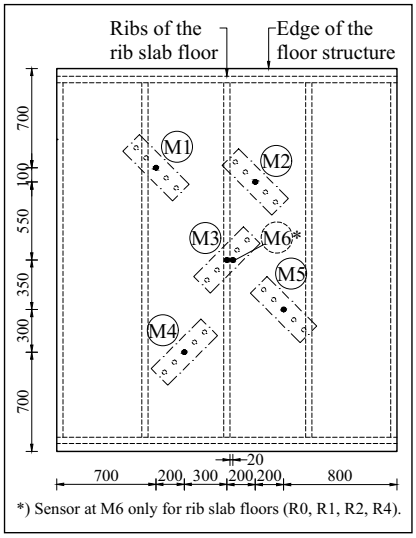

Figure 3. Measurement positions M1–M6 below the floor constructions. The black circles show the location of the sensors at the underside of the slabs. The rectangular boxes illustrate the orientation of the ISO tapping machine on the five source positions on the floors. Dimensions in the figure are presented in millimetres.

recorded at measurement positions M1–M6 below the slabs during the operation of the ISO tapping machine. The acceleration sensors (Kistler types 8704B50M1 and 8702B50M1) were glued to the underside of the CLT slab or to the underside of the deck of the rib slab, however, the position M3 lied below the centre rib of the rib slab where the sensor was glued to the underside of the rib. The measurements were conducted with and without the floor coverings using LMS system for vibration testing (Test.Lab 11b). In addition, the background noise levels were recorded at each receiver.

Figure 3 shows the measurement positions M1–M6 below the slabs and the orientation of the ISO tapping machine at the source positions on the floor. All the positions were kept the same for all studied floor constructions, but the additional measurement position M6 was used only for the rib slab floors R0, R1, R2 and R4 because (different from the other positions) the M3 lied below the centre rib of the floor. The results were derived so that the vibratory acceleration levels directly below the source position were neglected.

The experiments were performed for the multilayer parquet and the underlayment (floor covering (a)) on all the wooden slabs and for the cushion vinyl (floor covering (b)) on the floors C0 and R0. The reason for testing the floor covering (a) on all the slabs, and the floor covering (b) only on two slabs, was that in literature there already exists more information of the resilient coverings' performance on different types of floors, but the parquets or laminates have been minorly discussed (see Section 1). Furthermore, according to the authors' knowledge, a parquet (or a laminate) on a soft underlayment is one of the most common floor covering types in Nordic apartment buildings.

Standard tests on a concrete mock-up slab. To compare the ΔL_a results of the floor coverings on wooden and concrete slabs, standard tests using the ISO 16251-1[5] were carried out on the concrete mock-up slab. The measurements were performed by the Acoustics Laboratory of Turku University of Applied Sciences. The tests on this concrete slab were carried out for the same floor covering specimens that were used in the experiments on wooden slabs.

Force level reduction of a resilient floor covering

The behaviour of the resilient floor covering (b) on the wooden slabs was assessed by comparing the ΔL_a results to the force level reduction (ΔL_{force}). The ΔL_{force} presents the ΔL values calculated from the input force generated by the ISO tapping machine on the floors equipped with a soft floor covering. The purpose for computing the ΔL_{force} was to simply verify the ΔL_a results and to find out if the behaviour of the floor covering (b) on wooden slabs can be explained by its effect on the input force. According to Vér,[26] the ΔL_{force} can be derived from the known driving force spectra by

$$\Delta L_{force} = 20\log\left(\frac{F_{without}}{F_{with}}\right), \tag{3}$$

where F_{with} [N] and F_{without} [N] are the root-mean-square (rms) forces exciting the floor construction when the floor is equipped with and without the soft floor covering, respectively.

The input force with (F_{with}) and without (F_{without}) the soft floor covering were gained from the impact force excitation measurements.[12] In the measurements,[12] the centre hammer of the ISO tapping machine was instrumented to measure the impact force generated by the apparatus upon the floor surface. The impact force measurements[12] were simultaneous with the vibration measurements. For further details of the impact force measurements, see Lietzén et al.[12] The results for ΔL_{force} were calculated from the measured 1/3-octave driving forces in the frequency range 50–5000 Hz.

This method of deriving ΔL_{force} is restricted to describe the ΔL_a of soft floor coverings only. Thus, the comparison of ΔL_a and ΔL_{force} was carried out for the cushion vinyl, that is, the floor covering (b). However, the equation (3) considers purely the change in the input force neglecting any other possible effects of the floor coverings on the slabs. Thus, it is likely that the ΔL_{force} provides only approximate results of ΔL_a. It must also be noted that since the ISO tapping machine was equipped with one instrumented hammer in the impact force measurements,[12] the result of ΔL_{force} hereby assumes that the impact force generated by all hammers are uniform at the same source position. This assumption is slightly rough because there are differences in the driving force spectra between the source positions.[12]

Results

ΔL_a by floor coverings on wooden slabs

The measurement results for the ΔL_a by the floor coverings on the wooden slabs are shown altogether in Appendix A. The average results are illustrated in Figure 4, where Figure 4(a) shows the measurement results on the CLT slabs and Figure 4(b) on the rib slabs. In the figure legend, the first two characters denote the bare wooden slab (see Figure 2), and the third character shows the ID of the floor covering (see Table 1), for example, the curve (C0a) illustrates the ΔL_a for the floor covering (a) (the multilayer parquet on the soft underlayment) on the wooden slab (C0) (the bare CLT slab).

The results show that the vibration level reduction ΔL_a was positive almost in the entire frequency range for all the studied floor covering and wooden slab configurations (Figure 4). In the low-frequency range up to 250 Hz band, the values were rather constant apart from the individual peaks illustrated in Figure 4. The values of ΔL_a in this range varied from 1 to 9 dB depending on the configuration. In the mid-frequency range after the 250 Hz band, the ΔL_a began to increase until at higher frequencies it decreased or at least remained at constant level compared to the latter.

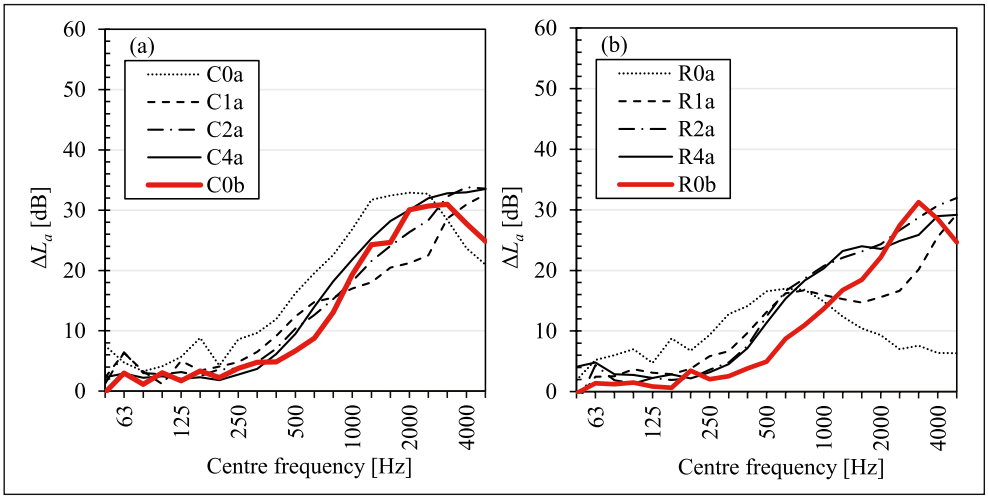

Figure 4. Measurement results of ΔL_a in 1/3-octave centre frequencies in the frequency range 50–5000 Hz on (a) CLT slabs, and on (b) rib slabs.

The measured ΔL_a levels of the floor coverings depended on the type of the wooden slabs (Figure 4). The results for the floor covering (a) showed high dependency between the ΔL_a and the bare wooden slab. If we limit the review to the frequencies under 2000 Hz, it can be noted that there were also significant differences between the maximum ΔL_a values of the floors. In case of the lightest slabs, that is, C0 and R0, the ΔL_a levels were higher in the low-frequency range and lower in the high frequencies than on the slabs where plasterboards were added. On these light slabs, the maximum ΔL_a values occurred at lower frequencies than on the others. In case of the slab C0, the maximum ΔL_a was at 2000 Hz whereas on R0 the values begin to diminish at the mid-frequencies and the maximum level occurred at 630 Hz.

The differences of the ΔL_a results C0b and R0b for the floor covering (b) were minor but prominent in the frequency range between 800 and 2500 Hz (Figure 4). However, the peak values of the ΔL_a were near the same level at 3150 Hz octave band. The ΔL_a levels for the floor coverings (a) and (b) were different when measured on the same wooden slab. When comparing the results C0a to C0b and R0a to R0b, it is obvious that the floor covering (a) produced larger ΔL_a levels than (b) in the low- and mid-frequency ranges. On the bare CLT slab C0, the ΔL_a levels were larger even up to 2000 Hz frequency band. It is also notable that the shapes of the ΔL_a curves for the floor coverings (a) and (b) were completely different on the rib slab R0 whereas on the CLT slab the curves showed a frequency shift.

Adding plasterboards to the load-bearing slabs gradually evened out the differences between the floors on the same load-bearing wooden slab (Figure 4). It can also be seen that the additional mass reduced the ΔL_a in low- and mid-frequencies and increased it at high frequencies. However, adding four plasterboard layers instead of two was not beneficial with respect to the ΔL_a (see especially Figure 4(b)) although this would improve the impact sound insulation of the corresponding floor.

Comparison of ΔL_a and ΔL_{force} on wooden slabs

In addition to the results determined from the vibrational acceleration level measurements shown in Figure 4, the ΔL_{force} of the floor covering (b) was calculated according to the equation (3) based

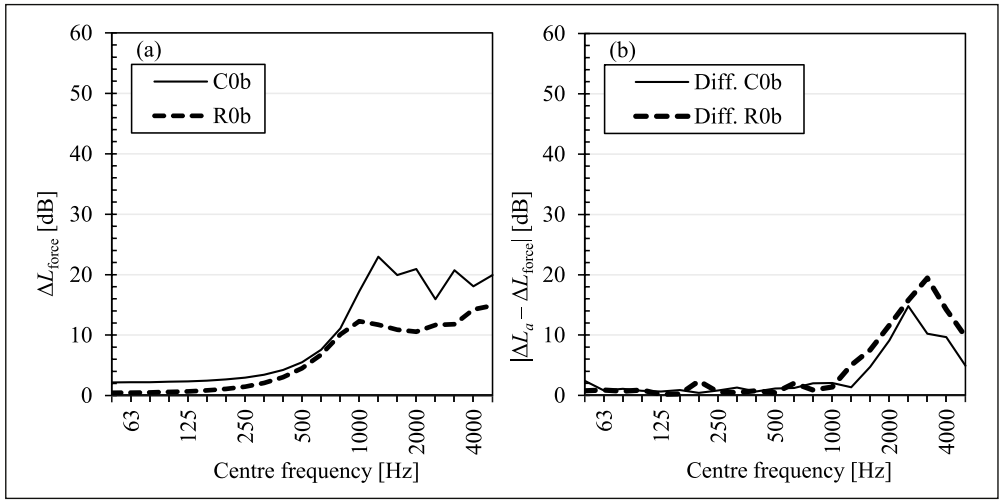

Figure 5. Measurement results of ΔL_{force} (a) and the absolute difference between the measurement results ΔL_a and ΔL_{force} on the corresponding wooden slabs (b) in 1/3-octave centre frequencies in the frequency range 50–5000 Hz.

on the measured rms force spectra generated by the ISO tapping machine on the wooden slabs C0 and R0 with and without the floor covering. The results for the ΔL_{force} are shown in Figure 5(a). These results were compared to the ΔL_a presented in Figure 4 and the absolute differences between the values are illustrated in Figure 5(b).

The comparison of ΔL_a and ΔL_{force} (Figure 5(b)) shows that the measurement methods produce corresponding results at least up to frequencies 1000 and 1250 Hz for the rib slab and the CLT slab, respectively. In this frequency range, the ΔL_{force} followed closely the measurement results of ΔL_a presented in Figure 4 and the absolute difference varied from 0 to 2 dB. The differences above these frequencies were probably caused by the measurement accuracy, the measurement method used for determining the ΔL_{force}, and the behaviour of the floor covering (b) on the wooden slabs. These effects should be taken into consideration when comparing the results of different measurements. The main issue is that there are some shortcomings in determining the ΔL_{force}.

The ΔL_{force} was determined on the basis of the impact force measurements from the single hammer of the ISO tapping machine,[12] even though the tapping machine operated on the wooden slabs normally using all of its five hammers. This means that it has been presumed that the impact force measured from this single hammer would represent the impact force produced by the other hammers, too, as discussed in Section 2.4. However, as noted in Lietzén et al.,[12] there are differences in the impact force between source positions, which could lead to mispredictions of the ΔL_{force}, especially in the high-frequency range.

Comparison of ΔL_a by floor coverings on wooden slabs and on a concrete mock-up slab

The results ΔL_a for the concrete mock-up slab are shown in Figure 6 for the floor coverings (a) and (b). The ΔL_a was positive in the low-frequency range and rather constant up to 250 Hz band. In this range, the values of ΔL_a varied from 1.4 to 2.8 dB and from 2.7 to 3.2 dB for the floor coverings (a) and (b), respectively. The maximum values of the ΔL_a were between 53 and 55 dB. The differences

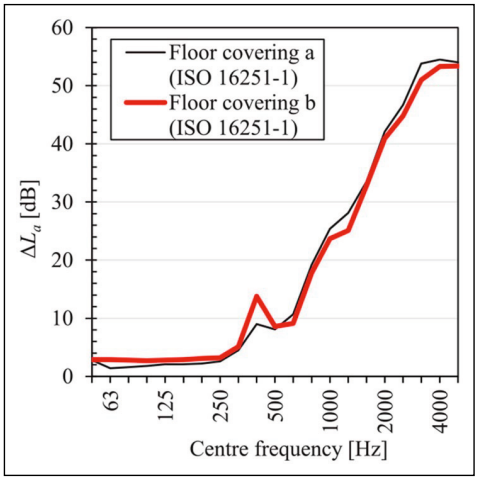

Figure 6. Measurement results of ΔL_a of the floor coverings (a) and (b) on the concrete mock-up slab in 1/3-octave centre frequencies in the frequency range 50–5000 Hz.

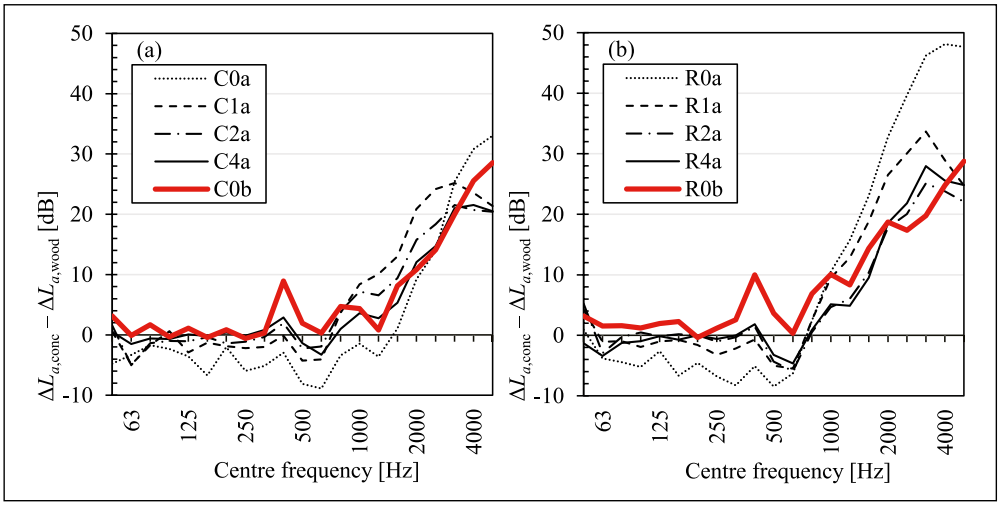

Figure 7. The difference between the measurement results on concrete mock-up slab ($\Delta L_{a,conc}$) and wooden slabs ($\Delta L_{a,wood}$) in 1/3-octave centre frequencies in the frequency range 50–5000 Hz. The figure (a) compares the results on the concrete mock-up slab with the results on the CLT slabs and (b) compares the results on the concrete mock-up slab and on the rib slabs.

between ΔL_a on the concrete mock-up slab and on the wooden slabs, that is, $\Delta L_{a,conc} - \Delta L_{a,wood}$, have been illustrated in Figure 7, where the ΔL_a on the concrete mock-up slab has been compared to the ΔL_a gained on the CLT slabs in Figure 7(a) and correspondingly with the rib slabs in Figure 7(b).

The ΔL_a results for the two floor coverings on the concrete mock-up slab seemed to be close to each other (Figure 6). As discussed above (Section 3.1), this was not the case for the wooden slabs. In the mid-frequencies, resonance frequencies were evident for both floor coverings probably due to the interaction between the hammers and the soft floor covering, and due to the floating floor constituted by the multilayer parquet and the soft underlayment. At the higher frequencies, the values increased until the highest frequencies in consideration.

The differences between the measurement results of ΔL_a on the concrete mock-up slabs and the wooden slabs were major especially in the high frequencies (Figure 7). A significant characteristic of the differences was that in the low-frequency range, the differences were rather constant and floor dependent and in the mid-frequencies a turning point was prominent after which the differences began to increase. In the low frequencies, the ΔL_a on wooden slabs was larger than on the concrete mock-up for the floor covering (a), especially in case of the lightest floors. The turning point frequency seemed to vary slightly depending on the floor covering and on the wooden slab. In addition, for the floor covering (a), the differences diminished when the plasterboards were added to the wooden floors.

Discussion

ΔL_a *by floor coverings on wooden and concrete slabs*

It is evident that the two floor coverings studied in this paper behave differently on different slabs. First, the multilayer parquet on the underlayment (floor covering (a)) forms a floating structure on the floor. Secondly, the cushion vinyl (floor covering (b)) is a resilient topping which affects the impact sound insulation by reducing the impact force level directed to the floor. These types of performances explain the results for the ΔL_a on the different floor constructions.

The ΔL_a of the floor covering (a) was clearly at its highest in the low-frequency range when the wooden slab was light weighted, that is, the bare CLT slab C0 or the rib slab R0 (Figure 4). In this frequency range, the values were several decibels higher than on the concrete mock-up slab. The reason for this phenomenon is presumably the relative increase of mass brought by the floor covering (a) to the bare slab.[27] This was also supported by the other results: when mass and stiffness of the slab increased by adding plasterboards, the differences in comparison with the concrete mock-up slab diminished in the low-frequency range (as well as in high frequencies). Another reason for the results is the differences in the impact force produced by the ISO tapping machine on the bare wooden slabs and the slabs with the floor covering.[12] When the floor covering is installed, the level of the impact force decreases compared to the bare wooden slab even in this low-frequency range.

In the mid-frequencies there seemed to be a turning point for the floor covering (a), where the ΔL_a began to suffer from the lightness of the wooden slab compared to the concrete mock-up slab (Figure 7). This occurs most probably due to the sinking impact force levels on the bare wooden slabs.[12] In other words, the softness of the bare wooden slab drops the impact force in the mid-frequency range whereas on the bare concrete mock-up slab the force levels continue to increase until the highest frequencies under consideration. These effects are seen from the mid- to high frequency results. Thus, even though the floor covering would affect the impact force similarly, the different basis for comparison makes the ΔL_a values lower on the wooden slabs. When plasterboards were added to the slabs, the results approached the ones received from the concrete mock-up measurements.

In the high-frequency range, the shape of the ΔL_a curves for the floor covering (a) could suggest – in addition to the lowering force levels – that the multilayer parquet acts resonantly on the wooden slabs.[28] Because of this phenomenon, the growth rate of the values begins to slow down in this range. On the concrete mock-up slab, apparently this does not occur, but the slight flattening of the curve after 2500 Hz is probably caused by the lowering impact force levels.

For the floor covering (b), the overall equivalence between the ΔL_a results received on the wooden slabs and concrete mock-up slab was better in comparison with the floor covering (a) on the same floors (Figure 7). In the low frequencies up to 630 Hz band, the correspondence of the results was reasonable apart from the 400 Hz peak evident in the ΔL_a on the concrete mock-up slab (Figure 6).

However, using the ΔL_a measured on the concrete mock-up instead of the ΔL_a measured on the rib slab, would slightly overestimate the performance of this topping in the low frequencies.

The ΔL_a of the floor covering (b) on the wooden slabs began to differ from the result on the concrete mock-up slab after the 630 Hz band (Figure 7). After this turning point, the differences increased up to the highest frequencies. This occurs due to the impact force differences on the different bare slabs, similarly as with the floor covering (a) discussed above. The differences of the results between the two wooden slabs C0 and R0 were also prominent because of the impact force differences. When the impact force acting on the rib slab is lower, especially between the ribs, than on the CLT slab, the ability to reduce the impact force of the resilient floor covering is lowered by the basis of the comparison. These results confirm the observations from the literature,[18–22] discussed in Section 1.

In addition to the impact force differences, it is possible that the ΔL_a of the floor covering (b) on the wooden slabs would be affected by the damping effect provided by the cushion vinyl (Figure 5(b)). When the soft floor covering is installed on the floor, the vibrational levels of the wooden floors could also be reduced by the damping properties of the material.[29] This effect could increase the values of ΔL_a in comparison with the ΔL_{force} because this damping effect is not considered by the equation (3).

To conclude, the ΔL_a results for the concrete mock-up were usually higher than the ΔL_a on the wooden floors, but there were exceptions (Figure 7). As noted, however, in the low-frequency range the differences were prominent but minor in comparison with the higher frequencies, which is important since the low-frequency performance is important for the subjective rating of the wooden floors.[30,31] In the high- and mid-frequency ranges the differences between the ΔL_a on concrete and wooden slabs became increasingly larger. These issues suggest that using the ΔL_a measured on the concrete floors instead of the ΔL_a measured on wooden floors could lead to mispredictions when designing the impact sound insulation between the apartments of wooden buildings.

Measurements of ΔL *of floor coverings used in timber construction industry*

According to the results (Figures 4, 6 and 7) and to the literature,[18–22] it is obvious that the ΔL measured on concrete slabs do not fully correspond to the ΔL gained on wooden slabs in the whole frequency range of interest. This should raise an interest to measure the floor covering products also on the wooden slabs.[4] In any case, this would increase the applicability of the products for use in the timber construction. However, the results also illustrate that there are differences between wooden slabs. Thus, it is important to measure the floor covering products on the wooden slabs corresponding to the floors the products are expected to be used.

There is also a need to develop a standardized test method for wooden mock-up slabs corresponding the method presented in the standard ISO 16251-1.[5] Because of the differences between the results brought by the standard[11] and the wooden mock-up tests in Sommerfeld,[6] the compact wooden floor should at least be larger than the corresponding concrete mock-up slab. As noted in Section 4.1, it is possible that the floating floor coverings, such as the floor covering (a), act resonantly on the wooden slabs, which should also be taken into consideration in the development of the method. In addition, it would be beneficial to include alternative floor types in the method, at least those as in ISO 10140-5.[4]

Limitations and need for further research

It must be noted that the measurement method[6] used in this study is not standardized on the wooden slabs. Thus, the vibration level reduction ΔL_a by the floor coverings on the wooden slabs have not

been confirmed to correspond with the improvement of impact sound insulation ΔL.[2–4] For example, increasing the measurement positions below the wooden slabs would have improved the accuracy of the results. Therefore, the results of this study should not be considered absolute, and the conclusions remain preliminary until they are confirmed by a further research conducted in a full-scale building acoustics laboratory.

Conclusions

It is known that ΔL of floor coverings depend upon the bare slab it is installed. The problem is, however, that the products are usually tested on concrete slabs even though laboratory standards[2–4] acknowledge also wooden slabs. Therefore, two floor coverings, a multilayer parquet on an underlayment, and a cushion vinyl, were tested on wooden slabs and on a concrete mock-up slab by applying the method presented by Sommerfeld[6] and the standard ISO 16251-1,[5] in this study. The object of this was to study the behaviour and the vibration level reduction ΔL_a by the floor coverings on different types of slabs. The findings suggest that the ΔL results achieved on concrete slabs do not correspond the results on wooden slabs. In case of the parquet, novel results were brought to light since, according to the authors' knowledge, systematic studies comparing the ΔL_a by a parquet on several floor types has not been previously published. The results for the cushion vinyl represent similar behaviour as seen in the literature.

Possible reasons for the discrepancies between the results on different slabs were found from the behaviour of the slabs and floor coverings. The main reason for the different results of both specimens on different slabs was the different impact force levels generated by the ISO tapping machine on the bare slabs. Secondly, the behaviour of the ΔL_a of the parquet on the underlayment was explained by the floating structure composed by the floor covering. In the low-frequency range, the relative increase of mass brought by the parquet to the slab increased the ΔL_a levels on wooden slabs in comparison with the concrete mock-up slab. In high frequencies it was noted that it is possible that the parquet acts resonantly, thus reducing its ability to improve impact sound insulation. Adding plasterboards to the floors seemed to diminish the discrepancies. Third, in case of the cushion vinyl, it is possible that the results were affected by the damping effects of the floor covering.

The results suggest that the floor coverings should be measured on wooden slabs when they are to be used within the timber construction industry. This should be done even though the results would not be as promising as on concrete slabs, and because using the ΔL measured on concrete slabs instead of the ΔL measured on wooden slabs could lead to mispredictions when designing the impact sound insulation of wooden floors. Additionally, there is a need for developing a fast and affordable standardized test method for wooden mock-up slabs corresponding the method presented in ISO 16251-1.[5] These findings and suggestions should be confirmed in a follow-up full-scale laboratory research.

Acknowledgements

This paper was written within the Doctoral School in Industrial Timber Construction of Tampere University. The authors would like to thank Dr Valtteri Hongisto and Mr Pekka Saarinen from Turku University of Applied Sciences for conducting the tests on the concrete floor mock-up. The authors are grateful for the constructive comments to the manuscript given by Dr Valtteri Hongisto.

Declaration of Conflicting Interests

The author(s) declared no potential conflicts of interest with respect to the research, authorship, and/or publication of this article.

Funding

The author(s) received no additional financial support for the research, authorship, and/or publication of this article.

ORCID iD

Jesse Lietzén https://orcid.org/0000-0002-7326-8556

References

1. Kylliäinen M, Lietzén J, Kovalainen V, et al. Correlation between single-number-quantities of impact sound insulation and various noise ratings of walking on concrete floors. *Acta Acust United Acust* 2015; 101: 975–985.
2. ISO 10140-1. *Acoustics – laboratory measurement of sound insulation of building elements – part 1: application rules for specific products*. Geneva: International Organization for Standardization, 2016.
3. ISO 10140-3. *Acoustics – laboratory measurement of sound insulation of building elements – part 3: measurement of impact sound insulation*. Geneva: International Organization for Standardization, 2010.
4. ISO 10140-5. *Acoustics – laboratory measurement of sound insulation of building elements – part 5: requirements for test facilities and equipment*. Geneva: International Organization for Standardization, 2010.
5. ISO 16251-1. *Acoustics – laboratory measurement of the reduction of transmitted impact noise by floor coverings on a small floor mock-up – part 1: heavyweight compact floor*. Geneva: International Organization for Standardization, 2014.
6. Sommerfeld M. A simplified measurement method for the determination of impact sound reduction. In: *Proceedings of DAGA*, Rotterdam, The Netherlands, 2009.
7. Pereira A, Godinho L, Mateus D, et al. Assessment of a simplified experimental procedure to evaluate impact sound reduction of floor coverings. *Appl Acoust* 2014; 79: 92–103.
8. Schmidt JH, Wittstock V and Langer SC. Uncertainties and validation procedures for the compact measurement setup. In: *Proceedings of 43rd international congress on noise control engineering inter-noise 2014*, Melbourne, Australia, 16–19 November 2014.
9. Schmidt JH, Wittstock V, Foret R, et al. Measuring the impact sound reduction at a compact measurement setup—design, results and uncertainties. *Build Acoust* 2013; 20: 107–139.
10. Keränen J, Lietzén J, Kylliäinen M, et al. Improvement of impact sound reduction by floor coverings - measurements using a small floor mock-up and an impact sound laboratory. In: *Proceedings of the 42nd international congress and exposition on noise control engineering 2013, INTER-NOISE 2013: noise control for quality of life*, Innsbruck, Austria, 15–18 September 2013.
11. ISO 140-11. *Acoustics – laboratory measurement of sound insulation in buildings and of building elements – part 11: laboratory measurements of the reduction of transmitted impact sound by floor coverings on lightweight reference floors*. Geneva: International Organization for Standardization, 2005.
12. Lietzén J, Miettinen J, Kylliäinen M, et al. Impact force excitation generated by an ISO tapping machine on wooden floors. *Appl Acoust* 2021; 175: 107821.
13. Hopkins C. *Sound insulation*. London: Elsevier Ltd, 2007.
14. Kartous M and Jonasson HG. A simplified method to determine impact sound improvement on lightweight floors. Nord Proj 1544-01, SP Rapport 2001:37, 2002.
15. Zeitler B, Nightingale TRT and Schoenwald S. Effect of floor treatments on direct impact sound pressure level. In: *Proceedings of Euronoise 2009*, Edinburgh, Scotland, 26–28 October 2009, pp.1–9.
16. Balanant N, Guigou C and Villenave M. Acoubois, Respect des exigences acoustiques dans les bâtiments à ossature bois, à vocation logements, Etape 2, Rapport final, France, 2012.
17. Späh M, Liebl A and Leistner P. Acuwood, Acoustics in wooden buildings – field measurements in multistorey buildings. Report 2, SP Report 2014: 5, http://www.diva-portal.org/smash/get/diva2:962815/FULLTEXT01.pdf (2014, accessed 5 November 2011).

18. Scholl W and Maysenhölder W. Impact sound insulation of timber floors: interaction between source, floor coverings and load bearing floor. *Build Acoust* 1999; 6: 43–61.
19. Schmitz A. Comparison of impact sound insulation measurements of floor coverings using different floor types and excitation sources. In: *Proceedings of Inter-noise 2000*, Nice, France, 27–30 August 2000, pp.1–9.
20. Warnock ACC. Impact sound measurements on floors covered with small patches of resilient materials or floating assemblies. Internal Report IRC-IR-802, Institute for Research in Construction, January 2000.
21. Nowotny and Nurzyński J. Proposal of an assessment method of the impact sound insulation of lightweight floors. *Buildings* 2020; 10(1): 13.
22. Pereira A, Mateus D, Godinho L, et al. Evaluation of impact sound reduction of floor coverings on timber and timber-concrete floors using vibration measurements. In: *Proceedings of EuroRegio2016*, Porto, Portugal, 13–15 June 2016.
23. Alonso A, Patricio J and Suárez R. On the efficiency of impact sound insulation systems on prefabricated lightweight floor and on standard homogeneous base-floor. *Eng Struct* 2019; 191: 649–657.
24. Valjakka S. Floor coverings' effect on the impact sound reduction on wooden floors (In Finnish). Tampere University, http://urn.fi/URN:NBN:fi:tuni-202101101137 (2021).
25. ISO 9052-1. *Acoustics – determination of dynamic stiffness – part 1: materials used under floating floors in dwellings*. Geneva: International Organization for Standardization, 1989.
26. Vér IL. Impact noise isolation of composite floors. *J Acoust Soc Am* 1971; 50: 1043–1050.
27. Zeitler B, Schneider M and Sabourin I. On the relevance of impact source impedance at low frequencies – part 2: floors with floating toppings. In: *24th international congress on sound and vibration ICSV 2017*, London, 23–27 July 2017.
28. Rindel JH. *Sound insulation in buildings*. Boca Raton, FL: CRC Press, 2017.
29. Oulmane A and Ross A. *Effects of material parameters on the transient dynamics of an impacted plate with partial constrained layer damping treatment. J Acoust Soc Am* 2010; 147: 1939–1952.
30. Ljunggren F, Simmons C and Hagberg K. Correlation between sound insulation and occupants' perception – proposal of alternative single number rating of impact sound. *Appl Acoust* 2014; 85: 57–68.
31. Ljunggren F, Simmons C and Öqvist R. Correlation between sound insulation and occupants' perception – proposal of alternative single number rating of impact sound, part II. *Appl Acoust* 2017; 123: 143–151.

Appendix A

Measurement results

The measurement results for the ΔL_a of the floor coverings are shown altogether in Figures A1–A4 as follows: the results on the CLT slabs are depicted in Figures A1 and A2 for the floor coverings (a) and (b), respectively; and the corresponding results on the rib slabs are presented in Figures A3 and A4. In the figures, the grey lines illustrate the individual measurement results and the black lines the average measurement results.

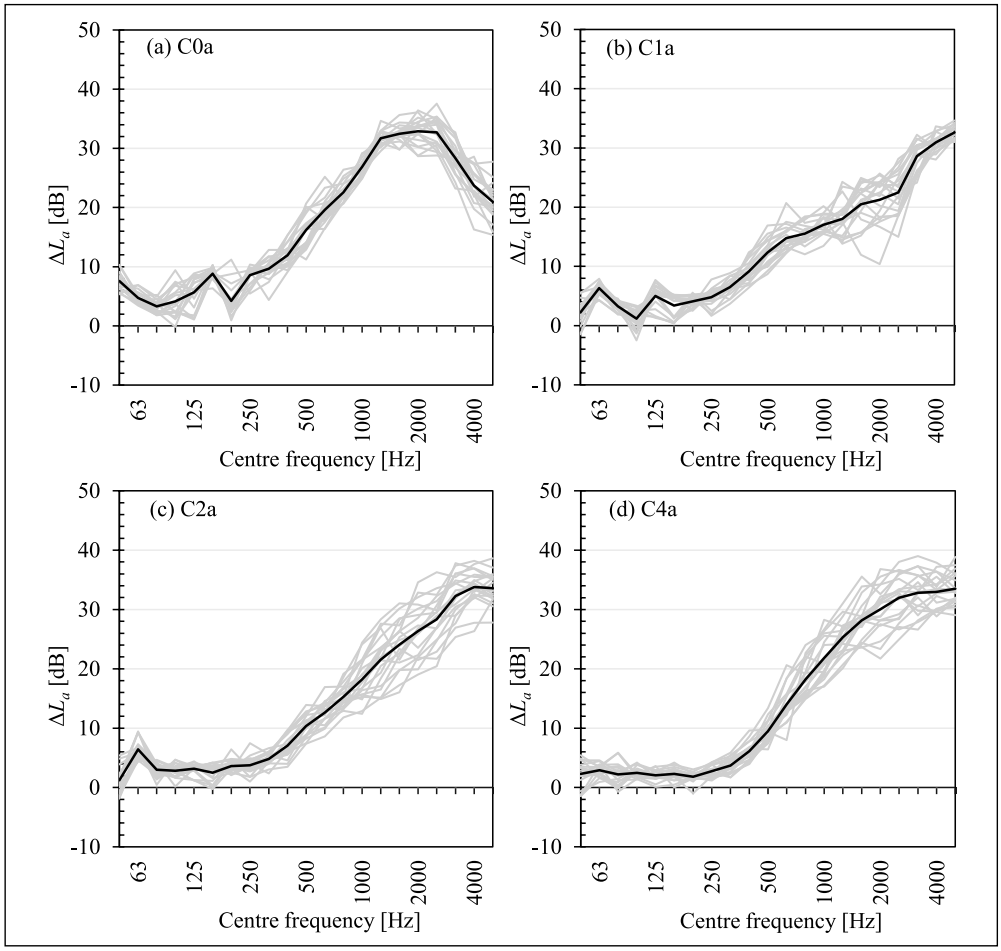

Figure A1. Individual measurement results of ΔL_a on the CLT slabs C0, C1, C2 and C4 for the floor covering (a) (grey lines), and the average results (black lines).

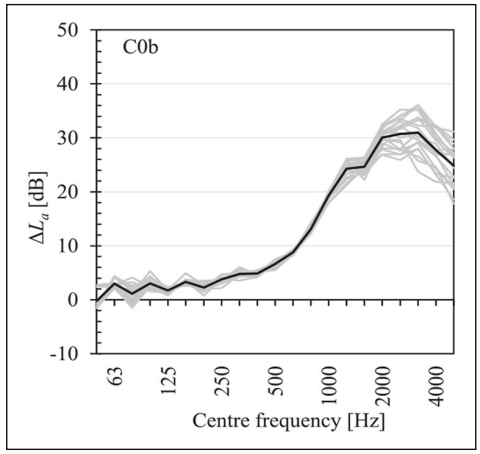

Figure A2. Individual measurement results of ΔL_a on the CLT slab C0 for the floor covering (b) (grey lines), and the average result (black line).

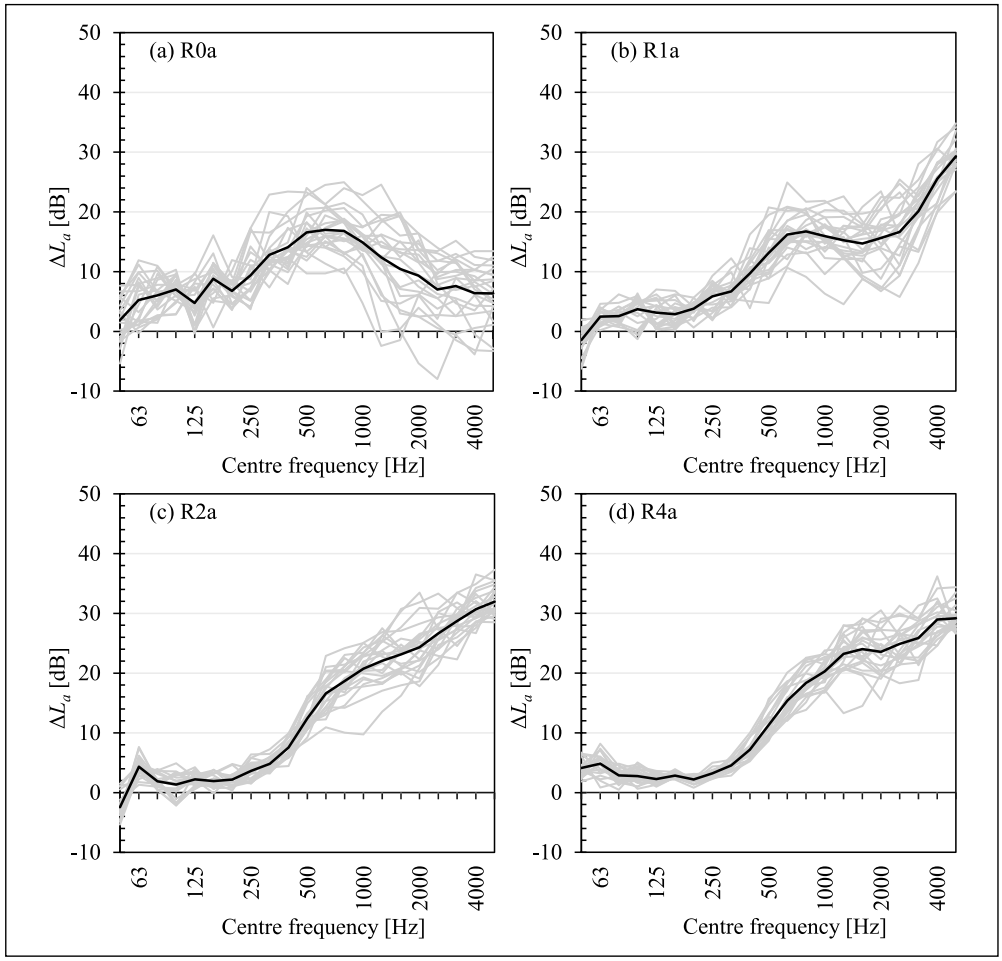

Figure A3. Individual measurement results of ΔL_a on the rib slabs R0, R1, R2 and R4 for the floor covering (a) (grey lines), and the average results (black lines).

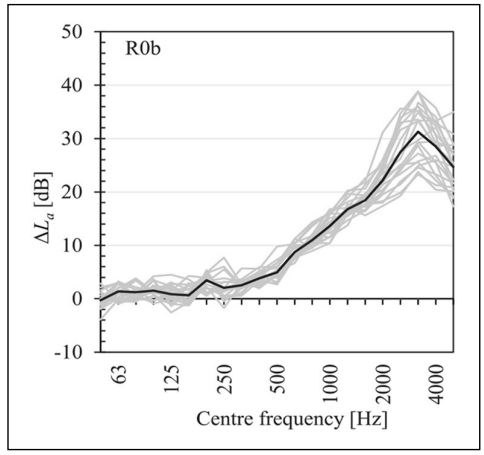

Figure A4. Individual measurement results of ΔL_a on the rib slab R0 for the floor covering (b) (grey lines), and the average result (black line).

PUBLICATION IV

Computational prediction of impact sound insulation of a full-scale timber floor applying a FEM simulation procedure

Jesse Lietzén, Ville Kovalainen, Mikko Kylliäinen, Sami Pajunen

Submitted to Engineering Structures on 3rd of August 2023, revised 15th of December 2023